Correlation and Capacity Analyses of Multi-input Multi-output Communications Systems

Jianmin Gong

A Thesis

In

The Department

Of

Electrical and Computer Engineering

Presented in Partial Fulfillment of the Requirements for the Degree of Doctor of Philosophy (Electrical Engineering) at Concordia University, Montreal, Quebec, Canada

June 2005

Your file Votre référence
ISBN: 0-494-09973-9
Our file Notre référence
ISBN: 0-494-09973-9

Abstract

Correlation and Capacity Analyses of Multi-input Multi-output Communications Systems

Jianmin Gong, Ph.D.

Concordia University, 2005

In this thesis, several factors which affect the channel capacity of multi-input multi-output communication systems have been studied under the assumption of a narrow-band Rayleigh fading channel.

The first factor is the capacity's diversity property. The previously known result is verified that the outage (a certain probability is out) capacity of N_1 transmit antennas and N_2 receive antennas systems is higher than that of N_2 transmit antennas and N_1 receive antennas when they have the same signal-to-noise ratio and $N_1 < N_2$ in the independent and identically distributed Rayleigh fading channel.

The second is the point of diminishing returns in the increase of capacity with the increase of the number of antennas. With the Monte Carlo simulation, it is found that six receive antennas reach the point of capacity diminishing returns for a small number of transmit antennas and four transmit antennas reach the point for a small number of receive antennas.

The third is the correlation between different paths in a correlated narrow-band Rayleigh fading channel. It is shown that the receive antenna polarization matrix must be orthogonal with the incident source polarization matrix to achieve zero correlation. An abstract spherical model is introduced so that the effect of antenna pattern on the correlation and thus the capacity can be studied. It is found that the broadside linear array

with the half-wave square patch microstrip antennas has higher outage capacity than that with half-wave dipole antennas in most orientations. This phenomenon still exists when both the transmit array and the receive array are square and rectangular arrays, respectively. Furthermore, a correlation model based on a statistical Student's t-distribution of angle-of-arrival is developed in order to investigate the effect of antenna pattern in a more realistic environment. It was found that the vertical linear array with half-wave patch microstrip elements has higher capacity than that with half-wave dipole elements in the orientation of the antenna visible region. However, for the horizontal linear array, the microstrip elements have different variation of capacity versus orientation with the dipole elements due to the effect of antenna pattern. The cross linear array illustrates higher capacity than the vertical and horizontal linear arrays, indicating that this array is closer to the condition of zero correlation.

Acknowledgement

As I finish writing my doctoral thesis, I look back on every stage of my Ph.D. program. First, I sincerely thank my supervisors, Prof. M. R. Soleymani and Prof. J. F. Hayes. Prof. M. R. Soleymani accepted me in the Ph.D. program and supported me with the financial program of research assistant/teaching assistant. Prof. J. F. Hayes also supported me under his grant of the Natural Science and Engineering Research Council of Canada. He led me into the field of channel modeling, in which I can combine my previous knowledge of electromagnetics with multiple-input multiple-output communication technology. During my research, I felt strongly that both of these professors spent a lot of their valuable time in helping me to understand the communication theory and technology, to discuss every academic point encountered, to suggest solutions for my problems, and to check results and correct errors I have made. I feel so grateful for these things.

Second, I appreciate professors, Y.R. Shayan, E.I. Plotkin, Ronggang Qi, A. Benyamin-Seyar, W. Hamouda, and Mustafa Mehmet Ali, who have taught the courses that I have taken.

Finally, I would like to thank Dr. Xiangmin Li, my fellow students M. Ghotbi, Yuandong Wang, Yingzi Gao, Le Feng, Z. Motamedi, J. Haghighat, P. Tooher, and H. Behroozi for their helpful discussions.

Table of Contents

List of Figures viii

List of Symbols and Abbreviations x

List of Contributions xii

1 Historical survey of multiple-input multiple-output systems 1

1.1 Information theory 4
1.2 Channel modeling and measurements 4
1.3 Space-time coding 7
1.4 Practical applications in 3G wireless systems and beyond 9

2 Capacity of multiple-input multiple-output Systems 11

2.1 Introduction 11
2.2 Mathematical model 12
2.3 The derivation of channel capacity 14
2.4 Examples of capacity 16
2.5 Distribution of capacity 17

3 Optimization of antenna number in the capacity of MIMO systems 22

3.1 Introduction 22
3.2 Mathematical model for MIMO channels 23
3.3 Higher capacity with more receive antennas 23
3.3.1 *Single Antenna Configurations* 24
3.3.2 *Two antenna configurations* 27
3.3.3 *Limiting Cases for Large Numbers of Antennas* 32
3.3.4 *General case of arbitrary* n_T *and* n_R 34
3.4 Antenna number for capacity saturation 37
3.5 Summary and conclusions 41

4 Correlation and capacity analyses with a spherical model 43

4.1 Introduction 43
4.2 Geometry and capacity 45
4.2.1 Capacity 45
4.2.2 The spherical model 47

4.3 Antenna arrays and radiation patterns 53
4.3.1 Capacity and the number of antennas 53
4.3.2 Two antenna arrays 54
4.3.3 Two kinds of antenna elements 57
4.3.4 Radiation field patterns 59
4.4. Simulation results 61
4.5. Conclusions 70

5 Correlation and capacity analyses with an experimentally based statistical model 73

5.1 Introduction 73
5.2 Condition for zero correlation 74
5.3 The covariance matrix based on the statistical power spectrum 77
5.3.1 Covariance in the rectangular coordinate system 77
5.3.2 Power spectrum 79
5.3.3 The covariance based on the power spectrum 83
5.4 Antenna array 84
5.5 Simulation results 88
5.6 Summary 96

6 Summary 98

Bibliography 104

Appendix A 117

Appendix B 124

List of publications 128

List of Figures

Fig. 1.1. Diagram of a MIMO wireless transmission system.

Fig. 3.1. Capacity increases with signal-to-noise ratio.

Fig. 3.2. Comparison of the transmit diversity with the receive diversity.

Fig. 3.3. The capacity increases with the number of receive antennas for n_T=1.

Fig. 3.4. The capacity increases with the number of receive antennas for n_T=2.

Fig. 3.5. The capacity increases with the number of receive antennas for n_T=3.

Fig. 3.6. The capacity increases with the number of transmit antennas for n_R=1.

Fig. 3.7. The capacity increases with the number of transmit antennas for n_R=2.

Fig. 3.8. The capacity increases with the number of transmit antennas for n_R=3.

Fig. 4.1. Illustration of the abstract spherical model. T_p, R_l, and $S(\theta, \varphi)$ are the transmitting antenna p, the receiving antenna l, and the scatterer, respectively.

Fig. 4.2. Antenna arrays of the transmitter.

Fig. 4.3. Antenna arrays of the receiver.

Fig. 4.4. (a) The half-wavelength dipole antenna; (b) the half-wavelength square patch microstrip antenna: $L=W=0.49\lambda_d$.

Fig. 4.5. The field pattern of the half-wave dipole.

Fig. 4.6. The field pattern of the half-wave square microstrip patch antenna.

Fig. 4.7. The pdf curves of the ordered eigenvalues of HH^+ in broadside case of linear transmitting and receiving arrays.

Fig. 4.8. The ccdf of capacity for various angle spreads for broadside case of linear transmitting and receiving arrays.

Fig. 4.9. Variations of outage capacity with θ_r for φ_r from 0° to 360° in the case of the linear transmitting and receiving arrays. Points of isotropic inline, dipole inline, and microstrip inline are almost merged.

Fig. 4.10. Variations of outage capacity with θ_r and φ_r for rectangular receiving arrays.

Fig. 4.11. (a) Magnitudes of correlations change with the receive antenna spacing for the broadside linear array. (b) $C_{0.1}$ versus dr.

Fig. 5.1. Electromagnetic waves propagate from the transmitter to the receiver.

Fig. 5.2. Distribution of complex scatterers.

Fig. 5.3. (a) The vertical linear array. (b) The antenna patterns.

Fig. 5.4. (a) The horizontal linear array. (b) The antenna patters.

Fig. 5.5. (a) The hybrid linear array. (b) The antenna patterns.

Fig. 5.6. Power spectrum from (5.19).

Fig. 5.7. (a) The correlation of $E[H_{11}H_{21}^*]$ changes with dr for the vertical linear array. (b) The 10% outage capacity $C_{0.1}$ changes with dr for the vertical linear array.

Fig. 5.8. The ccdf of capacity for various angle spreads for the vertical linear array.

Fig. 5.9. The 10% outage capacity $C_{0.1}$ changes with θ_r for the vertical linear array.

Fig. 5.10. The 10% outage capacity $C_{0.1}$ changes with θ_r for the horizontal linear array.

Fig. 5.11. The 10% outage capacity $C_{0.1}$ changes with θ_r for the hybrid linear array.

List of Symbols and Abbreviations

1. AOA	angle of arrival.
2. AWGN	additive white Gaussian noise.
3. BER	bit error rate.
4. BLAST	Bell labs space-time.
5. ccdfs	complementary cumulative distribution functions.
6. CSI	channel state information.
7. Fig	figure.
8. LOS	line of sight.
9. MIMO	multiple-input multiple-output.
10. ML	maximum-likelihood.
11. MOSI	multiple-input single-output.
12. NLOS	non-line of sight.
13. pdf	probability density function.
14. RV	random variable.
15. SISO	single-input single-output.
16. SNR	signal-to-noise ratio.
17. SOMI	single-input multiple-output.
18. STBC	space-time block code.
19. STC	space-time code.
20. STTC	space-time trellis code.
21. XPD	cross polar discrimination.
22. P_{out}	10% probability of outage.
23. n_T	transmitting antenna elements.
24. n_R	receiving antenna elements.
25. P_t	total transmission power.
26. $\boldsymbol{s}(t)$	n_T dimensional transmitting signal vector.
27. $\boldsymbol{v}(t)$	complex n_R dimensional AWGN vector.
28. $\boldsymbol{r}(t)$	n_R dimensional receiving signal vector.
29. P	the average power at the output of each of the receiving antennas.
30. ρ	$\rho=P/N$, signal-to-noise ratio at each receiver branch.
31. $g(t)$	the matrix channel impulse response.
32. H	the channel transfer matrix.
33. $\otimes$	convolution operator.
34. $'$	vector transpose.
35. +	transpose conjugate.
36. $det, \lvert\cdot\rvert$	determinant.
37. $\boldsymbol{I}_n$	$n \times n$ identity matrix.
38. $E[\cdot]$	expectation.
39. C	capacity
40. H_{lp}	path gain from the transmit antenna p to the receive antenna l.
41. $N_{\min}$	minimum of n_T and n_R.
42. W	Wishart matrix.
43. $\underline{\lambda}$	ordered eigenvalue vector of W.

44. λ_i	the i^{th} eigenvalue of W.
45. Σ_T	covariance matrix of the rows of H.
46. Σ_R	covariance matrix of the columns of H.
47. dt	distance between two adjacent transmit antenna elements.
48. dr	distance between two adjacent transmit antenna elements.
49. χ^2_{2n}	Chi-squared random variable with $2n$ degrees of freedom.
50. T_p	the transmitting antenna p.
51. R_l	the receiving antenna l.
52. $S(\theta,\varphi)$	the scatterer at (θ,φ).
53. D	distance between the base station and the mobile station.
54. Δ	angle spread.
55. R	radius of the scattering sphere.
56. Θ	angle of arrival.
57. $\phi(\theta,\varphi)$	phase shift at (θ,φ).
58. $F(\theta,\varphi)$	radiation field pattern.
59. D_a	maximum directivity of receiving antenna elements.
60. $\vec{E}_{\lambda p}$	the p^{th} incident source vector from the transmitting antenna T_p.
61. $\vec{E}_l$	the l^{th} dimensionless receive antenna electric field.
62. Ω	the solid angle (θ, φ).
63. A	the area of incident waves.
64. $d\Omega$	element of solid angle $=\sin\theta\, d\theta\, d\varphi$.
65. λ	wavelength.
66. R_{ji}	the distance from object j to object i.
67. Ω_k	the solid angle of the k^{th} scatterer.
68. σ^2_{lp}	the variance of H_{lp}.
69. s^2	measure of angular spread.

List of Contributions

1. We have analytically verified the previously known result that the outage (a certain probability is out) capacity of a MIMO system with N_1 transmit antennas and N_2 receive antennas is higher than that of a MIMO system with N_2 transmit antennas and N_1 receive antennas when they have the same signal-to-noise ratio and $N_1 < N_2$ in the independent and identically distributed Rayleigh fading channel.
2. We have numerically illustrated that six receive antennas reach the point of capacity diminishing returns for a small number of transmit antennas and four transmit antennas reach the point for a small number of receive antennas.
3. We have developed a spherical model to study the effect of antenna physics on the capacity of MIMO systems. We show that the microstrip patch antenna linear array has a higher capacity than the dipole linear array when they are in the broadside of the transmitter under the environment that scatterers are uniformly distribution over a sphere.
4. We have derived a condition of zero correlation for MIMO systems, i.e., the receive antenna polarization matrix must be orthogonal with the incident source polarization matrix, which extends the condition of zero correlation for the traditional communications systems, in which there is only one antenna in an end and multiple antennas in the another end.
5. We have derived a correlation model based on a statistical Student's *t*-distribution of angle-of-arrival, which is accurate in the micro-cell environment. With this model, we have shown that the cross linear array has

higher capacity than the vertical and horizontal linear arrays, indicating that this array is closer to the condition of zero correlation.

Chapter 1 Historical survey of multiple-input multiple-output systems

Future generation wireless communication systems will be required to have high voice quality as compared to current cellular mobile radio standards and to provide high bit rate data services. Moreover, they have to be reliable in different kinds of environments: Macro, micro, and pico-cellular; urban, suburban, and rural; indoor and outdoor. In other words, the coming systems need to provide better quality and coverage and more power and spectrum efficiency in diverse environments.

In traditional mobile radio communications, single-input single-output (SISO) systems are systems with one antenna at each end of the link. The fundamental phenomenon, which makes reliable wireless transmission difficult, is time-varying multipath fading [1]. It is this phenomenon, which makes wireless transmission a challenge as compared to fiber, coaxial cable, line of sight microwave or satellite transmissions.

Increasing the quality or reducing the effective error rate in a multi-path fading channel is extremely difficult. In the case of additive white Gaussian noise (AWGN), using typical modulation and coding schemes to reduce the bit error rate (BER) from 10^{-2} to 10^{-3} may require 1 dB or 2 dB higher signal-to-noise ratios (*SNR*). However, achieving the same in a multi-path fading environment may require up to 10 dB higher *SNR*. Improving *SNR* by increasing transmit power or bandwidth is precluded by the requirements of next generation systems. It is therefore crucial to effectively combat or reduce the effect of fading at both the mobile stations and base stations, without additional power or increase in bandwidth.

The most effective technique to mitigate multi-path fading in a wireless channel is transmitting power control. If channel conditions as experienced by the receiver are known at the transmitter, the transmitter can pre-distort the signal in order to overcome the effect of the channel at the receiver. However, there exist two fundamental problems. The major problem is the required transmitter dynamic range. For the transmitter to overcome a certain level of fading, it must increase its power by that same level, which is not practical in most cases due to radiation power limitations and the size and cost of amplifiers. The second problem is that the transmitter does not have any knowledge of the channel experienced by the receiver. So, the channel information has to be fed back from the receiver to the transmitter, which results in throughput degradation and considerable added complexity to both the transmitter and the receiver.

In most scattering environments, antenna diversity is a practical, effective, and widely applied technique for reducing the effect of multi-path fading [1]. By adding more antennas to one end of the link in order to increase the antenna diversity, the capacity can be increased as a result of the diversity and antenna array gain [2]. For the transmit diversity, there are multiple transmitting output antennas and single receiving input antenna (MOSI) [3, 4, 5, 6, 7]; for the receive diversity, there are a single transmitting output antenna and multiple receiving input antennas (SOMI) [8].

Adding more antennas at both ends of the link in which each transmitting antenna sends an independent signal forms multiple-input multiple-output communications (MIMO). This option had been disregarded in previous mobile communications standards due to the limited size of the handsets and the low frequency band of operation. Nowadays, the proliferation of wireless local area networks and the need for

sophisticated and bandwidth-consuming services such as video over the radio interface has motivated the reconsideration of this option. This option stands out among the emerging radio technologies, which are pushing the frontiers of wireless capacity with the promise of many orders of magnitude improvement in spectrum efficiency relative to what is achievable today. Pioneering work by Winters [9], Foschini [10,11], and Telatar [12,13] has ignited interest in this area by predicting remarkable spectral efficiencies for wireless systems when the channel exhibits rich scattering and its variations can be accurately tracked. Foschini, Telatar, et al, [11, 13] have shown that MIMO systems can provide radio channels capable of transferring parallel information within the same bandwidth and therefore increase the attainable capacity in ideal Rayleigh fading channels.

The core idea in MIMO systems is space-time signal processing in which time is complemented with the spatial dimension inherent in the use of multiple spatially distributed antennas. A key feature of MIMO systems is the ability to turn multi-path propagation, traditionally a pitfall of wireless transmission, into a benefit for the capacity. MIMO makes advantage of random fading [10, 11, 13] and multi-path delay spread when available [14, 15] for multiplying transmission rates.

The prospect of many orders of magnitude improvement in spectrum efficiency of MIMO has pushed progress in areas as diverse as channel modeling, information theory and coding, signal processing, antenna design and multiantenna-aware cellular design, fixed or mobile.

1.1 Information theory

Information-theoretical capacity provides a benchmark for practical systems to understand the tools needed to maximize capacity. For example, Information theory can show how the MIMO system capacity changes with different channel conditions.

For a single user MIMO system, Foschini et al [10] gave the channel capacity formulae of MIMO for independent and identically distributed (i.i.d.) Rayleigh fading channels when only the receiver knows the channel state information. Telatar analyzed the channel capacity of MIMO when the transmitter knows the channel state information [13]. Driessen et al [16] geometrically explained how to construct parallel sub-channels of MIMO in line of sight environments. When the fading channel of MIMO is correlated, the effect of fading correlation was studied by Shiu et al [17], Abdi et al [18], and Byers et al [19]. The probability distribution and characteristic function when the correlations are only among the transmitter or the receiver were given by Chiani et al [20]. The worst situation of MIMO channel capacity is with the keyhole indicated by Chizhik et al [21]. Upper bound of MIMO channel capacity [22] and asymptotic evaluation of MIMO channel capacity [23] were derived. For the multi-user MIMO systems, Goldsmith gave detailed analysis [24].

1.2 Channel modeling and measurements

Since MIMO algorithms are sensitive to channel matrix properties, the potential of high capacity of MIMO systems depends strongly on the nature of the underlying

multi-path environment. The properties of MIMO channels in pico, micro, and macro-cell environments are key to determining the channel capacity, achievable performance, and suitable system architectures and signal processing algorithms. Hence, channel modeling is critical to assess the relative performance of the various MIMO architectures discussed in the previous subsection. Key modeling parameters include path loss, shadowing, Doppler spread and delay spread profiles, and the Ricean K factor distribution. The Ricean K factor is the ratio between the power of the line of sight (LOS) component and the mean power of the non-line of sight (NLOS) component.

It is common to model a wireless channel as a sum of a LOS component and a NLOS component. The higher the Ricean K factor, the more dominant is the LOS component. Since the LOS component is a time-invariant, its effect is to increase correlation between antennas and to decrease the rank of the channel matrix [25]. High K channels show low useable spatial degrees of freedom and a low MIMO capacity for the same *SNR*.

Experimental measurements have been tried to characterize the distribution of the K factor [26,27,28]. An empirical model was derived for typical macrocell fixed deployment [26]. The K factor distribution was modeled as lognormal with the median as a function of season, antenna heights, antenna beamwidth, and distance. According to this model, the K factor decreases with the distance, which means that even though the use of MIMO does not improve the link throughout near the base station, where the signal strength is high, it improves the quality of service in areas that are far from the base station.

In a microcell deployment, the base station antenna is typically at about the same height as street lamp posts and hence the coverage radius is no more than a few hundred meters. Microcell channels frequently involve the presence of a LOS component [29]. The K factor also decreases with distance, but tends to be smaller than that in a macrocell.

In an indoor environment, many simulations [30] and measurements [31] have shown that the typical multipath scattering is so rich that the LOS component rarely dominates, which plays in favor of in-building MIMO deployments.

When the LOS component is absent, the channel matrix is usually modeled with circularly-symmetric complex Gaussian random variables (i.e., Rayleigh fading). The correlation between entries of the channel matrix can be caused by small antenna spacing, few dominant scatterers, and small spreading of angle of arrival (AOA). The effects of correlation on channel capacities are considered by Shiu et al [17], who have extended the "one-ring" model of Jakes [1] to the MIMO case and have shown that the correlation significantly reduces the channel outage capacities. Abdi et al have improved the "one-ring" model to consider the role of power azimuth distribution [18]. The power azimuth distribution studied in the literature is uniform, truncated normal and Laplacian [32]. Different power azimuth distributions lead to different relation between antenna correlation and AOA or angle spread. Byers et al have considered one ring around the transmitter and one ring around the receiver [19] in the investigation of correlation. Chuah et al have combined the Monte-Carlo simulation with electromagnetic field simulation in a practical indoor environment to observe the correlation and channel capacity [33]. The electromagnetic field simulation can be found in a large variety of studies[34-36].

Experiments have been carried out to clarify a number of issues. The capacity measured in microcell environments has been found to be 30% smaller than that of an idealized model [37]. Some stochastic channel models have been validated for picocell and microcell environments [38]. The multipath richness of MIMO has been investigated in [39]. The correlation measurements have shown that the receiver correlation is lower than the transmitter correlation [40]. The study of antenna polarization has shown that single polarization systems perform worse than the combined polarization systems in terms of achievable capacity [41]. Effects of antenna configurations and orientations in picocell and microcell environments on capacities have been studied in [42, 43].

1.3 Space-time coding

Since the information theoretic analysis provides the upper bound to capacity, new transmission schemes have to be developed to realize the capacity in practice with a reasonable bit error rate (BER) and a performance/complexity compromise. Transmission schemes over MIMO channels typically fall into two categories: data rate maximizing or diversity maximization schemes, although there has been some effort toward unification. The first kind is mainly to improve the average capacity, which is to perform spatial multiplexing when we send as many independent signals as we have antennas for a specific error rate (or a specific outage capacity [11]). The second kind is to maximize the outage capacity, or equivalently minimize the outage probability when individual streams are encoded jointly in order to protect transmission against errors caused by channel fading and noise plus interference.

Note that, when the level of redundancy increases between the transmit antennas through joint coding, the degree of independence between the signals decreases. Ultimately, the effective data rate goes back to that of a single antenna system, i.e., each transmit antenna sees a differently encoded, fully redundant version of the same signal. In this case, the multiple antennas only provide spatial diversity.

The schemes aimed at realizing joint encoding of multiple transmit antennas are called space-time codes. In these schemes, the number of code symbols is equal to the number of transmit antennas, one symbol from each antenna. These code symbols are generated by the space-time encoder and are transmitted simultaneously. Using the appropriate signal processing and decoding procedure at the receiver, the coding gain can be maximized.

Inspired by the delay diversity scheme of Wittneben [44], Seshadri et al made the first attempt to develop a space-time code [45]. The key development of the space-time code concept was originally presented by Tarokh et al [46] in the form of trellis codes, which required a multidimensional Viterbi algorithm at the receiver for decoding. These codes were shown to provide a diversity benefit equal to the transmit antennas in addition to a coding gain that depends on the complexity of the code without loss in bandwidth efficiency. Since these original space-time trellis codes were hand crafted, they were not optimum designs. So, a large number of research proposals [47-52] have been proposed to construct new codes or to perform systematic searches for different convolution space-time trellis (STTC) code or some variant of the original design criteria proposed by Tarokh et al. These new code constructions provide an improved coding advantage over

the original scheme proposed by Tarokh et al, however, only marginal gains were obtained in most cases.

The decoding complexity of space-time trellis coding (measured by the number of trellis states at the decoder) increases exponentially with the number of trellis states as a function of the diversity level and transmission rate. Alamouti [53] discovered a space-time block coding (STBC) scheme with two antennas, which has very simple structure and supports maximum-likelihood (ML) detection based only on linear processing at the receiver. The code construction is a very attractive scheme and currently part of both the W-CDMA and CDMA-2000 standards.

The space-time codes (STCs), initially developed to provide transmit diversity in the MISO case, are readily extended to the MIMO case. The extension of the space-time block code to more than two transmit antennas was studied in [54-57], in which a general technique for constructing STBCs for large antennas that provide the maximum diversity promised by the number of transmit and receive antennas was developed.

1.4 Practical applications in 3G wireless systems and beyond

With MIMO-related research entering a mature stage and with recent measurement campaign results further demonstrating the benefits of MIMO channels, the standardization of MIMO solutions in third generation wireless systems has recently begun. Current MIMO examples include the Lucent's Bell Labs space-time (BLAST) chip and proprietary systems intended for specific markets such as Iospan Wireless' AirBurst system for fixed wireless access [58]. Many practical issues, such as antenna

element numbers and interelement spacing, receiver complexity, system integration and signaling, MIMO channel model, and channel state information, remain before commercial development. The wide scale commercial deployment of MIMO systems should be expected in the future.

The following chapters are arranged as follows. Chapter 2 introduces the basic formulae of capacity of MIMO given by Foschini et al, which we will use throughout this dissertation. Chapter 3 discusses the comparison of more antennas at the transmitter with the inverse configuration and the diminishing return of capacity with receiver antenna elements. Chapter 4 discusses the effect of antenna physics on capacity with an abstract model. Chapter 5 continues to discuss the effect with a statistical model. Chapter 6 gives a summary.

Chapter 2 Capacity of Multiple-input multiple-output Systems

2.1 Introduction

In this chapter we introduce the basic information theoretic results of Foschini et al [10] in wireless LANs and building-to-building wireless communication links, which will be the basis of our work. The work of Foschini et al [10] was carried out in an idealized propagation context in order to give insight into wireless LAN applications and other applications where there is extremely limited mobility. The changes occurring in the propagation environment of the idealized model are on a very slow time scale compared to the burst rate. However, the channel, fixed during a burst, can randomly change from burst to burst. These properties allow the application of the "quasi-static" analysis, in which a randomly selected channel is unchanged during a burst and the burst is of long enough duration so that the standard infinite time horizon view of information theory gives meaningful results. The channel state information (CSI) is unknown at the transmitter but known at the receiver. The lack of the CSI at the transmitter can avoid the additional complication of accommodating another layer of processing to include a feedback link. Furthermore, if there is a feedback link, the extra time involved in incorporating the feedback loop could erode the validity of assuming that the channel is virtually unchanged.

The bandwidth is assumed to be narrow enough that the channel can be treated as flat over frequency. It has often been assumed that there are many scatterers in the

propagation environment so that the Rayleigh fading model is appropriate. The total transmitted power is fixed.

Since the capacity is treated as a random variable, a key goal is to find the complementary cumulative distribution functions (ccdfs). Setting a threshold percentage, for example, 90%, we can read from the ccdf graphs the capacity that we can provide with 90% probability. The 90% level amounts to 10% probability of outage (write P_{out}=10%).

2.2 Mathematical model

Fig. 1.1 illustrates a MIMO wireless transmission system. In this system, we limit our discussion for a single point-to-point channel in a complex baseband. The channel is fixed during a burst and randomly changes from burst to burst. The number of antennas at the transmitter is n_T and the number of antennas at the receiver is n_R. We use (n_T, n_R) to denote the antenna numbers at the transmitter and receiver, respectively. The total transmission power is constrained to P_t regardless of the value of n_T. The transmitted signal $\boldsymbol{s}(t)$ is n_T dimensional so that every transmit antenna sends one vector component. The channel bandwidth is narrow enough that we can treat the channel frequency characteristic as flat over frequency. The noise ν (t) at the receiver is complex n_R dimensional additive white Gaussian noise (AWGN) with statistically independent components of identical power N at each of the receiver branches. The received signal $\boldsymbol{r}(t)$ is n_R dimensional so that every receive antenna receives one complex vector component at each point in time. When there is only one transmit antenna, it radiates

power P_t and the average power at the output of each of the receiving antennas is denoted by P. So, the average signal-to-noise ratio (SNR) at each receiver branch is $\rho=P/N$ independent of n_T.

The matrix channel impulse response $g(t)$ has n_T columns and n_R rows. In accordance with the narrowband assumption, $g(t)$ is zero except for $g(0)$. Therefore, its Fourier transform is $G(f)=G$, i.e., independent of frequency. It will be convenient to represent the matrix channel response in normalized form $h(t)$. The Fourier transform of $h(t)$ is H. H is related to G by the equation $P_t^{1/2}G = P^{1/2}H$. So, $g(t) = (P/P_t)^{1/2}h(t)$.

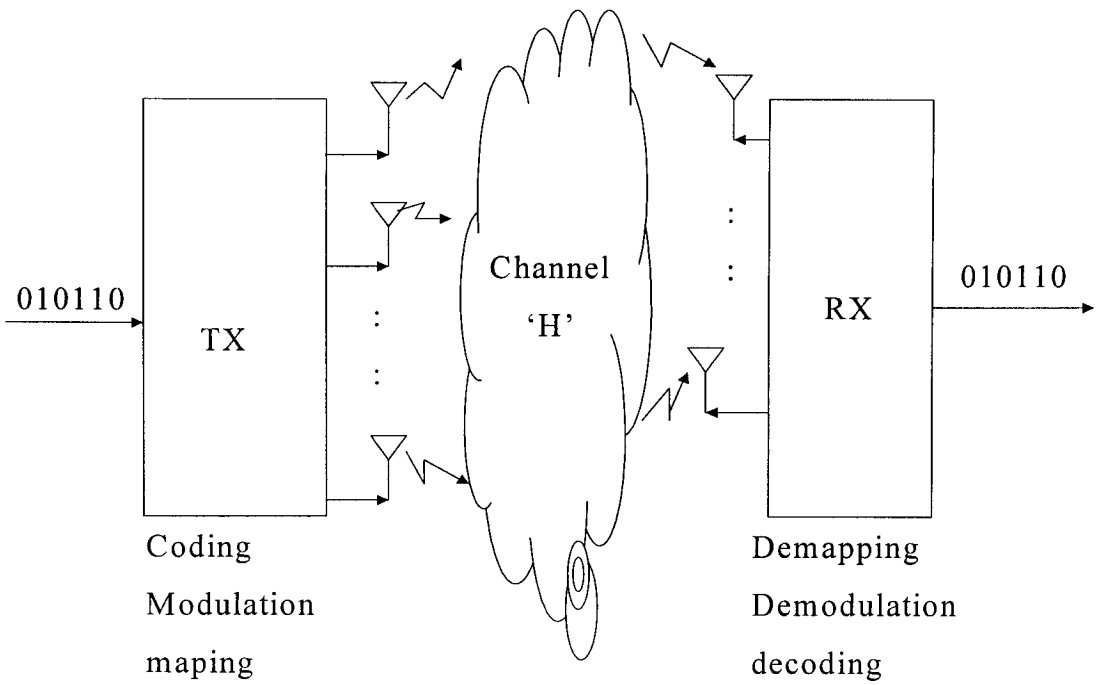

Fig. 1.1 Diagram of a MIMO wireless transmission system.

2.3 The derivation of channel capacity

The basic vector equation describing the channel operating on the signal is

$$r(t) = g(t) \otimes s(t) + v(t), \tag{2.1}$$

where $\otimes$ is for convolution. The other standard notation will be used: $'$ for vector transpose, + for transpose conjugate, *det* and $|\cdot|$ for determinant, $\boldsymbol{I}_n$ for $n \times n$ identity matrix, $E[\cdot]$ for expectation.

As the channel state information is unknown at the transmitter, P_t is distributed equally over the n_T transmitting antennas. The n_T transmitted signal components are taken to be statistically independent Gaussian random variables. The virtue of a Gaussian distribution for the transmitted signal is well established [59], and more details involving matrix channels are given in [60]. Using the narrowband assumption, the convolution can be replaced by product, so that

$$r(t) = g(0) \cdot s(t) + v(t). \tag{2.2}$$

The channel capacity for the transmitted signal vector of n_T statistically independent equal power components, each with a Gaussian distribution is [61-63]

$$C = \log_2[detA_s \cdot detA_r / detA_\mu], \tag{2.3}$$

where

$$A_s = E[ss^+] = \frac{P_t}{n_T} I_{n_T}, \tag{2.4}$$

$$A_r = E[rr^+] = NI_{n_R} + \frac{P_t}{n_T} G \cdot G^+, \tag{2.5}$$

$$A_\mu = E[\mu\mu^+] = \begin{bmatrix} A_s & \frac{P_t}{n_T} G^+ \\ \frac{P_t}{n_T} G & A_r \end{bmatrix}, \tag{2.6}$$

and where μ is the $n_T + n_R$ dimensional vector $(s, r)'$.

According to the following identity [64]

$$det\begin{bmatrix} A & B \\ C & D \end{bmatrix} = det[A] \cdot \det[D - CA^{-1}B], \tag{2.7}$$

which requires that A be nonsingular and while A and D need to be square, they do not need to be of the same size. From (2.7), we have

$$det[A_\mu] = det[A_s] \cdot det[A_r - \frac{P_t}{n_T} G \cdot A_s^{-1} \cdot \frac{P_t}{n_T} G^+]. \tag{2.8}$$

Since $A_s A_s^{-1} = I_{n_T}$, we have $A_s^{-1} = (n_T / P_t) I_{n_T}$. Using this equation and the equation (2.5), (2.8) can be written as

$$\begin{aligned} det[A_\mu] &= det[A_s] \cdot det[A_r - \frac{P_t}{n_T} G \cdot G^+] \\ &= det[A_s] \cdot det[N \cdot I_{n_R}] \end{aligned} . \tag{2.9}$$

Substituting the equations (2.4), (2.5), and (2.9) into (2.3) produces

$$C = \log_2 \{detA_r \cdot det[N^{-1} \cdot I_{n_R}]\} . \tag{2.10}$$

Based on the following relations $detA \cdot detB = det(A \cdot B)$ and $P_t^{1/2} G = P^{1/2} H$, equation (2.10) can be finally written as

$$C = \log_2 det[I_{n_R} + \frac{\rho}{n_T} HH^+], \tag{2.11}$$

which is the convenient formula for generalized capacity.

2.4 Examples of capacity

When n_T =n_R =1, the capacity of (2.11) reduces to

$$C = \log_2 (1 + \rho |H|^2) \text{ bps/Hz}, \tag{2.12}$$

which is the standard formula for the Shannon capacity [65-67] expressed in bps/Hz. H is a complex scalar. It can be seen that, for high *SNR*s, every 3 dB increase in ρ increases capacity by one bps/Hz.

When $n_T = n_R = n$ and $H = I_n$, the capacity of (2.11) becomes

$$C = n\log_2(1+\rho/n) \to \rho/\ln 2 \quad \text{as } n \to \infty. \tag{2.13}$$

In contrast with (2.12), the capacity of (2.13) scales linearly, rather than logarithmically, with an increase of *SNR*. $H = I_n$ means that there are orthogonal parallel channels offered by the multiple antennas at both sites.

It is helpful to consider (2.13) in terms of a specific example of n uncoupled transmission lines ($H = I_n$). If all the power is on one of these lines, the capacity is only $\log_2(1+\rho)$, which is much less than indicated in (2.13). If the power is equally divided between the n lines and n equal rate independent signals are sent, (2.13) can be achieved.

When the channel is the independent and identically distributed (i.i.d.) Rayleigh fading channel, H has i.i.d., complex, zero mean, unit variance entries. With the Monte-Carlo method, capacity ccdfs can be plotted and the outage capacity of (2.11) can be numerically obtained.

2.5 Distribution of capacity

As we mention above, the channel capacity is treated as a random variable. For uncorrelated Rayleigh fading channels, the entries of H are i.i.d. Gaussian random

variables with zero-mean, independent real and imaginary parts having equal variance of 1/2. For correlated Rayleigh fading channels, the elements (H_{lp}) of H are correlated with one other.

We define a $N_{\min} \times N_{\min}$ matrix W as

$$W = \begin{cases} H^{+}H, & n_{\mathrm{R}} > n_{\mathrm{T}} \\ HH^{+}, & n_{\mathrm{R}} \le n_{\mathrm{T}} \end{cases}, \tag{2.14}$$

where $N_{\min}=\min(n_R,n_T)$. W is called Wishart matrix. Let $\underline{\lambda}=[\lambda_1, \cdots,\lambda_{Nmin}]^T$ denote the ordered eigenvalue vector of W, where the superscript T represents the transpose, (2.11) can be rewritten by the singular value decomposition as [9,13,17]

$$C = \sum_{i=1}^{N_{\min}} \log_2(1+\frac{\rho}{n_T}\lambda_i). \tag{2.15}$$

Since W is a positive or positive semidefinite Hermitian matrix, the eigenvalues of W are non-negative. The maximum number of non-zero eigenvalues is $N_{\min}$. For an uncorrelated Rayleigh fading channel, i.e., no correlation between any different H_{lp} and H_{mq}^{*}, where the superscript * represents the complex conjugate, there are $N_{\min}$ positive eigenvalues. For the correlated Rayleigh fading channel, the number of non-zero eigenvalues could be less than $N_{\min}$ because the correlation might reduce the rank of W. In fact, an eigenvalue represents a single-input single-output channel.

We denote Σ_T and Σ_R as the covariance matrices of the rows and columns of H, respectively. Σ_T is the matrix of order $n_T \times n_T$ and its elements are given by $E[H_{lp}H_{lq}^*]$ for $l = 1, \cdots, n_R$, $p = 1, \cdots, n_T$, and $q = 1, \cdots, n_T$, where H_{lp} is the normalized complex path gain from transmitting antenna T_p to receiving antenna R_l. Similarly, $\Sigma_R = E[H_p H_p^+]$ is an $n_R \times n_R$ matrix for $p = 1, \cdots, n_T$ and is the same for any p, whose elements are $E[H_{lp}H_{mp}^*]$ for $l = 1, \cdots, n_R$, and $m = 1, \cdots, n_R$. H_p is the p^{th} column vector of $H = [H_1, H_2, \cdots, H_{n_T}]$

The distribution of the unordered eigenvalues of W for $n_T \geq n_R$ is obtained by [19, 86, 87],

$$p(\underline{\lambda}) = K \cdot {}_0\widetilde{F}_0(\Sigma_T^{-1}, \Lambda, -\Sigma_R^{-1}) \prod_{l=1}^{n_R} \lambda_l^{n_T - n_R} \prod_{l<m}^{n_R} (\lambda_l - \lambda_m)^2 , \tag{2.16}$$

where

$$K = \frac{\det(\Sigma_T)^{-n_R} \det(\Sigma_R)^{-n_T}}{n_R! \prod_{l=1}^{n_R} (n_T - l)! \prod_{l=1}^{n_R} (n_R - l)!},$$

$$\Lambda = diag(\lambda_1, \cdots, \lambda_{n_R}),$$

and ${}_0\widetilde{F}_0(\cdot, \cdot, \cdot)$ is the hypergeometric function of three matrix arguments. This function can be evaluated by a series of expansion of zonal polynomials. However, (2.16) is not tractable with realizable complexity because the zonal polynomials are extremely difficult to compute and the expansion is slow to converge.

When the distance, *dt*, between two adjacent elements in the transmitter is large enough, one would expect that the signal correlation between any two different transmitting elements tend to zero and only the receiver has correlated signals. When $n_T \geq n_R$ so that W is a full rank central Wishart matrix, the joint probability density function (pdf) of the distinctly ordered eigenvalues $\lambda_1 \geq \lambda_2 \geq \cdots \geq \lambda_{n_R}$ of W is [20,68]

$$p(\underline{\lambda}) = K_{\Sigma} \det(\exp(-\lambda_l / \sigma_m)) \cdot \prod_{l=1}^{n_R} \lambda_l^{n_T - n_R} \prod_{l<m}^{n_R} (\lambda_l - \lambda_m) \quad , \tag{2.17}$$

where

$$K_{\Sigma} = \frac{\prod_{l=1}^{n_R} (l-1)! \cdot |\Sigma_R|^{-n_T}}{\prod_{l=1}^{n_R} (n_T - l)! \cdot \prod_{l=1}^{n_R} (n_R - l)! \cdot \prod_{l<m}^{n_R} (\sigma_m^{-1} - \sigma_l^{-1})},$$

$$\exp(\lambda_l / \sigma_m) = \begin{pmatrix} \exp(\lambda_1 / \sigma_1) \cdots\cdots \exp(\lambda_{n_R} / \sigma_1) \\ \vdots \\ \vdots \\ \exp(\lambda_1 / \sigma_{n_R}) \cdots\cdots \exp(\lambda_{n_R} / \sigma_{n_R}) \end{pmatrix},$$

and $\sigma = [\sigma_1, \sigma_2, \cdots, \sigma_{n_R}]$, with $\sigma_1 \geq \sigma_2 \geq \cdots \geq \sigma_{n_R} \geq 0$, is the distinctly ordered eigenvalues of Σ_R. Then, the pdf of capacity can be obtained by

$$p_C(x) = \int_{-\infty}^{\infty} \phi_C(z) \exp(-j2\pi xz) dz \quad , \tag{2.18}$$

where

$$\phi_C(z) = K_\Sigma \cdot \det G_{n_R} \tag{2.19}$$

is the characteristic function of capacity derived in terms of (2.17) by [20] and G_{n_R} is an $n_R \times n_R$ matrix with lm^{th} elements [eq. 30, 20]

$$g_{l,m}(z) = \int_0^\infty x^{n_T - n_R + m - 1} \cdot \exp(-x/\sigma_l) \cdot (1 + \rho\, x/n_T)^{j2\pi z/\ln 2}\, dx\,.$$

So, cdf or ccdf of capacity is given analytically by (2.18).

When $n_T < n_R$, W is singular and no distribution for W exists.

Chapter 3 Optimization of antenna number in the capacity of MIMO systems

3.1 Introduction

A multiple-input multiple-output (MIMO) system has multiple antennas at both the transmitter and the receiver. Using multiple antennas at both locations makes it possible to form multiple channels and therefore to increase channel capacity significantly. This phenomenon was first recognized by simulation studies in the late 1980 [9], and has received wide attention mainly with the analytical results given in references [10,12, 69]. The analytical results of reference [10] show that the channel capacity increases linearly with the number of antenna elements under the assumptions that the multiple channels are independent and the fading is frequency flat. After this breakthrough, interest in MIMO systems has exploded. Space-time codes developed for these systems have come close to achieving channel capacity [46]. If, as in some practical systems, the scattering environment is not rich, the multiple channels correlate with one another and capacity is reduced. Ways to reduce correlation in actual deployments have been studied [7, 70]. Measurements of the statistical and correlative properties of the multiple channels have been carried out [37], and commercial products are under development [71].

The transmitter and receiver use multiple antennas, thus a pertinent question is how they should be deployed in order to achieve greater capacity, i.e. more antennas at the transmitter or at the receiver? Secondly, how many antennas should be reasonably used in

both transmitter and receiver for the channel capacities to reach their saturation level, i.e., the point of diminishing returns for different situation of multiple antennas?

To address the above questions, we explore the case of when the channel characteristics are only known at the receiver. If the channel is known at the transmitter, relevant discussions can be found in references [13, 72]. Section 3.3 contains results showing that more diversity can be achieved by putting more antenna elements in the receiver than the reverse. In Section 3.4, simulation results are given to illustrate the number of antenna elements required to reach the saturation level of the capacity for different signal-to noise ratios (*SNR*s).

3.2 Mathematical model for MIMO channels

In order to simplify the presentation, we will discuss and obtain primary results, using the same mathematical model as we have presented in chapter 2. We assume n_T transmit antennas and n_R receive antennas. The channel between transmit antennas and receive antennas is single point-to-point, and is assumed to be quasi-static Rayleigh flat fading, i.e. the channel is fixed during a burst and changes randomly from burst to burst. A complex baseband model involving a fixed linear matrix channel with additive white Gaussian noise is used.

3.3 Higher capacity with more receive antennas

The capacity of a MIMO wireless system with n_T transmit antennas and n_R receive antennas with an average received *SNR* ρ (independent of n_T) at each receive antenna has been presented in Chapter 2 as

$$C = \log_2 \det[I_{n_R} + (\rho / n_T) HH^+] \; bps / Hz, \tag{3.1}$$

where det denotes determinant, I_{n_R} is the $n_R \times n_R$ identity matrix, ρ is the average signal-to-noise ratio (*SNR*) per receiving antenna, H is the normalized channel transfer matrix with n_R rows and n_T columns, and + indicates transpose conjugate. In denoting a system we use the shorthand (n_T, n_R).

Since the channel is the Rayleigh channel model, the entry H_{lk} (l=1,2,···, n_R, k=1,2,···, n_T) in H is expressed as $H_{lk} = Normal(0,1/\sqrt{2}) + jNormal(0,1/\sqrt{2})$ for any l and k. It follows that the capacity expressed by Eq. 3.1 is a random variable. The measure of the capacity that is the basis of comparisons is the complementary cumulative distribution function (ccdf) of the capacity. In this section, we show that, channel capacity for a configuration in which $n_T < n_R$ is larger than that of its inverse ($n_T > n_R$). We proceed from the simple case to more general cases.

3.3.1 *Single Antenna Configurations*

The first step of the study is a comparison of receive diversity (1, n) with that of transmit diversity (n, 1).

For (1, n), the capacity C_R can be written directly from (3.1) as

$$C_R = \log_2(1+\rho\chi^2_{2n}), \tag{3.2}$$

where χ^2_{2n} is a Chi-squared random variable (RV) with $2n$ degrees of freedom. As in Chapter 2, we set a threshold percentage of 90% for the ccdf, i.e., channels are less than the specified capacity only 10% of the time. From the distribution of χ^2_{2n}, we can determine the distribution of C_R. From the distribution of C_R, we obtain the ccdf of C_R

$$F_{cR}(C_R > z) = \exp[-\tfrac{1}{\rho}(2^z-1)]\cdot\sum_{i=0}^{n-1}\tfrac{(2^z-1)^i}{\rho^i\, i!} \tag{3.3}$$

Similarly, for (n,1), the capacity of C_T and its 90% ccdf are respectively,

$$C_T = \log_2[1+(\rho/n)\chi^2_{2n}], \tag{3.4}$$

and

$$F_{cT}(C_T > z) = \exp[-\tfrac{1}{(\rho/n)}(2^z-1)]\cdot\sum_{i=0}^{n-1}\tfrac{(2^z-1)^i}{(\rho/n)^i\, i!}. \tag{3.5}$$

As one would expect, the capacity expressions are the same in both cases when n_T=n_R=1, i.e., n=1 in Eqs. 3.2-3.4. Also, notice that, when n=1, Eqs. 3.2 and 3.4 are simply the standard formula for the Shannon capacity [65, 67] expressed in *bps/Hz*. Of course, we still have the random element due to the fading channel,

$$C_1 = \log_2(1+\rho\chi_2^2), \tag{3.6}$$

and

$$F_{c1}(C_1 > z) = \exp[-\tfrac{1}{\rho}(2^z - 1)]. \tag{3.7}$$

From Eqs. 3.2-3.7, we can make several observations:

A. As expected, the capacity increases with the *SNR* in both cases of (1, *n*) and (*n*,1). That is because their ccdfs increase with the *SNR*. A simple proof for Eq. 3.3 is: $dF_{cR}(C_R > z)/d\rho = \exp[-(2^z-1)/\rho](2^z-1)^n/[\rho^{n+1}(n-1)!] > 0$. Similarly, the proof for Eq. 3.4 is the same with the simple substitution $\rho_{eff} = \rho/n$. In Fig. 3.1, which draws curves of the ccdfs of Eqs. 3.3, 3.5 and 3.7, it can be seen that the capacities of (2, 1) and (1,2) with a *SNR* of 9 dB are greater than these with a *SNR* of 3 dB.

B. A comparison of Eqs. 3.3 and 3.5 shows that the capacity of (1, *n*) is always greater than that of (*n*,1) for the same value of ρ. Since the capacity increases with the *SNR*, if we treat ρ/n as an effective *SNR*, the effective *SNR* in F_{cT} is *n* times less than the *SNR* of ρ in F_{cR}. In Fig. 2, the capacity of (1,2) is greater than that of (2,1) as shown by square dotted lines and circle dotted lines, respectively.

C. Capacity increases as the number of receiving antennas increases. This follows from the fact that the sum in Eq. 3.3, for F_{cR}, is always greater than or equal to 1 and increases with *n*.

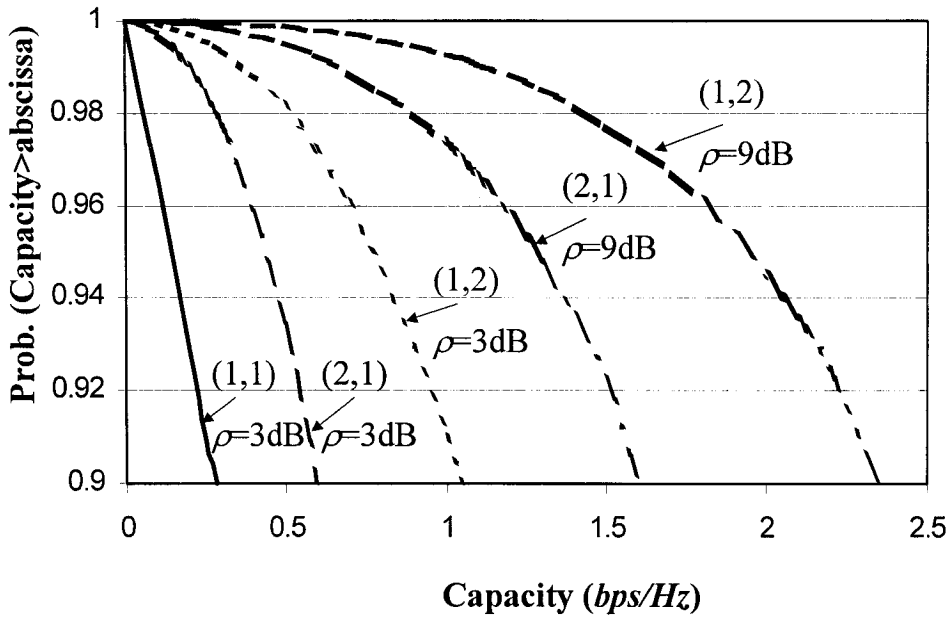

Fig. 3.1 Capacity increases with signal-to-noise ratio.

3.3.2 *Two antenna configurations*

Let's compare the capacity values of the (n, 2) case with its inverse, the (2, n) case. It is noted that in both cases the channel matrices consist of $2n$ independent variables $(H_{11}, H_{12}, ...H_{n2})$ and $(H_{11}, H_{12}, ...H_{2n})$, respectively. In either case, we have $2n$ Gaussian RV's having identical mean zero and variance ½. We denote C_{2n} and $D_{nn,2}$ as the capacity and determinant in Eq. 3.1 for (2, n), respectively, and C_{n2} and $D_{22,n}$ for the capacity and determinant in Eq. 3.1 for (n, 2), respectively. As it is shown in Appendix A, the determinant $D_{nn,2}$ in Eq. 3.1 for (2, n) has the same form as a function of these

variables as $D_{22,n}$ for (n, 2). Because $C_{2n} = \log_2 D_{nn,2}$ and $C_{n2} = \log_2 D_{22,n}$, C_{2n} has the same form as C_{n2}.

For (2, n), we have from Eq. 3.1 (see Appendix A)

$$C_{2n} = \log_2[1 + \sum_{i=1}^{n}\sum_{j=1}^{2}\left|\overline{H}_{ij}\right|^2 + \sum_{i=1}^{\binom{n}{2}}\left|\overline{H}_{Mi,2}\right|^2] = S_{nn,2}(\overline{H}_{11}, \overline{H}_{12},..., \overline{H}_{n2}) \quad , (3.8)$$

where $\overline{H}_{ij} = \sqrt{\alpha_{n2}} H_{ij}$ (i=1,…,n, j=1,2) with $\alpha_{n2}=\rho/2$, $|a| = (a \cdot a^+)^{1/2}$ represents the norm of a vector a, $\overline{H}_{Mi,2}$ is i^{th} major determinant[1] of the matrix H of order (n,2), and $\binom{n}{2} = n!/2!(n-2)!$ is simply the number of ways that major determinants of order (2, 2) can be formed from a matrix of order (n, 2) by eliminating rows. Since the components of the channel matrix are Gaussian RV's, we may write $\overline{H}_{ij} = x_{ij} + jy_{ij}$, x_{ij} and y_{ij} are Gaussian random variables with mean zero and variance of $0.5\alpha_{n2}$. Thus, $S_{nn,2}(\overline{H}_{11}, \overline{H}_{12},..., \overline{H}_{n2}) = S_{nn,2}(x_{11}, y_{11},..., x_{n2}, y_{n2})$. The cumulative distribution function (cdf) of C_{2n} is

$$P(C_{2n} < z) = P[S_{nn,2}(x_{11}, y_{11}, \cdots, x_{n2}, y_{n2}) < z] = \int\cdots\int_{S_{nn,2}(x_{11}, y_{11}, \cdots x_{n2}, y_{n2}) < z} f(x_{11}, y_{11}, \cdots x_{n2}, y_{n2}) dx_{11} \cdots dy_{n2}$$

(3.9)

[1] See Chapter two of Ref.73 or Appendix A

where $f(x_{11},y_{11},\cdots x_{n2},y_{n2})$ is the joint probability density function of $x_{11},y_{11},\cdots,x_{n2},y_{n2}$. Because $x_{11},y_{11},\cdots,x_{n2},y_{n2}$ are independent Gaussian RV's, $f(x_{11},y_{11},\cdots,x_{n2},y_{n2})$ can be written as the product of margin probability density functions of these variables

$$f(x_{11},y_{11},\cdots x_{n2},y_{n2}) = f(x_{11})f(y_{11})\cdots f(x_{n2})f(y_{n2})$$

where

$$f(w_{ij}) = \frac{1}{\sqrt{\pi\alpha_{n2}}}\exp(-\frac{w_{ij}^2}{\alpha_{n2}}) \ , \ w_{ij}=x_{ij},y_{ij}, \ i=1,2\ldots,n; j=1,2. \tag{3.10}$$

It can be seen that $f(x_{11},y_{11},\cdots,x_{n2},y_{n2})$ is circularly symmetrical on $x_{11},y_{11},\cdots,x_{n2},y_{n2}$ and is centered at zero.

For $(n, 2)$, the capacity is (see Appendix A)

$$C_{n2} = \log_2[1+\sum_{i=1}^{2}\sum_{j=1}^{n}\left|\overline{H}_{ij}\right|^2 + \sum_{i=1}^{\binom{n}{2}}\left|\overline{H}_{Mi,n}\right|^2 = S_{22,n}(\overline{H}_{11},\overline{H}_{12},...,\overline{H}_{2n}), \tag{3.11}$$

where $\overline{H}_{ij} = \sqrt{\alpha_{2n}}H_{ij}$ (i=1,2, j=1,2,…,n) with $\alpha_{2n}=\rho/n$ and $\overline{H}_{Mi,n}$ is i^{th} major determinant of the matrix H of order $(2, n)^2$. It is seen that $S_{22,n}(\overline{H}_{11},\overline{H}_{12},...,\overline{H}_{2n})$ is equivalent to

---

[2] In this case, $\binom{n}{2}$ is the number of major determinants of order (2, 2) that can be derived from a matrix of order (2, n) by eliminating columns.

$S_{nn,2}(\overline{H}_{11}, \overline{H}_{12},..., \overline{H}_{n2})$ except for the variable subscripts. If we set $\overline{H}_{ij} = u_{ij} + jv_{ij}$, then u_{ij} and v_{ij} are Gaussian random variables with mean zero and variance of $0.5\alpha_{2n}$; accordingly, $S_{22,n}(\overline{H}_{11}, \overline{H}_{12},..., \overline{H}_{2n}) = S_{22,n}(u_{11}, v_{11},..., u_{2n}, v_{2n})$. The cdf of C_{n2} is

$$P(C_{n2} < z) = P[S_{22,n}(u_{11}, v_{11},\cdots u_{2n}, v_{2n}) < z] = \int\cdots\int_{S_{22,n}(u_{11}, v_{11},\cdots u_{2n}, v_{2n})<z} g(u_{11}, v_{11},\cdots u_{2n}, v_{2n}) du_{11}\cdots dv_{2n} \tag{3.12}$$

where $g(u_{11},v_{11},\cdots u_{2n},v_{2n})$ is the joint probability density function of $u_{11},v_{11},\cdots u_{2n},v_{2n}$. As u_{11}, $v_{11},\cdots u_{2n},v_{2n}$ are independent Gaussian RVs, $g(u_{11},v_{11},\cdots u_{2n},v_{2n})$ can be rewritten as

$$g(u_{11}, v_{11},\cdots u_{2n}, v_{2n}) = g(u_{11})g(v_{11})\cdots g(u_{2n})g(v_{2n})$$

where

$$g(w_{ij}) = \frac{1}{\sqrt{\pi\alpha_{2n}}}\exp(-\frac{w_{ij}^2}{\alpha_{2n}}) \ , \ w_{ij}=u_{ij},v_{ij};\ i=1,2;j=1,2\ldots,n. \tag{3.13}$$

$g(u_{11},v_{11},\cdots u_{2n},v_{2n})$ is also circularly symmetrical on $u_{11},v_{11},\cdots, u_{2n},v_{2n}$ and centered at zero. Since $S_{nn,2}(x_{11}, y_{11},..., x_{n2}, y_{n2})$ and $S_{22,n}(u_{11}, v_{12},..., u_{2n}, v_{2n})$ have the same expression, the integration regions defined by $S_{nn,2}(x_{11}, y_{11},..., x_{n2}, y_{n2}) < z$ and $S_{22,n}(u_{11}, v_{12},..., u_{2n}, v_{2n}) < z$ are exactly the same. On the other hand, both $f(x_{11},y_{11},\cdots x_{n2},y_{n2})$ and $g(u_{11},v_{11},\cdots u_{2n},v_{2n})$ are joint probability densities of independent Gaussian

variables having identical mean values (zero) but different variances ($0.5\alpha_{n2}$ or $0.5\alpha_{2n}$), respectively. Since $\rho/2 > \rho/n$ for n>2, the variance, $0.5\alpha_{n2}$, of $f(x_{11},y_{11},\cdots x_{n2},y_{n2})$ is larger than the variance, $0.5\alpha_{2n}$, of $g(u_{11},v_{11},\cdots u_{2n},v_{2n})$.

The implications of this in the two dimensional case, i.e., for example, in the cross-sections of $f(x_{11},0,...,0) \sim x_{11}$ or $g(u_{11},0,...,0) \sim u_{11}$ planes, is that the region of the integration defined by $S_{nn,2}(x_{11},0,...,0,0) < z$ or $S_{22,n}(u_{11},0,...,0,0) < z$ become $|x_{11}| < (2^z - 1)^{1/2}$ or $|u_{11}| < (2^z - 1)^{1/2}$. As a result, Eqs. 3.9 and 3.12 become, respectively,

$$P(C_{2n} < z)\Big|_{x_{11}} = \int_{|x_{11}|<\sqrt{2^z-1}} \frac{1}{\sqrt{\pi\alpha_{n2}}} \exp(-\frac{x_{11}^2}{\alpha_{n2}}) dx_{11}, \qquad (3.14)$$

and

$$P(C_{n2} < z)\Big|_{u_{11}} = \int_{|u_{11}|<\sqrt{2^z-1}} \frac{1}{\sqrt{\pi\alpha_{2n}}} \exp(-\frac{u_{11}^2}{\alpha_{2n}}) du_{11}. \qquad (3.15)$$

Clearly, the relative values of the integrals in (3.14) and (3.15) depend only upon the variances. Since $\alpha_{n2} > \alpha_{2n}$, it follows directly that $P(C_{2n} < z)\Big|_{x_{11}} < P(C_{n2} < z)\Big|_{u_{11}}$.

This two dimensional result carries over to the multi-dimensional situation where two circularly symmetrical Gaussian distributions $f(x_{11},y_{11},\cdots,x_{n2},y_{n2})$ and $g(u_{11},v_{11},\cdots,u_{2n},v_{2n})$ have the same mean value but different variances and are integrated over a same region defined by $S_{nn,2}(x_{11},y_{11},...,x_{n2},y_{2n}) < z$ or

$S_{22,n}(x_{11}, y_{11},..., x_{2n}, y_{2n}) < z$, i.e. , $P(C_{2n} < z) < P(C_{n2} < z)$. Therefore, the ccdf of C_{2n}, which is $F_{2n}(C_{2n} > z) = 1 - P(C_{2n} < z)$, is larger than the ccdf of C_{n2}, which is $F_{n2}(C_{n2} > z) = 1 - P(C_{n2} < z)$; consequently, the average capacity for receiver diversity is higher.

3.3.3 *Limiting Cases for Large Numbers of Antennas*

The next step is to compare the capacity values of (*m*, *m*+*n*) case with that of its inverse case of (*m*+*n*, *m*) when *n* is a large number.

Because of the property of the determinant that exactly one element from each row and one element from each column appears in each term of the expansion of the determinant, for (*m*+*n*, *m*), Eq. 3.1 can be expressed directly as

$$C_{Tm+n} = \log_2\{1 + [\rho/(m+n)]\chi^2_{2m(m+n)} + [\rho/(m+n)]^2 G_2 + \cdots + [\rho/(m+n)]^m G_m\}, \quad (3.16)$$

where $G_2, \cdots, G_m$ are functions of H_{lk} and H_{qp}^*, l, q=1,2,…,m; k, p=1,2,…,m+n (The complex conjugate is denoted by superscript *.) When *n* becomes large, the third and higher terms in the bracket of (3.16) will become negligible; consequently, we have

$$C_{Tm+n} = \log_2\{1 + [\rho/(m+n)]\chi^2_{2m(m+n)}\}, \quad (3.17)$$

whose ccdf is obtained as before

$$F_{cTm+n}(C_{Tm+n} > z) = \exp[-\tfrac{1}{[\rho/(m+n)]}(2^z - 1)] \cdot \sum_{i=0}^{m(m+n)-1} \tfrac{(2^z-1)^i}{[\rho/m+n)]^i\, i!}. \quad (3.18)$$

For (m, $m+n$), Eq. 3.1 is shown in Appendix B to be

$$C_{Rm+n} = \log_2[1+(\rho/m)\chi^2_{2m(m+n)} + P], \quad (3.19)$$

where P is a positive term for any m and $m+n$. If we denote

$$C'_{Rm+n} = \log_2[1+(\rho/m)\chi^2_{2m(m+n)}], \quad (3.20)$$

then we have C_{Rm+n}>C'_{Rm+n} because P is positive. Similarly, the ccdf of C'_{Rn} is

$$F_{cRm+n}(C'_{Rm+n} > z) = \exp[-\tfrac{1}{(\rho/m)}(2^z - 1)] \cdot \sum_{i=0}^{m(m+n)-1} \tfrac{(2^z-1)^i}{(\rho/m)^i\, i!}. \quad (3.21)$$

If we denote an effective *SNR* as $\rho' = \rho/(m+n)$ and another *SNR* as $\rho'' = \rho/m$, it is obvious that $\rho'' > \rho'$ when ρ is the same for both and n is a large number. Moreover, Eqs. 3.18 and 3.21 have the same form, which is similar to Eq. 3.3, in terms of effective *SNR*s. As it has been shown for Eq. 3.3, both ccdfs of Eqs. 3.18 and 3.21 increase with their effective *SNR*s, respectively. Thus, for Eqs. 3.18 and 3.21, the larger *SNR* has larger

capacity. Since $\rho'' > \rho'$, we have $F_{cRm+n} > F_{cTm+n}$ with a same z, which means $C'_{Rm+n} > C_{Tm+n}$, and consequently $C_{Rm+n} > C_{Tm+n}$.

3.3.4 *General case of arbitrary n_T and n_R*

Finally, we compare the capacity when $n_T = N_1$, $n_R = N_2$ with the capacity when $n_T = N_2$, $n_R = N_1$. To begin with, we first cite the duality theorem: The capacity of MIMO systems with $n_T = N_1$, $n_R = N_2$, operating at $\rho = \rho_1$ in a Rayleigh fading environment with correlation among the transmitting antennas, characterized by correlation matrix Σ for the rows of the channel matrix H, is equal to the capacity of MIMO systems with $n_T = N_2$, $n_R = N_1$, operating at $\rho = \rho_1 N_2 / N_1$ in a Rayleigh fading environment with correlation among the receiving antennas, characterized by the correlation matrix Σ for the columns of the channel matrix H [20,74]. The theorem can be readily shown with the fact that HH^+ and H^+H have the same nonzero eigenvalues [74]. For the i.i.d. Rayleigh fading case, the correlation among the transmitting antennas is the same as the correlation among the receiving antennas. So, we extend the duality theorem to the i.i.d. Rayleigh fading environment as follows: The capacity of MIMO systems with $n_T = N_1$, $n_R = N_2$, operating at $\rho = \rho_1$, is equal to the capacity of MIMO systems with $n_T = N_2$, $n_R = N_1$, operating at $\rho = \rho_1 N_2 / N_1$.

Secondly, we use the equation of (2.15)

$$C = \sum_{i=1}^{N_{\min}} \log_2(1 + \frac{\rho}{n_T}\lambda_i). \tag{3.32}$$

For the i.i.d. Rayleigh fading case, the Wishart matrix is a positive definite matrix of order ($N_{\min}$, $N_{\min}$) because every entry of H is an i.i.d. complex Gaussian random variable. So, every eigenvalue λ_i is positive. By differentiating (3.32) over ρ as follows

$$\frac{dC}{d\rho} = \sum_{i=1}^{N_{\min}} \frac{1}{\ln 2} \frac{\lambda_i / n_T}{1 + (\rho / n_T)\lambda_i} > 0, \tag{3.33}$$

we can see that the capacity increases with ρ. With the duality theorem and the fact that the capacity increases with ρ, we can formulate a diversity theorem: The capacity of MIMO systems with $n_T = N_2$, $n_R = N_1$, , operating at ρ in an i.i.d. Rayleigh fading environment, is greater than the capacity of MIMO systems with $n_T = N_1$, $n_R = N_2$ operating at the same ρ in an i.i.d. Rayleigh fading environment, when $N_1 > N_2$.

The illustration of the phenomenon of greater receiver diversity gaining more capacity using the Monte-Carlo simulation is shown in Fig. 3.2. In this simulation, we randomly sample an H, and calculate a corresponding RV capacity of C in terms of Eq. 3.1. We set a total sample number of 10000 and a certain quantity of z. We count the number of $C>z$ among the total sample number and calculate the probability ($C>z$) by dividing the number of $C>z$ over the total sample number. As the threshold percentage of 90% is set for the ccdf, the outage capacity can be read out from the ccdf. Fig. 3.2 shows the difference between pairs of $C_{nT=m,nR=m+1}$ and $C_{nT=m+1,nR=m}$, $C_{nT=m,nR=m+2}$ and $C_{nT=m+2,nR=m}$,,

and $C_{nT=m,nR=m+3}$ and $C_{nT=m+3,nR=m}$, where m=1,2,…,7. It can be seen that the capacity of n_T=m, n_R=m+1 is always greater than that of n_T=m+1, n_R=m no matter how large m is. Moreover, the capacity with n_T=m, n_R=m+1 is even greater than that with n_T=m+2, n_R=m. When the difference between transmit antennas and receive antennas increases from one to two, i.e., n_T=m, n_R=m+2, or n_T=m, n_R=m+2, the difference of the capacity continues to increase. When the difference between transmit antennas and receive antennas increases from one to three, that is n_T=m, n_R=m+3 or n_T=m, n_R=m+3, the difference of the capacity increases even more.

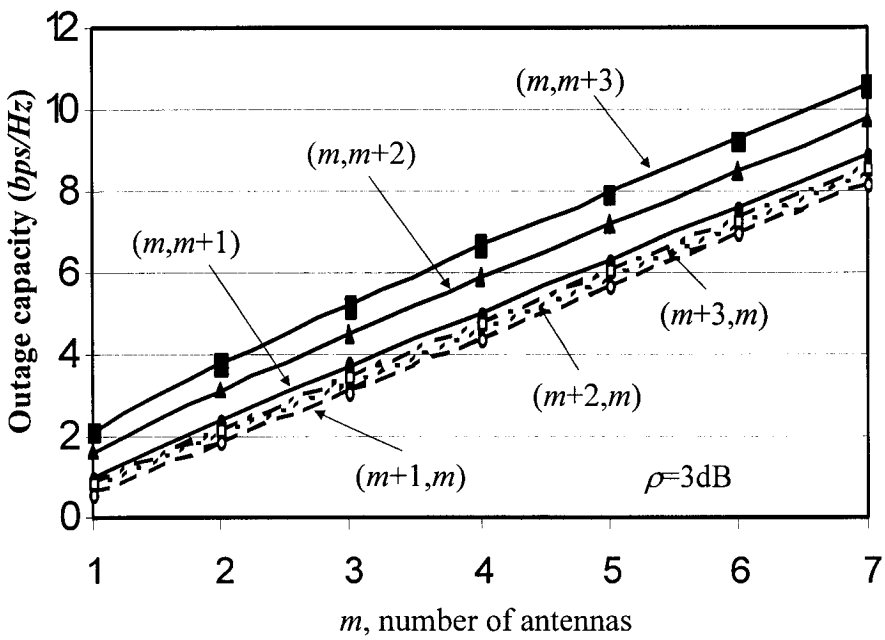

Fig. 3.2 Comparison of the transmit diversity with the receive diversity.

3.4 Number of antennas for capacity saturation

In order to investigate the capacity increase with the number of antenna elements, we use the Monte-Carlo method to compute the capacity ccdfs. From the ccdf graph with a certain outage probability, the outage capacity can be read out. Setting an outage probability of 10%, the capacity is computed in figures 3.3-3.8 with different *SNR*s.

In Fig. 3.3, n_T=1 and n_R varies from 1 to 16. For any of the values of *SNR* considered, four receive antennas can achieve about two thirds of the highest capacity, which we take to be the capacity with 16 antennas. When n_T=2 as shown in Fig. 3.4, five receive antennas are needed to obtain two thirds of the highest capacity. When n_T=3, almost 6 antennas are needed to obtain the same amount of the highest capacity as seen in Fig. 3.5.

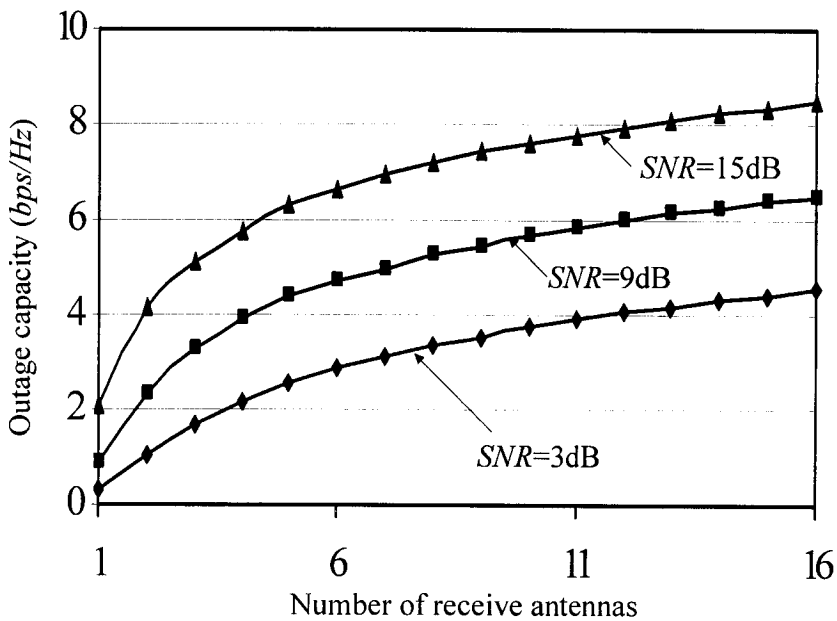

Fig. 3.3 The capacity increases with the number of receive antennas for n_T=1.

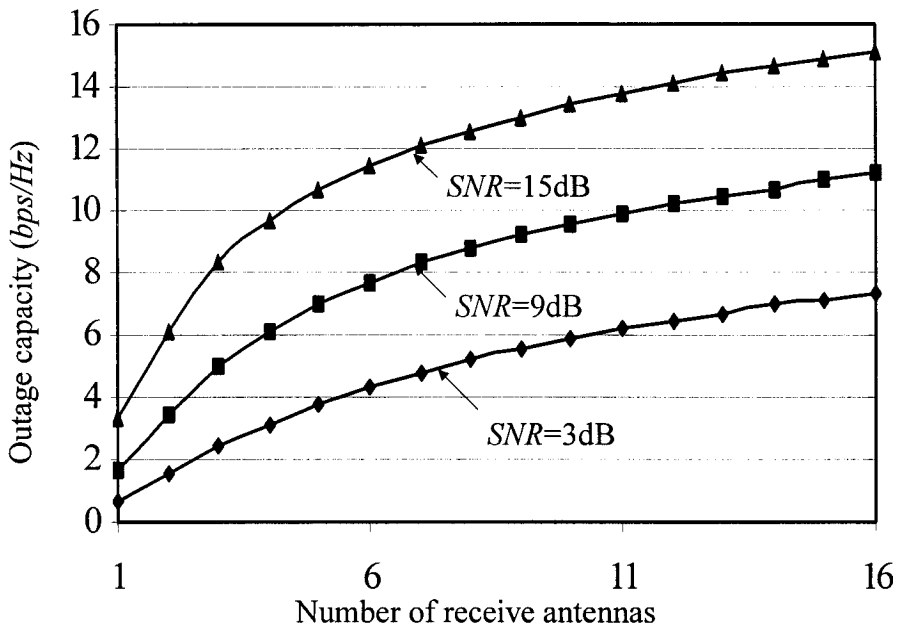

Fig. 3.4 The capacity increases with the number of receive antennas for n_T=2.

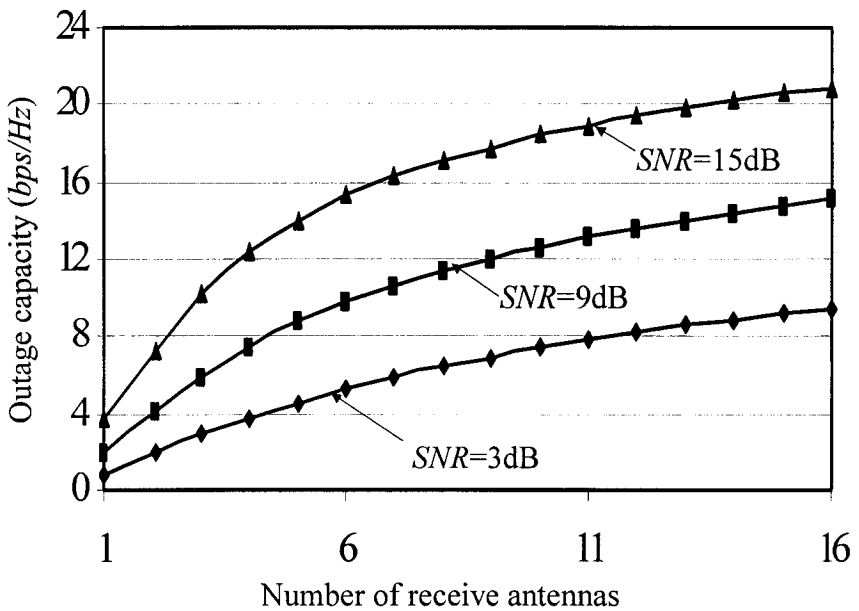

Fig. 3.5 The capacity increases with the number of receive antennas for n_T=3.

In contrast to above, we fix the receive antennas and increase the transmit antennas. In this case, it can be clearly seen from Figs. 3.6, 3.7 and 3.8 that four transmit antennas can achieve almost 90% of their highest capacity with 10 antennas, respectively, for fixed received antennas increasing from one to three. Moreover, it can seen that the highest capacity for the fixed number of the receive antennas is much lower than that for the fixed number of the transmit antennas if comparing Fig. 3.3 with Fig. 3.6, Fig. 3.4 with Fig. 3.7 and Fig. 3.5 with Fig. 3.8, respectively. This illustrates the receive diversity can gain higher capacity than the transmit diversity. These curves with fixed receive antennas, Figs. 3.6-3.8, are very flat, which demonstrates increase of the transmit antennas after four antennas does not give substantial diversity. In contrast, these curves with fixed transmit antennas, Figs. 3.3-3.5, are not flat, which means increase of the receive antennas can still gain some minor diversity.

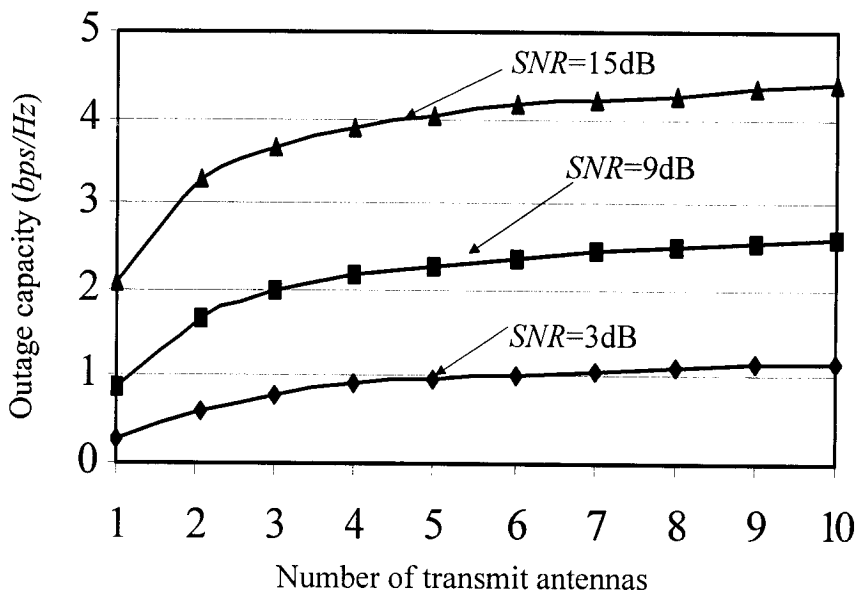

Fig. 3.6 The capacity increases with the number of transmit antennas for n_R=1.

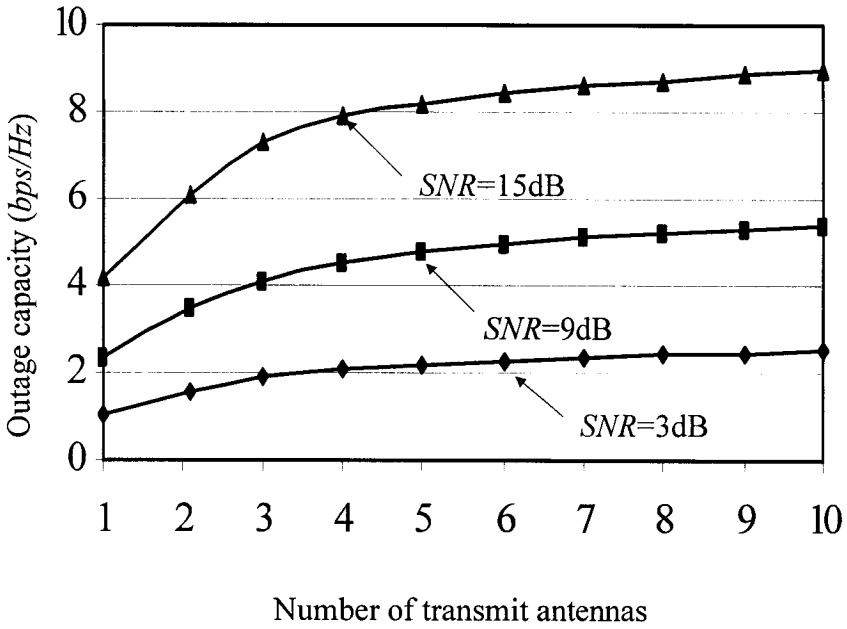

Fig. 3.7 The capacity increases with the number of transmit antennas for n_R=2.

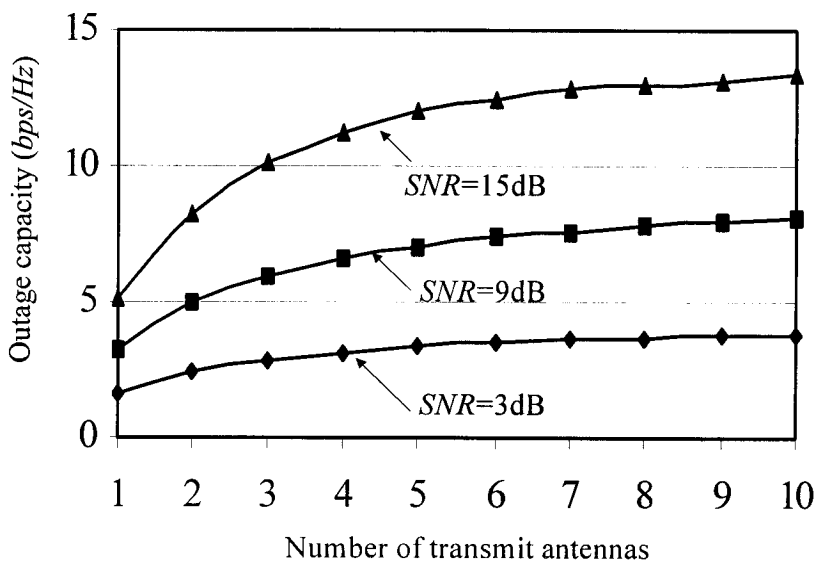

Fig. 3.8 The capacity increases with the number of transmit antennas for n_R=3.

3.5 Summary and conclusions

In this chapter of the thesis, we have studied the problem of optimizing antenna number with respect to channel capacity. We have analyzed four cases. In the first case, we have compared the capacity for one transmit antenna and n receive antennas with that for n transmit antennas and one receive antenna. In the second case, we have compared the capacity for two transmit antennas and n receive antennas with that for n transmit antennas and two receive antennas. In the third case, we have compared the capacity for a large number $m+n$ transmit antennas and m receive antennas with that for m transmit antennas and the large number $m+n$ receive antennas when n is a large number. In the fourth case, we have generalized the above three cases, comparing the capacity of arbitrary $n_T=N_1$ and $n_R=N_2$ with that of $n_T=N_2$ and $n_R=N_1$ when they have the same *SNR* based on the fundamental capacity formula. The analytical results of the four cases have shown that putting more antennas at the receiver gives more diversity, and consequently larger capacity. For other cases, we have demonstrated the same conclusion through simulation results. The physical explanation for this phenomenon should be: increasing the antennas at the transmitter increases the diversity, but reduce the effective *SNR* of ρ / n_T at the receiver at the same time because the signal power at the transmitter is fixed. In contrast to transmit diversity, increasing the antennas at the receiver increases the diversity without reducing the effective *SNR*. In summation, increasing the diversity by putting more antennas at the receiver is better than that putting more antennas at the transmitter.

When we fix the transmit antennas and increase the receive antennas, the number of receive antennas for capacity saturation goes up with the number of the fixed transmit antennas. For example, when the transmit antenna is fixed at one, Fig. 4, the number of the receive antennas achieving 2/3 of the maximum capacity with 16 receive antennas is about four. When the transmit antennas are fixed at two, Fig. 5, the number of the receive antennas achieving 2/3 of the maximum capacity with 16 receiver antennas is about five. However, When we fixed the receive antennas at one, two and three and increased the transmit antennas, the number of transmit antennas for capacity saturation is always almost four. This phenomenon is related to the first phenomenon as we discussed above. The capacity changes slowly with the increase of the transmit antennas. The diversity increased by the increase of the transmit antennas is partly compensated by the reduction of the effective *SNR* at the receiver. Therefore, four transmit antennas achieves almost 90% of the maximum capacity with 16 transmit antennas for all cases of the fixed receive antennas. On the other hand, the capacity changes fast with the increase of the receive antennas. Therefore, six receive antennas are required to reach the point of capacity diminishing return for small number of transmit antennas.

Chapter 4 Correlation and capacity analyses with a spherical model

4.1 Introduction

A multi-input multi-output (MIMO) system employs n_T antenna elements at the transmitter and n_R antennas at the receiver. The signals propagating through the wireless channel experience multi-path fades. Under the assumption that the transmitter does not know the channel but the receiver does, if the fades between pairs of transmit-receive antenna elements are i.i.d. Rayleigh random variables, the average channel capacity grows linearly with $N_{\min}=\min(n_T, n_R)$ as $N_{\min}$ approaches infinity for a given fixed average transmitter power [10,75]. If the fades are correlated, the channel capacity can be significantly smaller than the case of i.i.d. fades [30, 17, 20, 40]. The fading correlation is caused by the interaction of the scattering environment and the properties of antenna physics such as the antenna field pattern, antenna spacing, antenna orientation, and antenna array arrangement. In practice, correlation has to be taken into account since antenna elements in small mobile terminals have to be closely spaced in order to achieve small size and low cost.

To study the attainable capacity of MIMO systems under correlated fading propagation, a closed-form expression for the characteristic function of MIMO system capacity with arbitrary correlation among the transmitting antennas or among the receiving antennas has been derived for frequency-flat Rayleigh-fading environments [20]. Several experiments have been made to investigate the capacities [37], the relation of correlation with the distance between the transmitter and the receiver [40], and effects of different patterns and polarizations on capacities [41,42].

However, on one hand, the analytical expression of [20] itself cannot be used to calculate capacity without established correlation models. On the other hand, carrying out experiments is expensive, time-consuming, and applicable to particular environments. Between analytical and experimental approaches, there is a third technical approach: the construction of an abstract scattering model in order to provide a reasonable description of the scattering environments for the wireless application of interest. This is a simple, intuitive approach to obtain the essential characteristics of the channel. Reference [17] used the "one-ring" model [1] to model the multi-path propagation and the fading correlation. The "one-ring" model is appropriate in a fixed wireless communication context and can be used to determine the spatial fading correlation of a narrow-band fading channel from the physical parameters of the model such as antenna spacing, antenna arrangement, angle spread, and angle of arrival. Later, Abdi et al [18] extended the "one-ring" model to take into account space-time correlation. Byers et al [19] extended the "one-ring" model to a "two-ring" model so that scatterers are not only around the receiver but also around the transmitter. Furthermore, a vector geometrical scattering model is extended to study multipolarized transmissions [76]. However, since these models of [17, 18, 19, 76] are two-dimensional models, three dimensional antenna patterns and orientations cannot be taken into account.

The goal of our work is to extend the "one-ring" model of [17] to a three dimensional scattering environment in order to investigate the effects of the antenna field pattern and the antenna orientation on the fading correlation and consequently on the MIMO capacity. We use this model to determine, first, the fading correlation and then the channel transfer matrix of the point-to-point narrow-band communication system with additive Gaussian noise without co-channel (multi-user)

interference. We investigate the information-theoretic channel capacity as a function of the spatial fading correlation. It is noted that realistic three dimensional models have been used to understand spatial correlation [77, 78, 79] and to produce spatial-temporal characteristics [80]. However, we use this abstract model to focus on the effect of antenna physics on the fading correlation and the capacity. Since the channel capacity is modeled as a random variable resulting from the random channel realization, we employ Monte Carlo simulation to compute complementary cumulative distribution functions (ccdfs) of the channel capacity. By observing the ccdfs, we can quantify the effects of the antenna pattern and the antenna orientation.

In Section 4.2, the spherical model is defined and the relevant mathematical background is introduced. Antenna arrays and antenna patterns are described in Section 4.3. Section 4.4 gives simulation results and discussions. Conclusions are given in Section 4.5.

4.2 Geometry and Capacity

4.2.1 Capacity

The MIMO system investigated in this work consists of n_T transmitting and n_R receiving antennas. A basic assumption is that the transmitter has no channel state information and only the receiver knows the actual realization of the channel. Thus, uniform power allocation by the transmitter is reasonable. We also assume that the channel is flat fading within a narrow communication bandwidth. Under these assumptions, the capacity of the MIMO channel is given by [10]

$$C_{n_T,n_R} = \log_2 \left| I_{n_R} + (\rho / n_T) HH^+ \right| bps / Hz \qquad (4.1)$$

where every term has the same definition as it is in previous chapters. The channel matrix defined by $H=[H_1, H_2, \cdots, H_{nT}]$ is a random matrix with complex elements H_{ij} describing the gain of the radio channel between the j^{th} transmitting antenna and the i^{th} receiving antenna. The column vector H_i is the n_R-dimensional propagation vector corresponding to the i^{th} transmitted signal.

For uncorrelated Rayleigh fading channels, the entries of H are i.i.d. Gaussian random variables with zero-mean, independent real and imaginary parts having equal variance. For correlated Rayleigh fading channels, the elements (H_{lp}) of H are correlated with one another.

As in Chapter 2, we can rewrite (4.1) by means of the singular value decomposition [17] as

$$C_{n_T,n_R} = \sum_{i=1}^{N_{\min}} \log_2 (1 + \frac{\rho}{n_T} \lambda_i) . \qquad (4.2)$$

Since the Wishart matrix W is a positive or positive semi-definite Hermitian matrix, the eigenvalues of W are non-negative. The maximum number of non-zero eigenvalues is $N_{\min}$. For an uncorrelated Rayleigh fading channel, i.e., no correlation between any different H_{lp} and H_{mq}^*, there are $N_{\min}$ positive eigenvalues. For the correlated Rayleigh fading channel, the number of non-zero eigenvalues could be less than $N_{\min}$ because the correlation might reduce the rank of W. In fact, an eigenvalue represents a single-input single-output channel. Since the capacity depends on the number and the distributions of eigenvalues, it depends, in turn, on the correlation.

4.2.2 The Spherical Model

In order to study the correlation with directive receiving antennas, we extend the "one-ring" model to a spherical model as shown in Fig. 4.1.

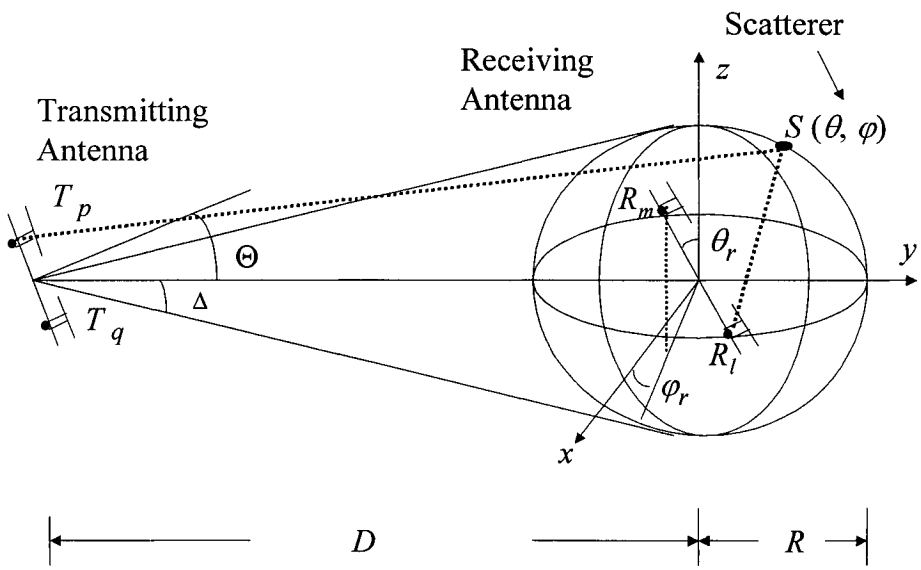

Fig. 4.1. Illustration of the abstract spherical model. T_p, R_l, and $S(\theta,\varphi)$ are the transmitting antenna p, the receiving antenna l, and the scatterer, respectively.

The model is valid in the fixed communication context because the parameters in Fig. 4.1 are fixed over a burst, where the base station is usually elevated and unobstructed by local scatterers, and the mobile station is surrounded by local scatterers. In this model, cross-correlations are among the transmitting and receiving elements. For convenience, we assume that the base station and the mobile station

play the roles of the transmitter and the receiver, respectively. It is noted that the capacity is invariant for the notational exchange of the transmitter and the receiver because W is invariant with respect to the transposition of H. The parameters in the model are the distance D between the base station and the mobile station, the angle spread Δ, the radius R of the scattering sphere, the angle of arrival, Θ, at the base station, the direction (θ_r, φ_r) of the axes of the receiving antenna array and antenna elements, and geometrical arrangement of the antenna sets. Here and in the sequel, the angle θ_r is relative to the z axis. It is analogous to latitude, in terrestrial terms. The angle φ_r is the projection on the x-y plane corresponding to longitude.

In the model, K actual scatterers are assumed to be distributed uniformly in θ andφ. Each actual scatterer at (θ,φ) to the receiver is represented by a corresponding effective scatterer, denoted by $S(\theta,\varphi)$, which is located at the same (θ,φ) on the scattering sphere centered on the receiver. The dielectric properties and radial displacement from the scattering sphere of the actual scatterer that $S(\theta, \varphi)$ represents are taken into account by $\phi(\theta,\varphi)$. So, rays reflected by $S(\theta,\varphi)$ have a phase change of $\phi(\theta,\varphi)$, which has an independent and identically uniform distribution for all scatterers. R can be determined by the root-mean-square delay spread of the channel [81]. We also assume that the rays being considered are those that are reflected by the effective scatterers only one time and the rays reach receiving antenna elements with equal power and in the same field direction as field patterns of the receiving antenna elements. Field patterns of transmitting antennas in the region of the scattering sphere are assumed to be isotropic. In many realistic environments, when a receiver is far from a transmitter, this assumption is often a good approximation to the realistic field pattern of the transmitting antenna. Receiving antenna elements are assumed to be identical and directive. Their radiation field

patterns are defined as $F(\theta,\varphi)=E(\theta,\varphi)/E_{max}$, where $E(\theta,\varphi)$ is the radiation electric field and E_{max} is the maximum value of $E(\theta,\varphi)$. So, $F(\theta,\varphi)$ is normalized. The maximum directivity of receiving antenna elements is denoted by D_a.

Following Collin and Zucker [82], we write the channel gain (signal voltage) from a transmitting antenna T_p to a receiving antenna R_l as

$$H_{lp} = \int_A \vec{E}_{\lambda p}(\Omega,t)\cdot\vec{E}_l(\Omega)d\Omega\,, \tag{4.3}$$

where $\vec{E}_{\lambda p} = E_{\theta p}\vec{a}_\theta + E_{\varphi p}\vec{a}_\varphi$ is the p^{th} incident source vector from the transmitting antenna T_p, which is a zero mean complex Gaussian random variable, $\vec{E}_l = E_{\theta l}\vec{a}_\theta + E_{\varphi l}\vec{a}_\varphi$ is the l^{th} dimensionless receive antenna electric field, $(\vec{a}_\theta,\vec{a}_\varphi)$ are the unit vectors in the direction of θ and φ, respectively, Ω is the solid angle (θ, φ), which is a part of the space bounded by straight lines issuing from the origin of the sphere in Fig. 4.1 (the vertex) to all points of an arbitrary closed curve, A is the area of incident waves, and $d\Omega$=element of solid angle $=\sin\theta\, d\theta\, d\varphi$.

In terms of ray tracing method, $E_{\lambda p}(\Omega,t)$ in a burst is given from Fig 4.1

$$E_{\lambda p}(\Omega,t) = \frac{1}{\sqrt{4\pi K}}\sum_{k=1}^{K}\exp[-j\frac{2\pi}{\lambda}(R_{pS(\Omega)} + R_{S(\Omega)l}) + j\phi(\Omega)]\delta(\Omega-\Omega_k)\,, \tag{4.4}$$

where λ is wavelength, R_{ji} is the distance from object j to object i, $\phi(\Omega)$, the phase shift caused by the scatter at Ω, is uniformly distributed over (-π, π), K is the number of scatterers, Ω_k is the solid angle of the k^{th} scatterer.

Since the transmitting power is fixed, (4.4) is the same for every type of antenna. The dimensionless receive electric field is chosen in terms of equal receive power of every type of antenna if the equal incident power is uniformly distributed over a sphere centered on the antenna as

$$E_l(\theta,\varphi) = \sqrt{D_{al}} F_l(\theta,\varphi) \quad , \tag{4.5}$$

where D_{al} is the maximum directivity of the l^{th} antenna, which represents the maximum value of directivity, F_l is the pattern of the l^{th} antenna. With (4.5), if the incident waves are uniformly distributed over a sphere centered on the antenna, every type of antenna receives the same power, which is the basic idea of the definition of antenna directivity. Under this condition, it is meaningful to compare the effect of different types of antenna.

Assuming the direction of $E_l(\theta,\varphi)$ is in the same direction of $E_{\lambda p}$, and putting (4.4) and (4.5) into (4.3), we have

$$H_{lp} = \frac{1}{\sqrt{4\pi K}} \int_0^{\pi} \int_0^{2\pi} \sum_{i=1}^{K} \delta(\Omega - \Omega_i) \exp[-j\frac{2\pi}{\lambda}(R_{pS(\Omega)} + R_{S(\Omega)l}) + j\phi(\Omega)] \sqrt{D_{al}} F_l(\Omega) d\Omega \quad . \tag{4.6}$$

(4.6) is in a form of normalization as seen from below that the auto-variance of H_{lp} is one for every type of antenna,

$$E[H_{lp} H_{lp}^*] = 1 \tag{4.7}$$

where the superscript * denotes the complex conjugate. If we substitute (4.7) into the following formula of capacity found in [42],

$$C = \log_2 | I_{n_R} + \frac{\rho}{n_T} R |$$

with

$$R = \frac{HH^+}{\frac{1}{n_T n_R} E[\sum_{t=1}^{n_R} \sum_{r=1}^{n_T} H_{r,t} H_{r,t}^*]} \tag{4.8}$$

we find that $R=HH^+$. So, H defined by (4.6) is already normalized. The other path gain in three dimensions can be found in [83].

In accordance with the central limit theorem, as K, the number of scatterers, approaches infinity, H_{lp} approaches to being a circularly symmetric complex Gaussian random variable with mean zero and variance one, and the channel becomes asymptotically purely Rayleigh fading [84].

Setting an $n_R n_T \times 1$ column vector of $vec(H) = (H_1^T, H_2^T, \cdots, H_{nT}^T)^T$ formed by stacking the columns of H under each other, we can determine the covariance matrix of the vector vec(H): $\text{cov}(vec(H)) = E[vec(H)vec(H)^+]$. Since $vec(H)$ constructed from the model is special complex Gaussian random variable, the second-order statistics of $vec(H)$ are completely specified by cov($vec(H)$) [85]. The covariance between H_{lp} and H_{mq} is

$$E[H_{lp} H_{mq}^*] = \frac{1}{4\pi} \int_0^{\pi} \int_0^{2\pi} \exp\{-j \frac{2\pi}{\lambda} [R_{pS(\theta,\varphi)} + R_{S(\theta,\varphi)l} - (R_{qS(\theta,\varphi)} + R_{S(\theta,\varphi)m})]\} \cdot \sqrt{D_{al} D_{am}} F_l(\theta,\varphi) F_m^*(\theta,\varphi) \sin\theta \, d\theta \, d\varphi \tag{4.9}$$

Since the spatial complex correlation $E[H_{lp}H_{lq}^{*}]$ at the transmitter between antenna p and q is dependent of l, and the correlation $E[H_{lp}H_{mp}^{*}]$ at the receiver between antenna l and m is independent of p, the spatial correlation matrix of (4.9) is the Kronecker product of the spatial correlation matrix at the transmitter and the receiver. This has been confirmed in [38, 86]. Here we denote Σ_T and Σ_R as the covariance matrices at the transmitter and receiver, respectively. Σ_T is the matrix of order $n_T \times n_T$ and its elements are given by $E[H_{lp}H_{lq}^{*}]$ in terms of (4.9) for $l = 1, \cdots, n_R$, $p = 1, \cdots, n_T$, and $q = 1, \cdots, n_T$. Similarly, $\Sigma_R = E[H_p H_p^{+}]$ is an $n_R \times n_R$ matrix for $p = 1, \cdots, n_T$ and is the same for any p, whose elements are $E[H_{lp}H_{mp}^{*}]$ of (4.9) for $l = 1, \cdots, n_R$, $p = 1, \cdots, n_T$, and $m = 1, \cdots, n_R$.

The distribution of the unordered eigenvalues of W for $n_T \geq n_R$ can be found in [19, 87, 88] based on Σ_T and Σ_R. When the distance, dt, between two adjacent elements in the transmitter is large enough, one would expect that the signal correlation between any two different transmitting elements tend to zero and only the receiver has correlated signals. In this case, the analysis of [20] can be applied. When $n_T < n_R$, W is singular and no distribution for W exists.

From the channel covariance matrix $\Psi = \mathrm{cov}(vec(H)) = \Psi^{1/2}(\Psi^{1/2})^{+}$, whose entries are determined by (4.9), the samples of $vec(H)$ can be generated by pre-multiplying a white channel $vec(H_w)$ by $\Psi^{1/2}$ as follows

$$vec(H) = \Psi^{1/2} vec(H_w), \tag{4.10}$$

from which we can obtain H. We have generated 10,000 samples of the channel and compute the statistics of MIMO capacity given in (4.1) such as cumulative distribution function (cdf) and complementary cdf (ccdf) using Monte Carlo simulation.

4.3 Antenna Arrays and Radiation Patterns

4.3.1 The Number of Antennas

As discussed in Sec. 4.2, the MIMO capacity $C_{nT,nR}$ depends on the number and the distribution of the eigenvalues of the Wishart matrix W. Since the number of the eigenvalues is given by $N_{\min} = \min(n_T, n_R)$, if we have a total of ten antennas in the simulation, we should put five antennas at the transmitter and five at the receiver in order to increase the potential number of eigenvalues over any other arrangement of antenna elements at the transmitter and receiver. Because of physical constraints, there may be situations where it may not be possible to put equal numbers of antenna elements in the transmitter and receiver. According to the duality theorem of [20] and the fact that $C_{nT,nR}$ in (4.2) increases with SNR, it is readily deduced from Eq.1 that having more antennas in the receiver gives higher MIMO capacities than having more antennas in the transmitter when the total number of antennas is fixed and SNR remains the same (see Chapter 3). Reference [89] gives several examples of this situation. Another aspect of the distribution of antennas between the transmitter and receiver is the point of diminishing return with the increase of receiving antenna number. As illustrated in Ref. 89, when the transmitter has small number of antennas, increasing beyond six receiving antennas increases capacity only marginally. Based

on the foregoing considerations, in our studies, we place four antennas in the transmitter and six antennas in the receiver for the ten antenna case. Since $n_T < n_R$ is set in our arrangement of antennas in the transmitter and receiver, the Monte Carlo simulation will be used to calculate the outage capacity and the ccdf of the capacity.

4.3.2 Two Antenna Arrays

We now consider the physical arrangement of the various antennas at the transmitter and the receiver. We consider two different antenna arrays for the four antenna elements in the transmitter: the linear array of Fig. 4.2a and the square planar array of Fig. 4.2b.

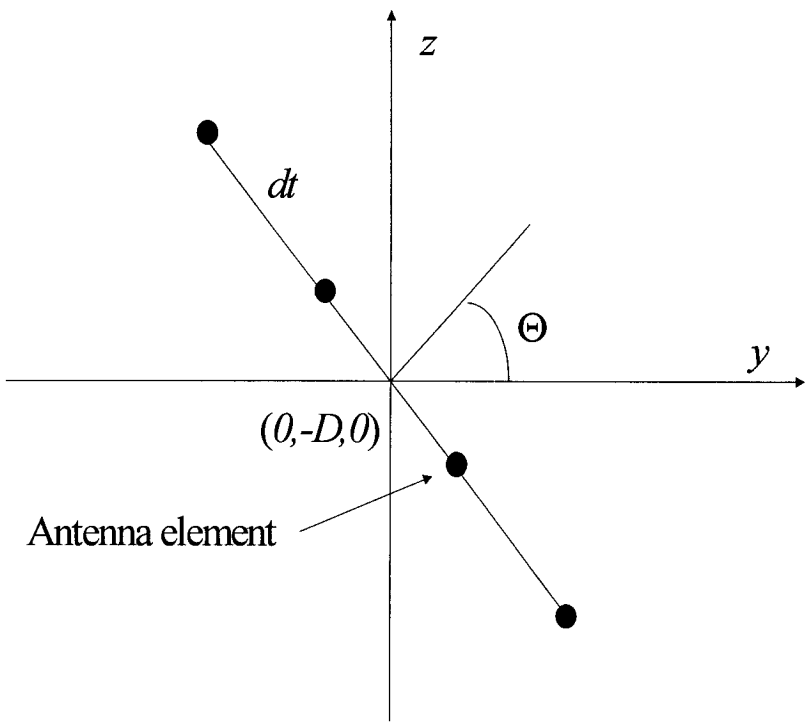

(a) Linear array at the transmitter

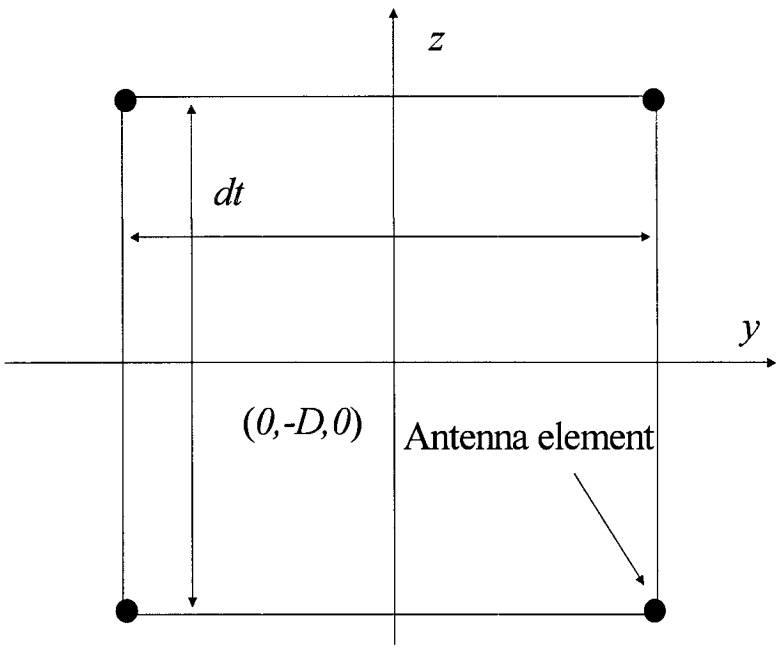

(b) Square array at the transmitter

Fig.4.2. Antenna arrays of the transmitter.

Antenna elements in Fig. 4.2a and Fig. 4.2b are equally spaced along a line and at the corners of a square, respectively. They are centered at *(0, -D, 0)*, where *D* is the distance to the receiver. The distance between two adjacent elements is denoted by *dt*.

We consider two orientations of the transmitting linear array for Fig. 4.2a. One is when $\Theta=0^{\circ}$. In this orientation, the receiver is broadside to the linear array in the transmitter, and this is termed the broadside case. Another is when $\Theta=90^{\circ}$ and the inline case occurs.

We also consider a linear antenna array, Fig. 4.3a, and a rectangular array, Fig. 4.3b, for the receiver.

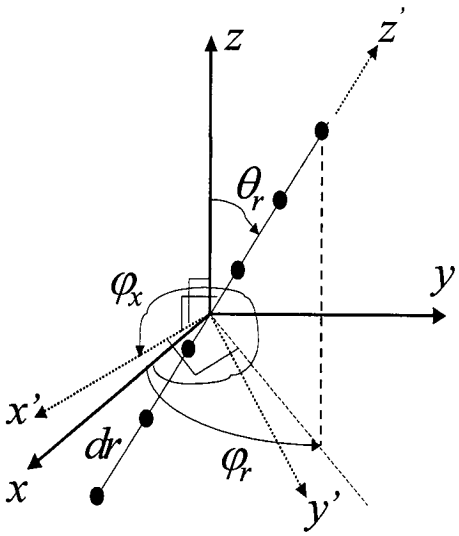

(a)

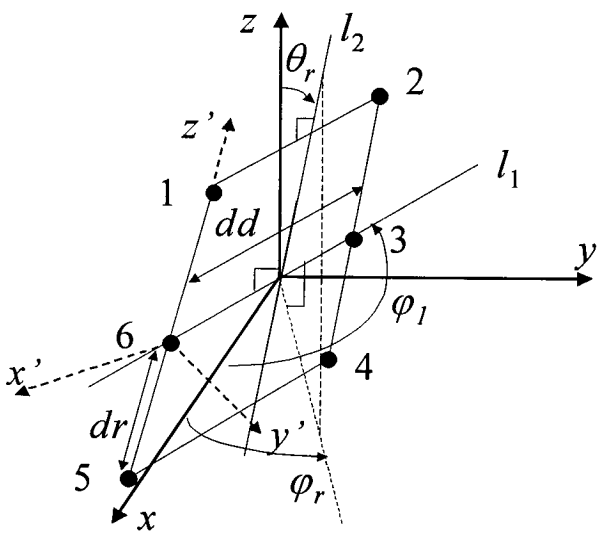

(b)

Fig.4.3 Antenna arrays of the receiver

In Fig. 4.3, We use two coordinate systems. The coordinate system of (x, y, z) is for the spherical model and the coordinate system of (x', y', z') is for the antenna element for convenient description of element patterns. However, we will transform the patterns from coordinates (x', y', z') to (x, y, z).

In the case of the linear array, Fig. 4.3a, z' axis coincides with the linear array and x' is set in the x-y plane. y' can be determined by the right hand rule of the coordinate system. The orientation of the array is determined by (θ_r, φ_r) in the (x, y, z) coordinate system. Since x' is vertical to the projection of the linear array on the x-y plane as shown in Fig. 4.3a, $\varphi_x = 2\pi - (\pi/2 - \varphi_r)$.

In the case of the rectangular array, Fig. 4.3b, l_1 and l_2, the cross median lines in the plane of the rectangle containing antennas from number one to six, are used to fix the rectangle. l_1 is set to remain in the x-y plane while the rectangle turns in different orientation angles. So, the rectangle can be determined by the angles θ_r and φ_r in (x, y, z) coordinate system instead of (φ_l, θ_r) because φ_l is not independent and is given by $\varphi_l = \varphi_r + \pi/2$. The rectangular array can be regarded as a combination of two linear arrays. One is formed by antenna elements 1, 6, and 5, and another by 2,3, and 4. The distance between the two linear arrays is *dd*, and the distance between adjacent antennas of the two linear arrays is *dr*.

4.3.3 Two Kinds of Antenna Elements

In order to study the effect of receiving antenna directivity, we compare half-wavelength dipoles and square microstrip patch antennas as the respective antenna elements for arrays. The maximum directivity of the dipole antenna is $D_a = 1.64$, and

the maximum directivity of the microstrip antenna is D_a=4.67. All elements in an array are identical dipoles or microstrip antennas. The coordinates of the dipoles and microstrip antennas are depicted in Fig. 4.4a and Fig. 4.4b, respectively.

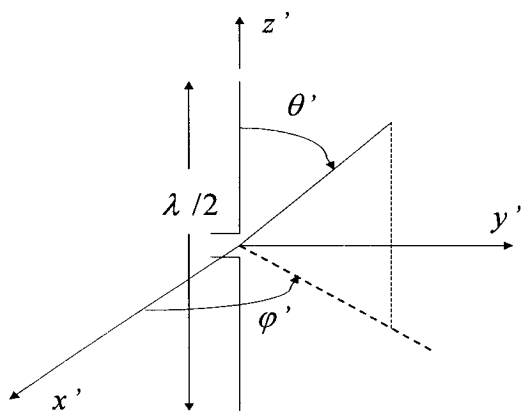

(a)

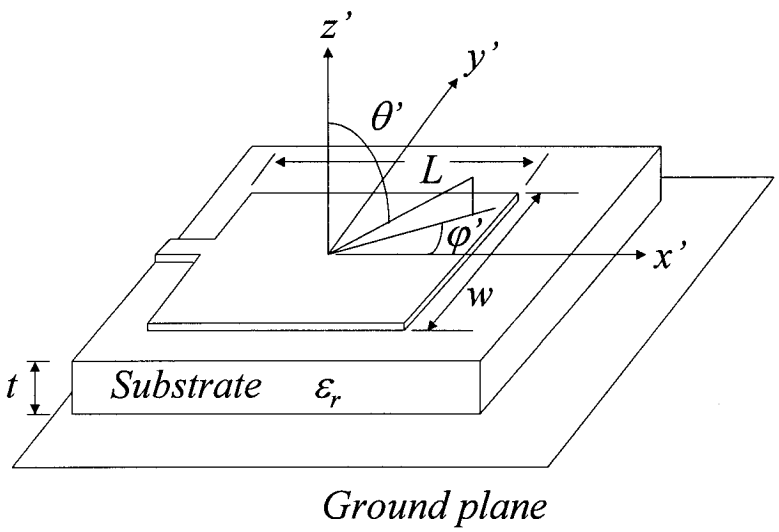

(b)

Fig. 4.4 (a) The half-wavelength dipole antenna; (b) the half-wavelength square patch microstrip antenna: L=W=0.49λ_d.

4.3.4 Radiation Field Patterns

The radiation field pattern for the half-wave dipole is given by [90]

$$F(\theta',\varphi') = \frac{\cos[(\pi/2)\cos\theta']}{\sin\theta'}, \tag{4.11}$$

whose cross section is illustrated in Fig.4.5. The pattern does not change with φ'; consequently, it is omni-directional in the x'-y' plane.

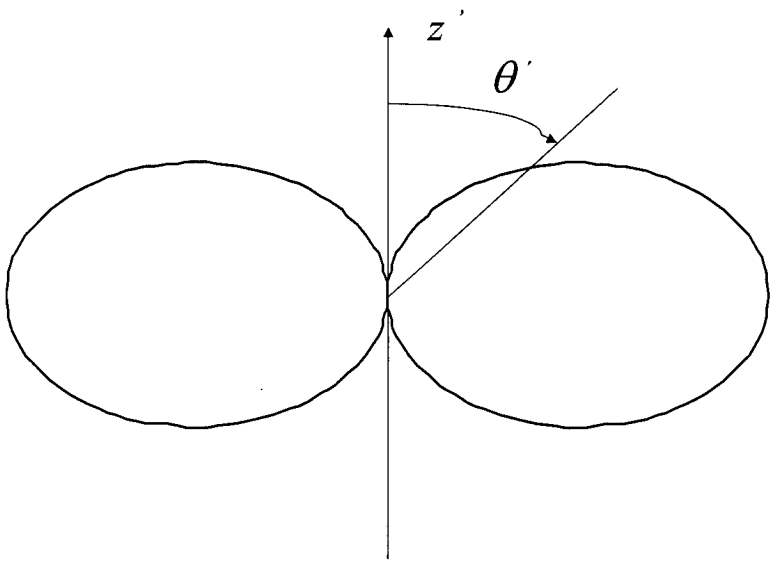

Fig.4.5 The field pattern of the half-wave dipole.

For the half-wave square microstrip patch antenna, where $L=W=0.49\lambda_d=0.49\lambda/\sqrt{\varepsilon_r}$ (ε_r is the substrate dielectric constant with value 2.35), its field pattern is [90]

$$F(\theta',\varphi') = \sqrt{\cos^2\varphi' + \sin^2\varphi'\cos^2\theta'}\, f_1(\theta',\varphi'), \tag{4.12}$$

where

$$f_1(\theta',\varphi') = \frac{\sin[(0.49\pi/\sqrt{\varepsilon_r})\sin\theta'\sin\varphi']}{(0.49\pi/\sqrt{\varepsilon_r})\sin\theta'\sin\varphi'}\cos[(0.49\pi/\sqrt{\varepsilon_r})\sin\theta'\cos\varphi'] .$$

The field pattern is a torus in the upper hemisphere, whose projections in the x'-z' and y'-z' planes are depicted in Fig. 4.6a and Fig. 4.6b, respectively.

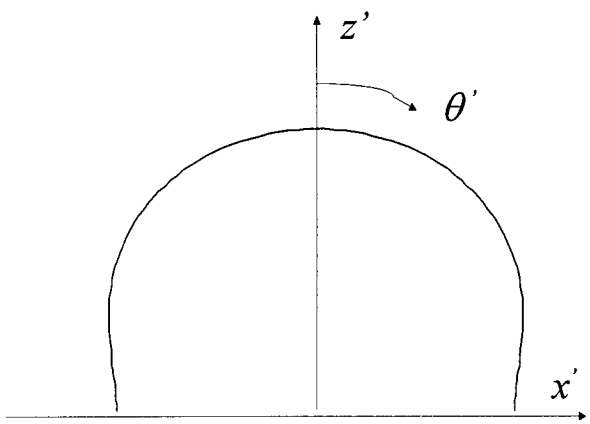

(a) the field pattern at φ'=0°

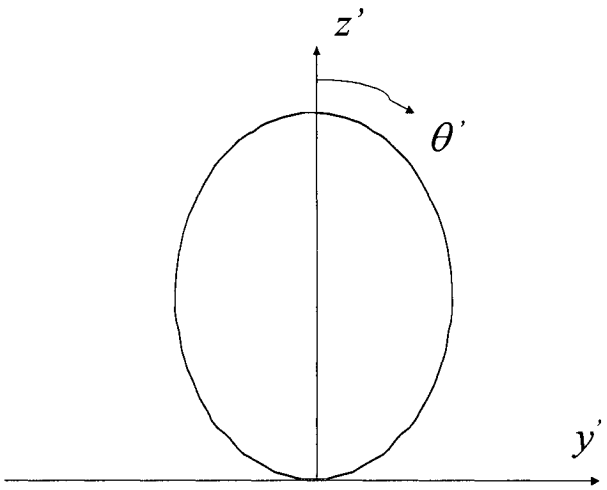

(b) the field pattern at φ'=90°

Fig.4.6 The field pattern of the half-wave square microstrip patch antenna.

In the following, we set *dt= 0.5λ, dr=0.5λ, dd=0.5λ , D=1000 λ* , and Δ=12° as default values. These can be overridden by new settings. The average received *SNR*, ρ, is chosen to be 18 dB. In the simulation of ccdfs of the MIMO capacity, 10% outage capacity is denoted by $C_{0.1}$. The term 10% outage capacity means that 90% of the values have higher capacity.

4.4. Simulation results

First, we examine the eigenvalues of the Wishart matrix. Fig. 4.7 gives the pdfs of the ordered eigenvalues of the Wishart matrix when both the transmitting and receiving arrays are linear and lie broadside of one another (θ_r=0°). The Wishart matrix has two eigenvalues for both the dipole and the microstrip arrays although the

potential maximum number of eigenvalues is $N_{\min} = \min(n_T, n_R) = 4$ for uncorrelated cases. The pdfs are normalized to have the same height for demonstration purposes. For the first eigenvalue, it can be seen from Fig.4.7 that pdfs of the dipole and microstrip elements have almost the same distribution. However, for the second eigenvalue, the pdf of the dipole elements is significantly different from the pdf of the microstrip elements. It is clear that the pdf of the microstrip elements has a greater mean value and variance.

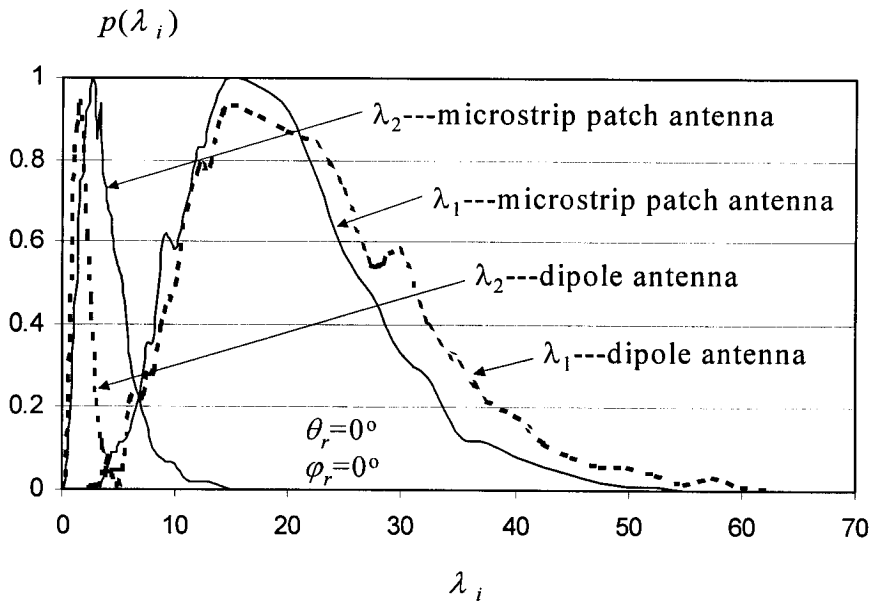

Fig. 4.7 The normalized pdf curves of the ordered eigenvalues of HH^+ in broadside case of linear transmitting and receiving arrays.

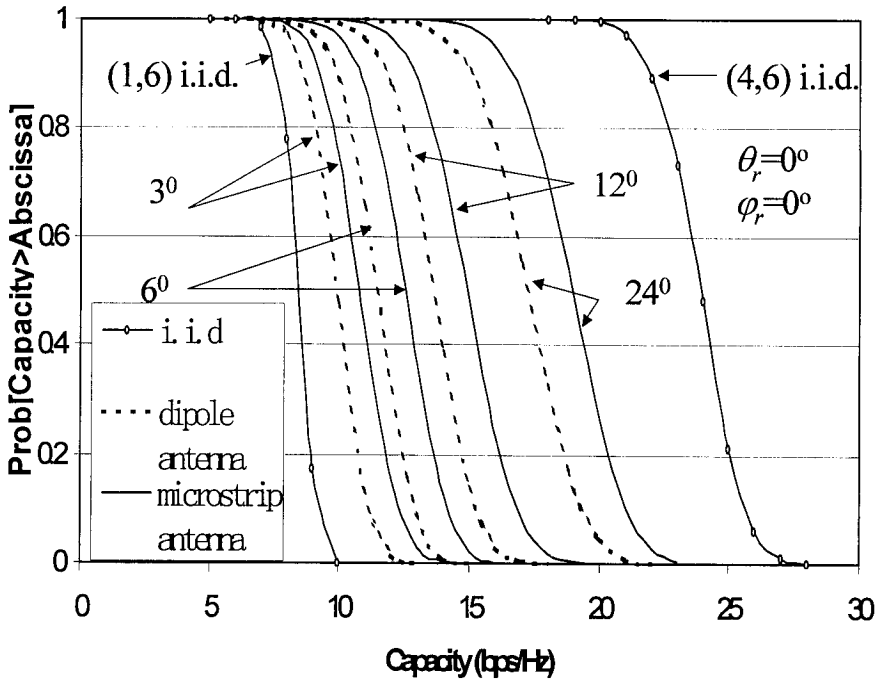

Fig. 4.8 The ccdf of capacity for various angle spreads for broadside case of linear transmitting and receiving arrays.

Second, we study curves of ccdfs as a function of correlations among entries of H at θ_r=0°. Fig.4.8 gives the simulation curves of ccdfs with different angle spreads. In this figure, (1, 6) i.i.d., the open dotted line, refers to the ccdfs curve of capacity when H of order 6×1 is composed of i.i.d. complex Gaussian entries with mean zero and variance one. Solid lines refer to the ccdfs of capacity for the array with microstrip patch antenna elements and dashed lines with dipole antenna elements, respectively. It can be seen that the values of the ccdfs with the dipole elements is significantly lower than that with the microstrip elements when they have the same angle spread at the same capacity. In other words, with a high probability,

for example, 90% of the time, the capacity of the dipole elements is significantly smaller than that of the microstrip elements.

This phenomenon is similar to the experimental results [42], which show that directive elements (patch antennas) result in 35% higher average capacities than those of the omnidirectional elements (dipole antennas). The experimental observation is obtained in an indoor environment. In fact, under the condition that the transmitting power and the average-to-noise ratio ρ are fixed, two mechanisms are at work here. One is the scattering richness. The richer the scatterers, the less is the correlation. Another is the antenna directivity. Antenna directivity can decrease or increase correlation, dependent on the incident waves and antenna field pattern. Usually, omnidirectional elements see more scatterers and therefore have lower correlation, but have low antenna directivity. Directive elements see lower scatterers and therefore have higher correlation, but have high antenna directivity. However, in a scatter-rich indoor environment, the antenna directivity plays a more positive role than the scatter-richness, which results in above measured results in [42].

On the other hand, this phenomenon can also be explained by Fig. 4.7, in which the pdfs of the first eigenvalues of both the dipole and microstrip elements have almost the same distribution, but the pdf of the second eigenvalue of the microstrip elements has a greater mean value and variance than that of the dipole elements. It should be noted that our model shown in Fig. 4.1 has rich scatterers over the sphere.

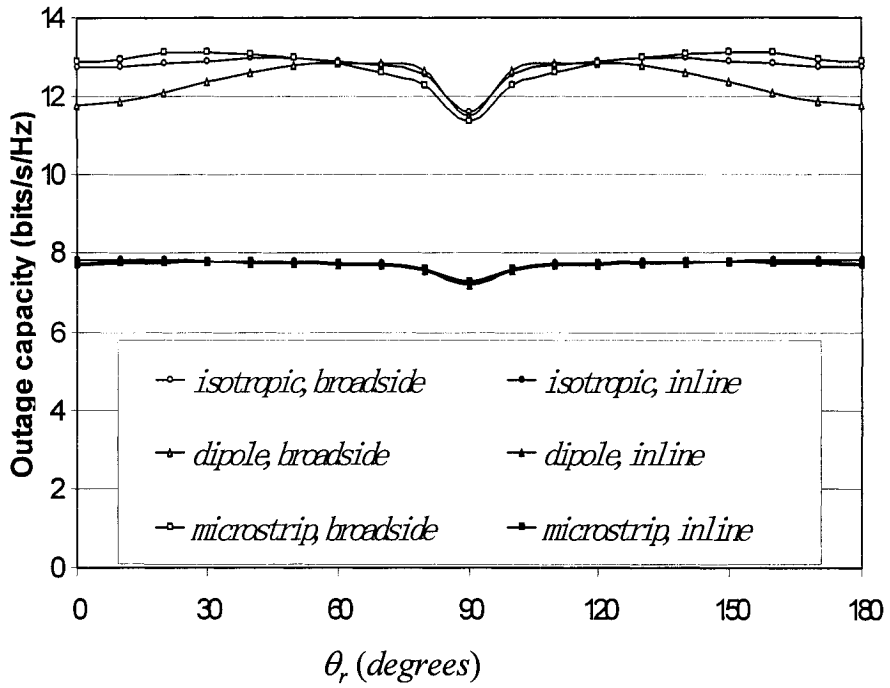

Fig. 4.9 Variations of outage capacity with θ_r for φ_r from 0° to 360° in the case of the linear transmitting and receiving arrays. Points of isotropic inline, dipole inline, and microstrip inline are almost merged.

Next, we study figures in which outage capacities $C_{0.1}$ change with orientation of the antenna array. In these figures, isotropic antennas (D_a=1) as array elements are included for comparisons. When both the transmitting array and the receiving array are linear arrays, the results are plotted in Fig. 4.9. The open dotted lines are for the cases that the receiving arrays on the broadside ($\Theta=0^o$) of the transmitting arrays and close dotted lines for the inline ($\Theta=90^o$) cases, respectively. The denotation of "isotropic, broadside" means the receiving array lies broadside to the transmitting array and has isotropic elements. In the broadside cases, the capacities of the

microstrip elements are higher than those of the dipole elements in most ranges of angles. The biggest difference between the microstrip capacity and the dipole capacity is about 1 bits/s/Hz, which is a 10% difference. This phenomenon indicates that the microstrip elements generate less correlation in the covariance matrix than the dipole elements in the scatter-rich environment of uniformly distributed scatterers around the receiver because of their field patterns. It is interesting to note that [42, 43] also observed that the capacity of directive elements depends on the azimuth direction of arrival of the incident field. In fact, the scatter-richness seen by antennas in different orientations in our model is different. Therefore, the dependence on θ_r is a result of interaction of the two working mechanisms we discussed above. The capacities of the isotropic elements lay in between those of the microstrip and dipole elements, indicating that the isotropic antennas have higher capacities than those of the dipole antennas. For the inline cases, the capacities of the isotropic, dipole, and microstrip elements are almost the same. They are much lower than those of the broadside cases, as previously shown by [17], because they produce higher correlation in the covariance matrix. At θ_r =90°, the capacities for all cases are the lowest because the transmitting arrays are on the inline of the receiving arrays. The capacity curves are symmetrical on θ_r and do not change with φ_r due to the uniformly distributed scatterers and the symmetric elements along the linear array.

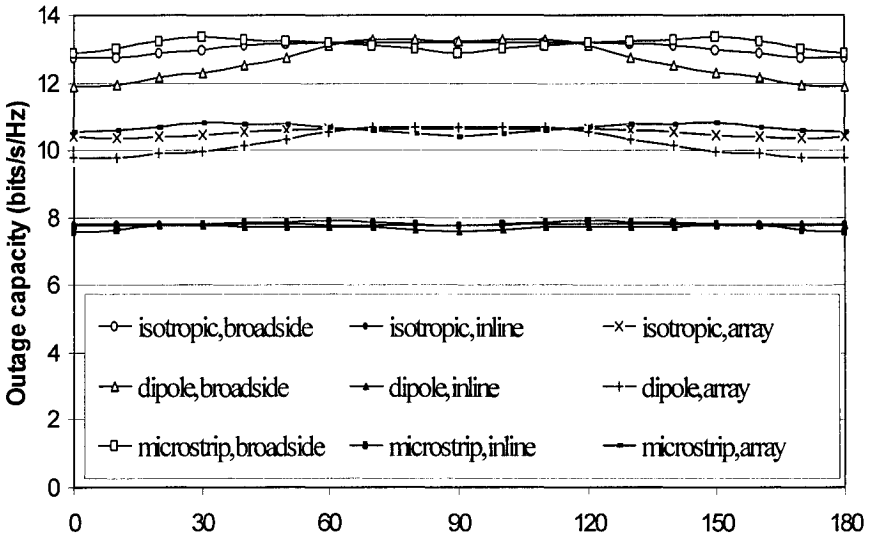

(*a*) $\varphi_r = -90^\circ$

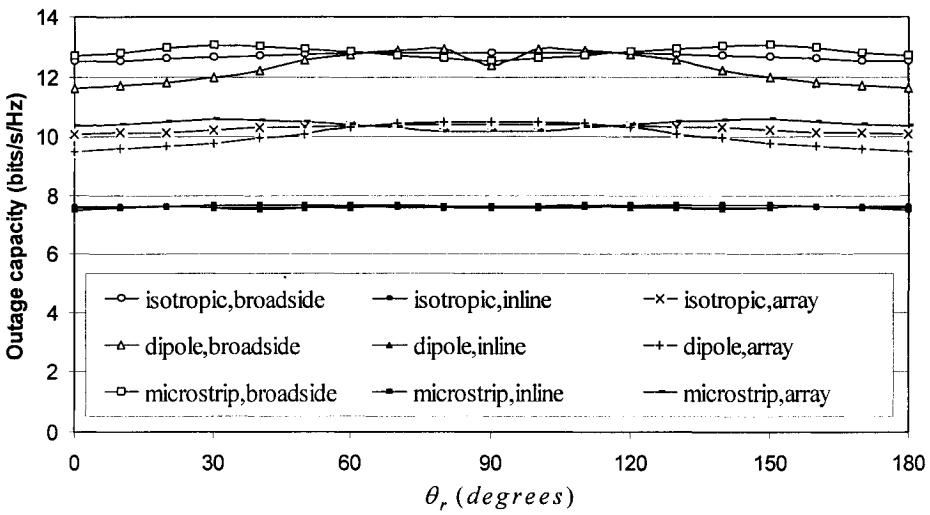

(*b*) $\varphi_r = 0^\circ$

Fig. 4.10 Variations of outage capacity with θ_r and φ_r for rectangular receiving arrays.

When the receiving array is rectangular and the transmitting arrays are broadside, inline, and square arrays, respectively, the variations of capacities with θ_r and φ_r are given in Fig. 4.10, in which the denotation of "isotropic, array" means the transmitting array is square and the receiving elements are isotropic. φ_r is set with two planes of φ_r = -90° and φ_r =0°, respectively. Fig. 4.10*a* is for φ_r = -90° and Fig. 4.10*b* for φ_r =0°. Comparing Fig. 4.9 with Fig. 4.10, it is seen that they are similar to each other. The important difference between Fig. 4.9 and Fig. 4.10 is that the variations of the capacities with θ_r in Fig. 4.10 are smoother than those in Fig. 4.9 due to the rectangular receiving arrays. The capacity curves of the square transmitting array are in between those of the broadside and inline arrays, which is also identical with that of [17]. Comparing Fig. 4.10a with Fig. 4.10b, we find that curves of Fig. 4.10b are slightly lower than those of Fig. 4.10a; thus,, the rectangular receiving array results in weak directivity of capacities on φ_r.

Finally, we examine the effect of the receive antenna spacing. Fig. 4.11a displays the magnitude of the correlation, $E[H_{11}H_{21}^*]$, versus *dr* for the broadside linear array. Fig. 4.11b shows $C_{0.1}$ versus *dr*. The receive elements are with dipole elements and microstrip elements, respectively. The magnitude's variations of $E[H_{11}H_{21}^*]$ with *dr* are like the zero-ordered Bessel functions, which don't monotonically decrease with *dr*. The decrease results in an increase in $C_{0.1}$. However, the increase reaches saturation at dr/λ =0.5, which explains that the degradation in capacity is small even with the spacing as small as dr/λ =0.5. Similar results can be found in the "one-ring" model [17], as it is well known in diversity reception systems [91].

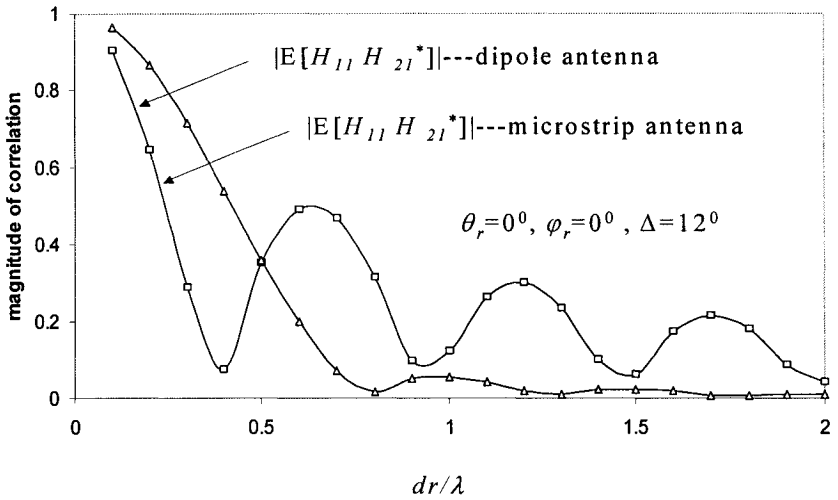

(a)

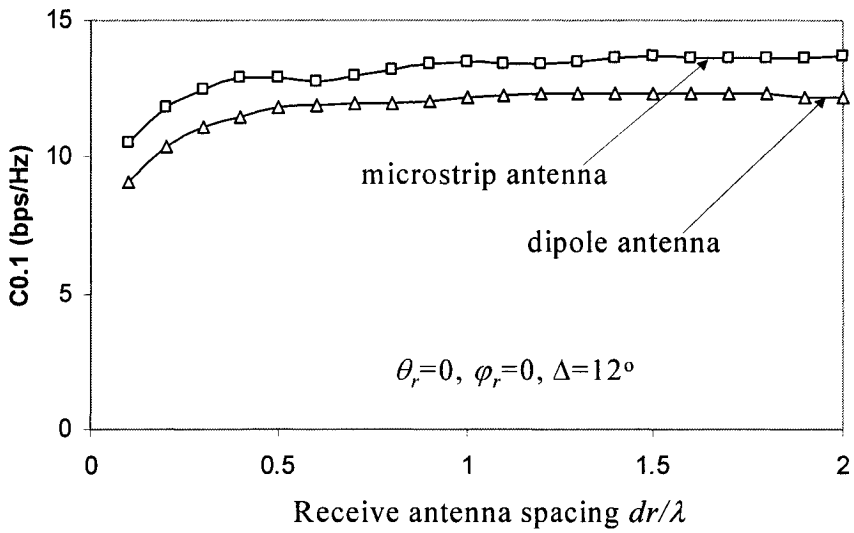

(b)

Fig. 4.11 (a) Magnitudes of correlations change with the receive antenna spacing for the broadside linear array. (b) $C_{0.1}$ versus dr.

4.5 Conclusions

In this chapter, we extend the "one-ring" model to the spherical model so that we can consider the effects of the antenna parameters such as the antenna field pattern and orientation on the information-theoretic capacity. In this model, scatterers around the subscriber unit (receiver) are distributed over the sphere centered on the antenna array in the subscriber unit. Based on assumptions that the transmitting power is constant and the receiving power is the same for any type of receiving antenna if the incident waves are uniformly distributed over the sphere centered on the receiving antennas, we present the expressions of the channel transfer function and its covariance matrix, which is appropriate for the study of different antenna types and different antenna orientations in the space in MIMO systems. In the simulations, the transmitting antenna elements are isotropic, and the receiving elements are half-wave dipole antennas and half-wave square patch microstrip antennas, respectively. The receiving isotropic antennas are taken for the purpose of comparison. In the transmitter, a linear array and a square array are chosen respectively. In the receiver, a linear array and a rectangular array are set respectively. The choice of antenna numbers at the transmitter and at the receiver is based on two considerations. The first is that, from the point of view of information-theoretic capacity, i.e., putting more antennas at the receiver provides higher capacities than vice-versa at the transmitter for the case that it may not be possible to put equal antenna elements in the transmitter and receiver because of physical constraints. The second is that the receiving antenna number at the point of outage capacities shows diminishing return. So, we set 4 elements in the transmitter and 6 in the receiver. The arrangement of unequal antenna numbers could be meaningful in a

realistic communications system. In the uplink, more antennas in the base station (transmitter) having lower capacity are compensated by higher transmitting power of the base station. In the downlink, lower transmitting power of the mobile station (transmitter) having lower capacity is compensated by more antennas in the base station (receiver) having higher capacity.

When both the transmitter and receiver are linear and lie broadside to one another ($\theta_r = 0^\circ$), the pdfs of the first eigenvalues with dipole and microstrip elements are almost the same, but the pdf of the second eigenvalue with microstrip elements has larger mean value and variance than that with the dipole elements, which gives the result that the outage capacities with the microstrip elements are higher than those with dipole elements for the same angle spread at different spread angles. As θ_r changes from 0° to 180° , the capacities with the microstrip elements are generally higher than those with the dipole elements, but the difference between them is small, about 1 bits/s/Hz or 10%. This means that the microstrip antennas provide lower correlation in the covariance matrix than the dipole antennas in the scatter-rich environment. It can be expected that antenna directivity play more important role when its directivity is higher and the incident waves are not from uniformly distributed scatterers. Similar experimental observation can be found in [42]. Furthermore, using the antenna field pattern to achieve the parallel channels in the line of sight environment of MIMO systems can be found in [16].

In all inline cases, the capacities change very slightly with θ_r for any type of antenna because the correlations are high.

In the case that both the transmitting array and the receiving array are square and rectangular arrays, respectively, the variations of the capacities with θ_r are smoother than when the transmitting array is linear broadside.

In all cases, the variations of the outage capacities with φ_r are very small. That is because the dipole antennas don't have directivity on φ_r, the microstrip antennas have weak directivity on φ_r, and the scatterers are uniformly distributed over these antenna elements.

Chapter 5 Correlation and capacity analyses with a experimentally based statistical model

5.1 Introduction

In Chapter 4 we have used the abstract spherical model to investigate the effect of antenna physics. The abstract model assumes the scatterers uniformly distributing over the sphere centered on the receive array. So, the electromagnetic waves come to the receiver array in every direction equi-probably (uniform probability). Since the correlation between two different path gains is the interaction of the scattered waves and the antenna patterns, it is important to have a good understanding of the propagation phenomena and the antenna issues.

Several experiments have been carried out with the objective of studying the distribution of incoming waves. In the indoor case, Spencer et al [92] have characterized the indoor wideband channel. They model the histogram of ray arrivals relative to the cluster mean of scatterers as a Laplacian (a double exponential) distribution. In the outdoor case, Pedersen et al [93] measured the angular response using an array and found the statistics of the distribution, where the pdf of arriving angles was modeled by a Gaussian distribution and the angular power spectrum by a Laplacian. Astely and Ottersten [94] have applied the MUSIC algorithm to find the statistics of the angle-of-arrival under the assumption that the angular spread is small. Recently, Andersen et al [95] have found a statistical Student's t-distribution of the angle-of-arrival in the limit where the antenna is not able to resolve the details of the distribution.

In this chapter, we will use the Student's *t*-distribution [95], which is accurate in the micro-cell environment, to further study the effect of antenna physics. To start with, in section 5.2, we derive a condition for zero correlation in general. Then, in section 5.3, we calculate the covariance matrix conditioned on the Student's t-distribution assumption. Also, angle-of-arrival statistics will be introduced. The effect of the arrangement of the antenna array is presented in section 5.4. Simulation is in section 5.5 and the conclusion is in Section 5.6.

5.2 Condition for zero correlation

As in subsection 4.2.2, the normalized path gain is

$$H_{lp}(t) = \frac{\sqrt{D_{al}}}{\sigma_{lp}} \int_A \vec{E}_{\lambda p}(\Omega, t) \cdot \vec{F}_l(\Omega) d\Omega, \tag{5.1}$$

where $\sigma_{lp}^2 = E[H_{lp} H_{lp}^*]$ is the variance of H_{lp}, A is the region of the incident waves, $\vec{E}_{\lambda p} = E_{\theta p}\vec{a}_\theta + E_{\varphi p}\vec{a}_\varphi$ is the p^{th} incident source vector from the transmitting antenna p, which is a zero mean complex Gaussian random variable, $\vec{F}_l = F_{\theta l}\vec{a}_\theta + F_{\varphi l}\vec{a}_\varphi$ and D_{al} are the pattern vector and maximum directivity of the l^{th} receive antenna, respectively, Ω is the solid angle (θ, φ), and appropriate time dependence has been introduced. To study the fading correlation, we still used the same notation as in Chapter 4; that is, if H=[H_1, H_2, $\cdots$,H_{nT}] is an $n_R \times n_T$ matrix, where H_i is an $n_R \times 1$ vector for $i = 1, \cdots, n_T$, then

$vec(H) = (H_1^T, H_2^T, \cdots, H_{nT}^T)^T$ is a vector formed by stacking the columns of H under each other. The covariance matrix of H is defined as the covariance matrix of the vector vec(H): cov(vec(H))=E[vec(H)vec(H)$^+$].

The correlation between H_{lp} and H_{mq} is

$$E[H_{lp}H_{mq}^*] = \frac{\sqrt{D_{al}}\sqrt{D_{am}}}{\sigma_{lp}\sigma_{mq}} E[\int_A \vec{E}_{\lambda p}(\Omega_1,t)\cdot\vec{F}_l(\Omega_1)d\Omega_1 \cdot \int_A \vec{E}_{\lambda q}^{\,*}(\Omega_2,t)\cdot\vec{F}_m^{\,*}(\Omega_2)d\Omega_2]$$

$$= \frac{\sqrt{D_{al}D_{am}}}{\sigma_{lp}\sigma_{mq}} \iint_A \{E[E_{\lambda\theta p}(\Omega_1,t)E_{\lambda\theta q}^*(\Omega_2,t)]F_{\theta l}(\Omega_1)F_{\theta m}^*(\Omega_2)$$
$$+ E[E_{\lambda\theta p}(\Omega_1,t)E_{\lambda\varphi q}^*(\Omega_2,t)]F_{\theta l}(\Omega_1)F_{\varphi m}^*(\Omega_2)$$
$$+ E[E_{\lambda\varphi p}(\Omega_1,t)E_{\lambda\theta q}^*(\Omega_2,t)]F_{\varphi l}(\Omega_1)F_{\theta m}^*(\Omega_2)$$
$$+ E[E_{\lambda\varphi p}(\Omega_1,t)E_{\lambda\varphi q}^*(\Omega_2,t)]F_{\varphi l}(\Omega_1)F_{\varphi m}^*(\Omega_2)\}d\Omega_1 d\Omega_2 \quad . \quad (5.2)$$

We define a two-element polarization matrix for the incident fields as

$$\Gamma_{pq}^t(\Omega_1,\Omega_2) = \begin{bmatrix} \Gamma_{\theta\theta pq}^t(\Omega_1,\Omega_2) & \Gamma_{\theta\varphi pq}^t(\Omega_1,\Omega_2) \\ \Gamma_{\varphi\theta pq}^t(\Omega_1,\Omega_2) & \Gamma_{\varphi\varphi pq}^t(\Omega_1,\Omega_2) \end{bmatrix}, \quad (5.3)$$

where the elements are of the form

$$\Gamma_{\theta\varphi pq}^t(\Omega_1,\Omega_2) = E[E_{\lambda\theta p}(\Omega_1,t)E_{\lambda\varphi q}^{\,*}(\Omega_2,t)], \quad (5.4)$$

which is only concerned with the correlation between the incident waves from transmitting antenna element p and q.

Similarly, we define a two-element antenna polarization matrix for the receive antenna elements as

$$\Gamma_{lm}^{r}(\Omega_1,\Omega_2)=\begin{bmatrix}\Gamma_{\theta\theta lm}(\Omega_1,\Omega_2) & \Gamma_{\theta\varphi lm}(\Omega_1,\Omega_2)\\ \Gamma_{\varphi\theta lm}(\Omega_1,\Omega_2) & \Gamma_{\varphi\varphi lm}(\Omega_1,\Omega_2)\end{bmatrix}, \tag{5.5}$$

in which a matrix element is defined

$$\Gamma_{\theta\varphi lm}(\Omega_1,\Omega_2)=F_{\theta l}(\Omega_1)F_{\varphi m}^{*}(\Omega_2). \tag{5.6}$$

Now, (5.2) can be rewritten as

$$\begin{aligned}&E[H_{lp}H_{mq}^{*}]\\ &=\frac{\sqrt{D_{al}D_{am}}}{\sigma_{lp}\sigma_{mq}}\iint_{A}[\Gamma_{\theta\theta lm}(\Omega_1,\Omega_2)\Gamma_{\theta\theta pq}^{t}(\Omega_1,\Omega_2)+\Gamma_{\theta\varphi lm}(\Omega_1,\Omega_2)\Gamma_{\theta\varphi pq}^{t}(\Omega_1,\Omega_2)\\ &\quad+\Gamma_{\varphi\theta lm}(\Omega_1,\Omega_2)\Gamma_{\varphi\theta pq}^{t}(\Omega_1,\Omega_2)+\Gamma_{\varphi\varphi lm}(\Omega_1,\Omega_2)\Gamma_{\varphi\varphi pq}^{t}(\Omega_1,\Omega_2)]d\Omega_1 d\Omega_2\\ &=\frac{\sqrt{D_{al}D_{am}}}{\sigma_{lp}\sigma_{mq}}\iint_{A}tr\{\Gamma_{lm}^{r}(\Omega_1,\Omega_2)[\Gamma_{pq}^{t}(\Omega_1,\Omega_2)]^{T}\}d\Omega_1 d\Omega_2\ ,\end{aligned} \tag{5.7}$$

where *tr* represents the trace of $\Gamma_{lm}^{r}(\Omega_1,\Omega_2)[\Gamma_{pq}^{t}(\Omega_1,\Omega_2)]^{T}$, meaning the sum of diagonal entries of $\Gamma_{lm}^{r}(\Omega_1,\Omega_2)[\Gamma_{pq}^{t}(\Omega_1,\Omega_2)]^{T}$.

It is clear that the lowest correlation between H_{lp} and H_{mq} with $l \neq m$ or $p \neq q$ for the Rayleigh fading channels is zero. So, we have

$$\iint_A tr\{\Gamma^r_{lm}(\Omega_1,\Omega_2)[\Gamma^t_{pq}(\Omega_1,\Omega_2)]^T\}d\Omega_1 d\Omega_2 = 0, \tag{5.8}$$

i.e., to achieve zero correlation, incident field polarization matrix must be orthogonal with the receive antenna polarization matrix. This condition extends the condition of zero correlation in the traditional wireless communications (there are a transmit antenna and multiple receive antennas for diversity) [2] to the MIMO systems.

5.3 The covariance matrix based on the statistical power spectrum

5.3.1 Covariance in the rectangular coordinate system

We apply (5.2) to a specific statistical distribution of angle-of-arrival so that we can study the effect of antenna pattern. Consider a point-to-point communication channel. Under the assumption that the incident polarizations are uncorrelated and each polarization is spatially uncorrelated, (5.2) becomes

$$E[H_{lp}H^*_{mq}] = \frac{\sqrt{D_{al}D_{am}}}{\sigma_{lp}\sigma_{mq}} \iint_A E[E_{\lambda\theta p}(\Omega_1,t)E^*_{\lambda\theta q}(\Omega_2,t)]\cdot \\ [XPD_{pq}F_{\theta l}(\Omega_1)F^*_{\theta m}(\Omega_2) + F_{\varphi l}(\Omega_1)F^*_{\varphi m}(\Omega_2)]d\Omega_1 d\Omega_2, \tag{5.9}$$

where

$$E[E_{\lambda\theta p}(\Omega_1,t)E^*_{\lambda\theta q}(\Omega_2,t)] = E[E_{\lambda\theta p}(\Omega_1,t)E^*_{\lambda\theta q}(\Omega_1,t)]\delta(\Omega_1-\Omega_2), \tag{5.10}$$

and

$$XPD_{pq} = \Gamma^{t}_{\theta\theta pq} / \Gamma^{t}_{\varphi\varphi pq} \tag{5.11}$$

is the cross polar discrimination (*XPD*). For vertically polarized antennas in urban areas, the *XPD* is given by Kozono et al [96] as a weak empirical function of the distance between the mobile and base station. However, it is also a function of the polarization of the mobile antenna and the type of terrain along the path. For a vertically polarized base station and a vertically polarized urban based mobile antenna, *XPD*=6 dB [97]. For a horizontally polarized base station, the value is –6 dB [97].

Using the selection property of the delta function, we obtain

$$E[H_{lp}H^{*}_{mq}] = \frac{\sqrt{D_{al}D_{am}}}{\sigma_{lp}\sigma_{mq}} \int_{A} E[E_{\lambda\theta p}(\Omega,t)E^{*}_{\lambda\theta q}(\Omega,t)] \cdot [XPD_{pq}F_{\theta l}(\Omega)F^{*}_{\theta m}(\Omega) + F_{\varphi l}(\Omega)F^{*}_{\varphi m}(\Omega)]d\Omega \tag{5.12}$$

Since the studied distribution of angle-of-arrival [95] is for the θ direction in a plane, we rewrite (5.1) in the rectangular coordinate system

$$H_{lp} = \frac{\sqrt{D_{al}}}{\sigma_{lp}} \int_{A} \vec{E}_{\lambda p}(\theta) \cdot \vec{F}_{l}(\theta,\varphi_0)d\theta, \tag{5.13}$$

where $\vec{E}_{\lambda p}(\theta) = E_{\lambda\theta p}(\theta)\vec{a}_\theta + E_{\lambda\varphi p}(\theta)\vec{a}_\varphi$ is the p^{th} incident field vector from the transmitting antenna p in the plane $\varphi = \varphi_0$, which is a zero mean complex Gaussian random variable, $\vec{F}_l(\theta,\varphi_0) = F_{\theta l}(\theta,\varphi_0)\vec{a}_\theta + F_{\varphi l}(\theta,\varphi_0)\vec{a}_\varphi$ and D_{al} are the pattern vector and maximum directivity of the l^{th} receive antenna, respectively. We omit t in (5.13). Consequently, the covariance (or correlation) between H_{lp} and H_{mq} is

$$E[H_{lp}H_{mq}^*] = \frac{\sqrt{D_{al}D_{am}}}{\sigma_{lp}\sigma_{mq}} \int_A E[E_{\lambda\theta p}(\theta)E_{\lambda\theta q}^*(\theta)] \cdot [XPD_{pq}F_{\theta l}(\theta,\varphi_0)F_{\theta m}^*(\theta,\varphi_0) + F_{\varphi l}(\theta,\varphi_0)F_{\varphi m}^*(\theta,\varphi_0)]d\theta \quad . \quad (5.14)$$

In general, the calculation of the cross-correlation of $E[E_{\lambda\theta p}(\theta)E_{\lambda\theta q}^*(\theta)]$ is a difficult task. Therefore, we assume that two adjacent transmit antenna elements are widely separated from each other so that the cross-correlation between any two transmit antenna elements is zero. Then

$$E[E_{\lambda\theta p}(\theta)E_{\lambda\theta q}^*(\theta)] = \begin{cases} E[\left|E_{\lambda\theta p}(\theta)\right|^2], p = q \\ 0, elsewhere \end{cases} . \quad (5.15)$$

5.3.2 Power spectrum

In order to calculate the power spectrum of $E[|E_{\lambda\theta p}(\theta)|^2]$, we consider a scattered model illustrated in Figure 21.

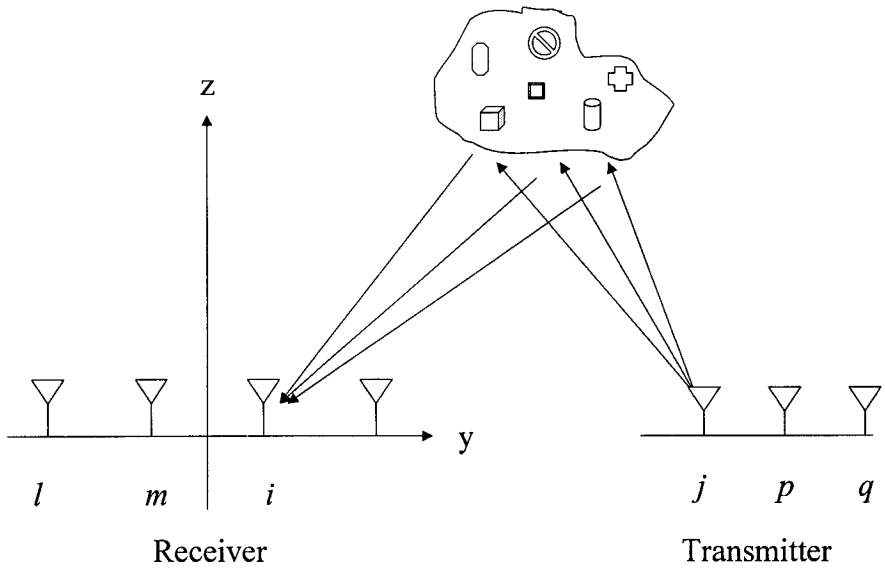

Fig. 5.1 Electromagnetic waves propagate from the transmitter to the receiver.

In Fig. 5.1, we consider plane waves from a transmit antenna element p impinging on a receive antenna element i. With a local plane wave approximation of the field with amplitude E_j and angle α_j, which is sent by the transmit antenna p and scattered by a cluster of scatterers, the field impinging on the i^{th} receiving antenna is

$$E_{\lambda\theta p} = \sum_j E_j \exp[-j(kr_j + \alpha_j)], \tag{5.16}$$

where α_j is the phase shift introduced by scatterers at θ_j (see Fig. 5.2) relative to the p^{th} transmit antenna element. E_j includes slowly varying distance factors the variation of

which may be neglected over short distances. In the phase, we make a first order far-field approximation for the variable distance r_j (see Fig. 5.2)

$$r_j = r_{0j} - y\sin\theta_j, \tag{5.17}$$

which leads to

$$\begin{aligned} E_{\lambda\theta p} &= \sum_j E_j \exp[-j(kr_j + \alpha_j)] = \sum_j E_{\lambda j} \exp[-j(kr_{0j} + \alpha_j - ky\sin\theta_j)] \\ &= \sum_j E_j' \exp(jky\sin\theta_j) \\ &= \left|E_{\lambda\theta p}\right| \exp(jky\sin\theta) \end{aligned}, \tag{5.18}$$

where $E_j' = E_j \exp[-j(kr_{0j} + \alpha_j)]$.

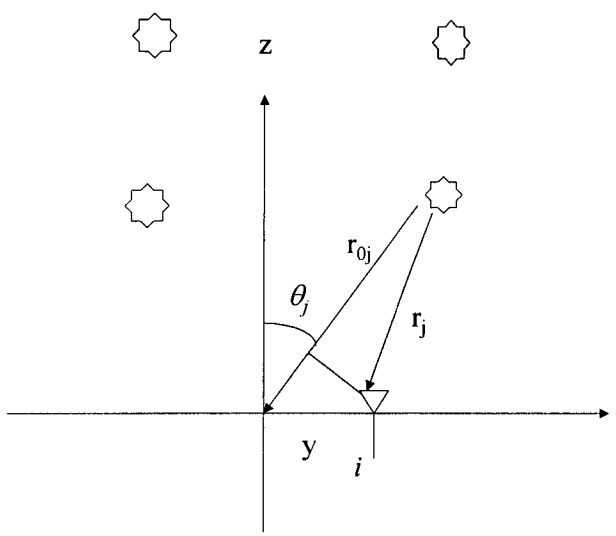

Fig. 5.2 Distribution of complex scatterers

$E_j^{'}$ is the complex scattering strength in the direction θ_j. When the mobile moves around in the environment, $|E_{\lambda\theta p}|$ will be Rayleigh fading. Clearly, θ in (5.18) represents the direction of arrival.

Andersen et al have described θ as a stochastic process and pointed out that $u=sin\theta$ has a known distribution [98], a Student's t-distribution [95]. They have derived the power conditioned on $u=sin\theta$ for (5.18) based on the Student's t-distribution of angle-of-arrival [95], i.e., the power spectrum,

$$E[|E_{\lambda\theta p}(u)|^2 \quad |u] = \frac{s^2}{(u-\bar{u})^2 + s^2}, \tag{5.19}$$

where $\bar{u} = \int uP(u)du/P$, $\overline{u^2} = \int u^2 P(u)du/P$ are the first and second moments of the average power distribution measured in u-space, and

$$s^2 = \overline{u^2} - \bar{u}^2 \tag{5.20}$$

is a measure of angular spread. Here $P(u)$ is the true distribution of power as a function of u and $P = \int P(u)du$ is the total power. This spectrum is identical for every receive antenna element because the distribution of angle-of-arrival is identical to every receive antenna element. This power spectrum is in agreement with indoor measurements for two

different building [92,99] and outdoor measurements for a macro-cellular typical urban environment [93].

5.3.3 The covariance based on the power spectrum

We transform the variable θ into $u=sin\theta$. Substituting (5.19) into (5.15) and (5.15) into (5.14) leads to

$$E[H_{lp}H_{mq}^{*}]=\begin{cases}\dfrac{\sqrt{D_{al}D_{am}}}{\sigma_{lp}\sigma_{mp}}\displaystyle\int_{A}\dfrac{s^{2}}{(u-\bar{u})^{2}+s^{2}}[XPD_{pq}F_{\theta l}(u,\varphi_{0})F_{\theta m}^{*}(u,\varphi_{0}) \\ \qquad +F_{\varphi l}(u,\varphi_{0})F_{\varphi m}^{*}(u,\varphi_{0})]\dfrac{1}{\sqrt{1-u^{2}}}du, & p=q, \\ 0, \qquad p\neq q\end{cases} \tag{5.21}$$

where

$$\sigma_{ip}=[D_{al}\int_{A}\frac{s^{2}}{(u-\bar{u})^{2}+s^{2}}\frac{[XPD_{pp}\mid F_{\theta i}(u,\varphi_{0})\mid^{2}+\mid F_{\varphi i}(u,\varphi_{0})\mid^{2}]}{\sqrt{1-u^{2}}}du]^{1/2}, \tag{5.22}$$

and $\varphi_{0}=\pi/2$.

It is seen that $E[H_{lp}H_{mq}^{*}]$=1 when l=m. In (5.21), the parameters are the range of incident waves A, the angel spread s, the XPD, the antenna pattern, the distance between two adjacent receive antenna elements, and the arrangement of the antenna array.

5.4 Antenna array

As in Chapter 4, we choose ten antennas in the simulation: four antennas in the transmitter and six antennas in the receiver. For the transmit antennas, the space between any two antenna elements is so large that there is no correlation between them although they don't occur explicitly in (5.21). For the receive antennas, we choose three linear arrays. In each linear array, the antenna elements are identical. They are either the half-wave dipole antennas or half-wave square patch microstrip antennas as we have employed in Chapter 4. The distance between two adjacent antenna elements is *dr*.

Case 1 : The vertical linear array

The vertical linear array is shown in Fig. 5.3. There are two coordinate systems. One is the *z-y* coordinate system for the receive array. Another is the *z'-y'* coordinate system for the receive antennas. The relation between θ and θ' is defined by $\theta' = \theta_r - 90^0 - \theta$.

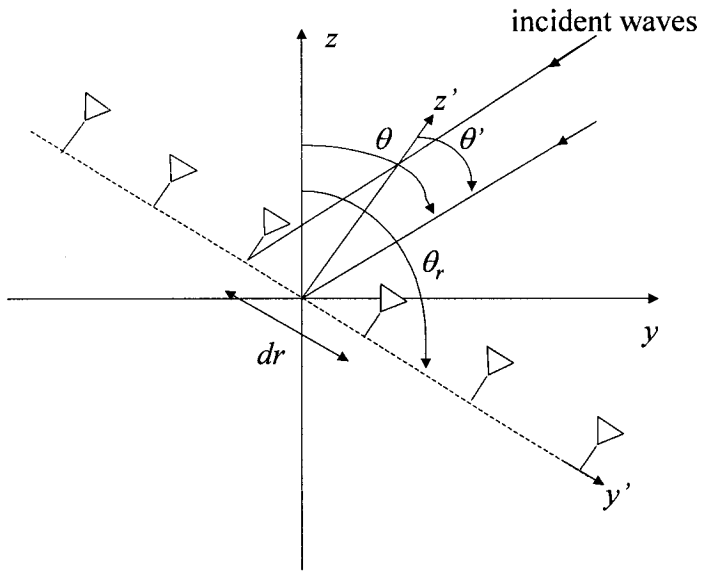

(a)

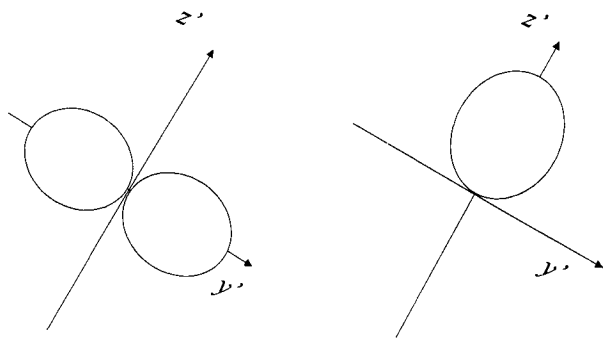

(b)

Fig. 5.3. (a) The vertical linear array. (b) The antenna patterns.

Case 2: The horizontal linear array

The horizontal linear array is shown in Fig. 5.4, in which θ' related to θ is given by $\theta' = 180^0 - \theta_r + \theta$.

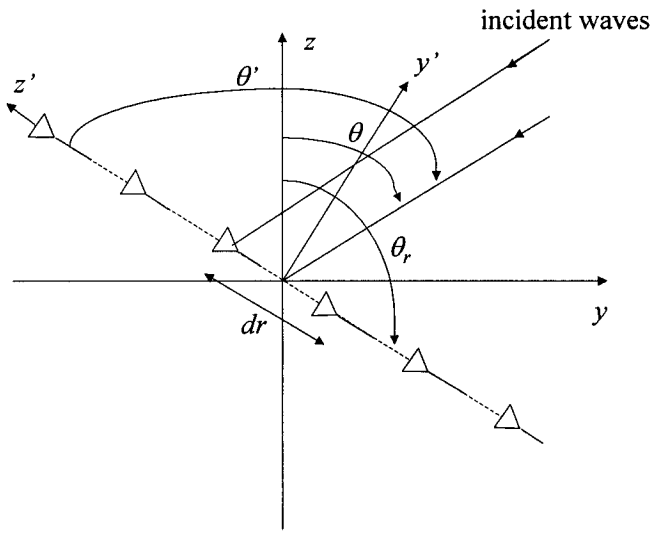

(a)

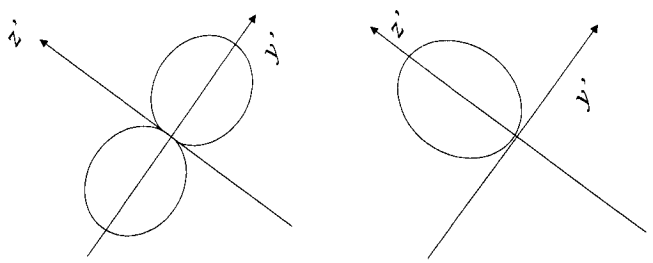

dipole antenna microstrip antenna

(b)

Fig. 5.4. (a) The horizontal linear array. (b) The antenna patters.

Case 3: The hybrid linear array.

The hybrid linear array is shown in Fig. 5.5. In this case, we use three coordinate systems: *z-y*, *z'-y'*, and *z"-y"*. θ' and θ'' related to θ are given as in the first two cases.

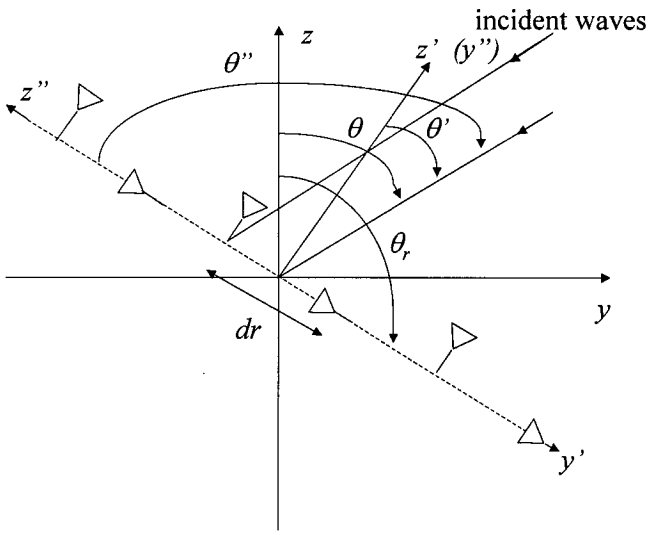

(a)

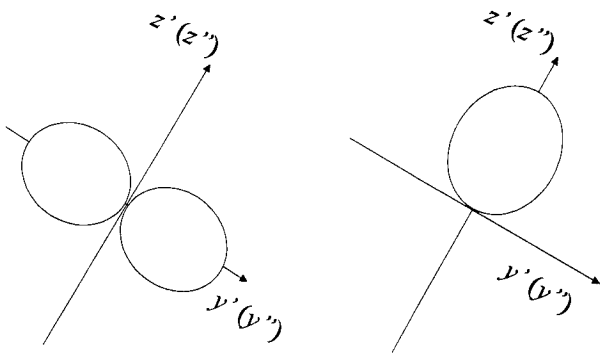

(b)

Fig. 5.5. (a) The hybrid linear array. (b) The antenna patterns.

5.5 Simulation results

We follow the same procedure to calculation the covariance matrix, and then to get the channel transfer matrix and capacity as in section 4.2.2. Since the chosen plane is *y-z*, $\varphi_0 = \pi/2$, the pattern of dipole antenna at $\varphi_0 = \pi/2$ is still (4.11) because the pattern of dipole antenna is not a function of φ

$$F_\theta(\theta', \pi/2) = \frac{\cos[(\pi/2)\cos\theta']}{\sin\theta'}, \tag{5.23a}$$

$$F_\varphi(\theta', \pi/2) = 0. \tag{5.23b}$$

The pattern of microstrip antenna at $\varphi_0 = \pi/2$ is [90]

$$F_\theta(\theta', \pi/2) = 0, \tag{5.24a}$$

$$F_\varphi(\theta', \pi/2) = \frac{\sin[(0.49\pi/\sqrt{\varepsilon_r})\sin\theta']}{(0.49\pi/\sqrt{\varepsilon_r})\sin\theta'}\cos\theta'. \tag{5.24b}$$

(5.23a) and (5.24b) are plotted in Fig. 23b, Fig. 5.4b, and Fig. 5.5b.

With (5.23) and (5.24), the covariance (5.21) can be reduced to

$$E[H_{lp}H^*_{mq}] = \begin{cases} \dfrac{1}{\sigma_{lp}\sigma_{mp}} \displaystyle\int_A \frac{s^2}{(u-\bar{u})^2 + s^2} \frac{F_{al}(u,\varphi_0)F^*_{am}(u,\varphi_0)}{\sqrt{1-u^2}}\,du, & p = q \\ 0, & p \neq q \end{cases}, \tag{5.25}$$

where

$$\sigma_{ip} = [\int_A \frac{s^2}{(u-\bar{u})^2 + s^2} \frac{|F_{\alpha i}(u,\pi/2)|^2}{\sqrt{1-u^2}} du]^{1/2}, \tag{5.26}$$

and $F_{\alpha i}(\theta,\pi/2)$ is (5.23a) for dipole antenna and (5.24b) for microstrip antenna, respectively.

As in Section 5.4, there are four transmit antennas and six receive antennas. The average received SNR ρ is 18 dB. 10% outage capacity is denoted by $C_{0.1}$. For convenience in reading, we use degrees to represent the measure of angular spread s, i.e., $s(degrees) = (s/\pi)\cdot 180^0$. In the following, we set dr/λ=0.5, s=12°, and θ_r=0° as default. However, these can be overridden by new settings. The incident angel is between -30° and 30°, i.e., $-30^0 \le \theta \le 30^0$. So, the incoming waves are mainly from z direction. The power spectrum is plotted in Fig. 5.6.

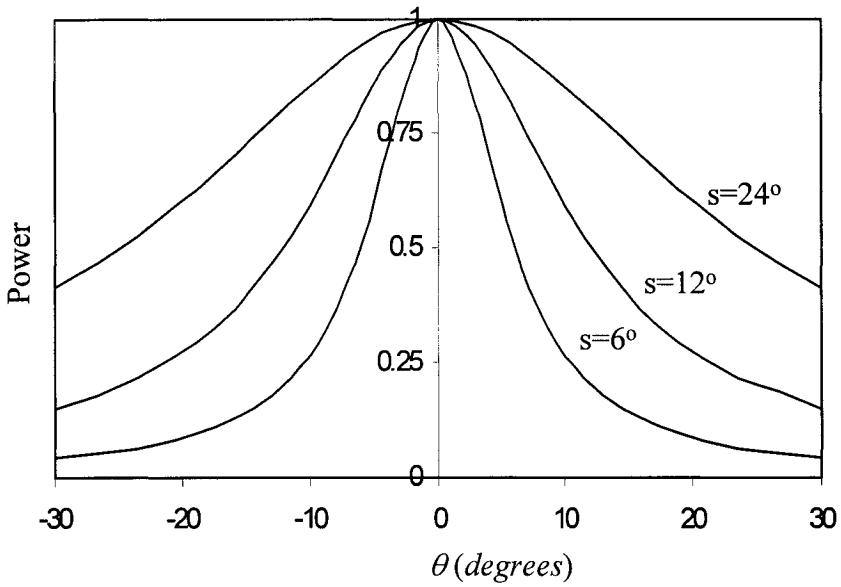

Fig. 5.6. Power spectrum from (5.19).

Fig. 5.7, 5.8, and 5.9 cover case 1. In case 1, the maximum directivity of the microstrip elements is pointed to the z direction, the direction of incident waves when θ_r =90°. However, the maximum directivity of the dipole elements is pointed in the y direction, the null direction of incident waves when θ_r =90°. In Fig. 5.7, we see that the change of $C_{0,1}$ with the spacing is identical with the variation of magnitude of correlation, $E[H_{11}H_{21}^*]$, versus the spacing. Unlike the slow increase of $C_{0,1}$ with the spacing in the "one-ring" model [17] and in Fig. 4.11b, $C_{0,1}$ increases rapidly with the spacing before dr/λ=0.7, as in the "two-ring" model, where there are nonisotropic distributions of scatters around the transmitter and receivers [19]. This is due to the fact that the nonisotropic distribution of scatterers (here and [19]) gives rise to larger correlation than the isotropic distribution of scatterers (Chapter 4 and [17]) when the spacing between

two adjacent antenna elements is small, which can be seen by comparing Fig. 5.7a with Fig. 4.11a. So, dr/λ=0.7 is a critical point, in which the fading correlation coefficients is about 0.5, that the degradation in capacity is small after it. [91] has stated that the degradation in capacity is small even with fading correlation coefficients as high as 0.5 for the diversity reception systems.

Fig. 5.8 shows the ccdfs of capacity increase with s, the measure of angular spread. Similarly, the ccdfs of capacity increase with Δ, the another measure of angle spread, in Figure 4.8 of Chapter 4 and "one-ring" model, et al, [17-19].

Fig. 5.9 shows that $C_{0.1}$ changes with θ_r. When the linear array rotates from the broadside to the incident waves to the inline to the incident waves (see Fig. 5.3), $C_{0.1}$ decreases toward the inline direction (see Fig. 5.9). This is because the difference of signals seen by antenna elements becomes small; consequently, the correlation becomes large when the array rotates from the broadside to the inline. The microstrip $C_{0.1}$ is higher than dipole $C_{0.1}$, which indicates the same results as in Chapter 4.

Fig. 5.10 is for case 2. In case 2, the microstrip elements have maximum directivity in y direction and null in z direction when θ_r =90°, as seen from Fig. 5.4. The dipole elements have maximum directivity in z direction and null in y direction when θ_r =90°.

In contrast with Fig. 5.9, the microstrip $C_{0.1}$ increases with θ_r. That is to say, when the linear array rotates from the broadside to the incident waves to the inline to the incident waves, the microstrip $C_{0.1}$ becomes higher. This is because of the pattern of the microstrip antennas, which is only in the up half-plane. At θ_r =90°, the broadside case, although the difference of signals seen by the microstrip elements is maximum, the

signals received by the microstrip elements are minimum, half signals of $0^0 \leq \theta \leq 30^0$ can not be received by the elements as seen from Fig. 5.4. At θ_r =180°, the inline case, the difference of signals seen by the elements is minimum. However, all signals can be received by the elements.

Similar to Fig. 5.9, the dipole $C_{0.1}$ decreases with θ_r as it is in Fig. 5.9 because the dipole elements are omnidirectional. However, $C_{0.1}$ in Fig. 5.10 is higher than $C_{0.1}$ in Fig. 5.9 because the maximum directivity of dipole elements in Fig. 5.4 is pointed to the incident waves.

Fig. 5.11 covers case 3. In case 3, the antenna elements are cross placed. It is explicitly seen that $C_{0.1}$ in Fig. 5.11 is higher than $C_{0.1}$ in Fig. 5.9 and Fig. 5.10. The cross arrangement of two adjacent elements causes the two elements to have different patterns, which increases the difference of signals received by the two elements and thus reduces the correlation between them. In fact, the cross arrangement of two adjacent elements causes the two elements to have two cross polarizations. Recently, the measurement [42] and analysis [41,100] have indicated that the use of orthogonally polarized receive elements is better than the use of copolarized receive elements. Furthermore, the variation of $C_{0.1}$ in Fig. 5.11 with θ_r is less than it is in Fig. 5.9 and Fig. 5.10.

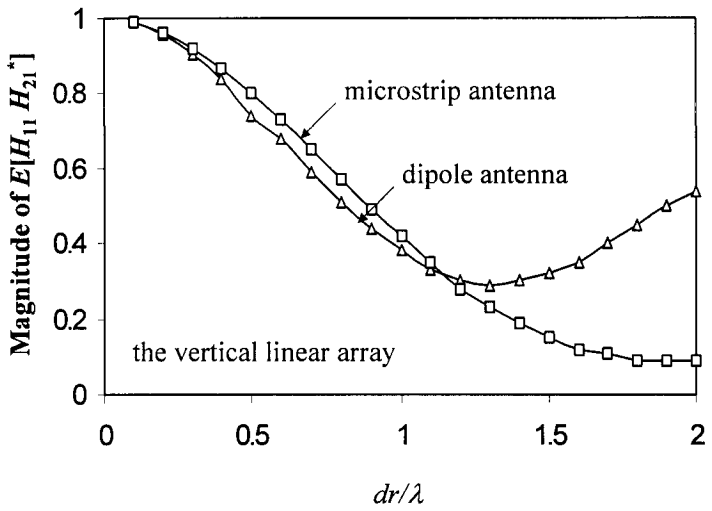

(a)

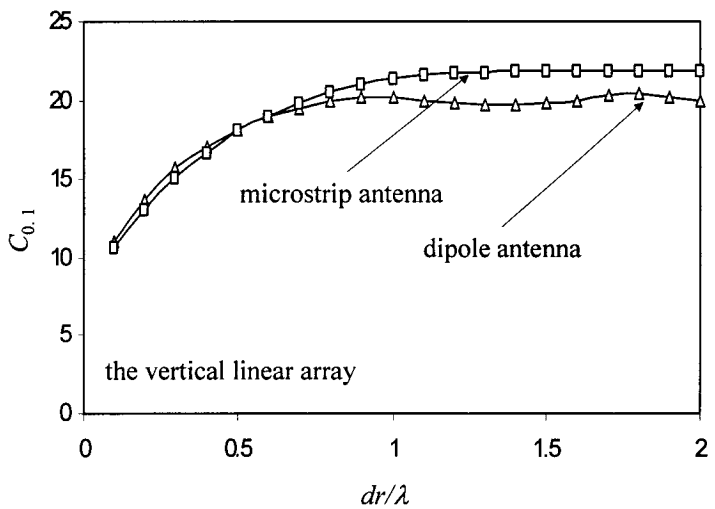

(b)

Fig. 5.7 (a) The correlation of $E[H_{11}H_{21}^*]$ changes with dr for the vertical linear array.

(b) The 10% outage capacity $C_{0.1}$ changes with dr for the vertical linear array.

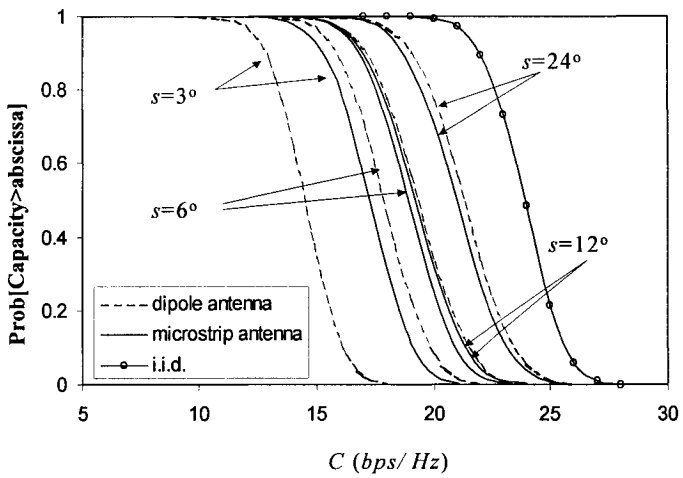

Fig. 5.8 The ccdf of capacity for various angle spreads for the vertical linear array.

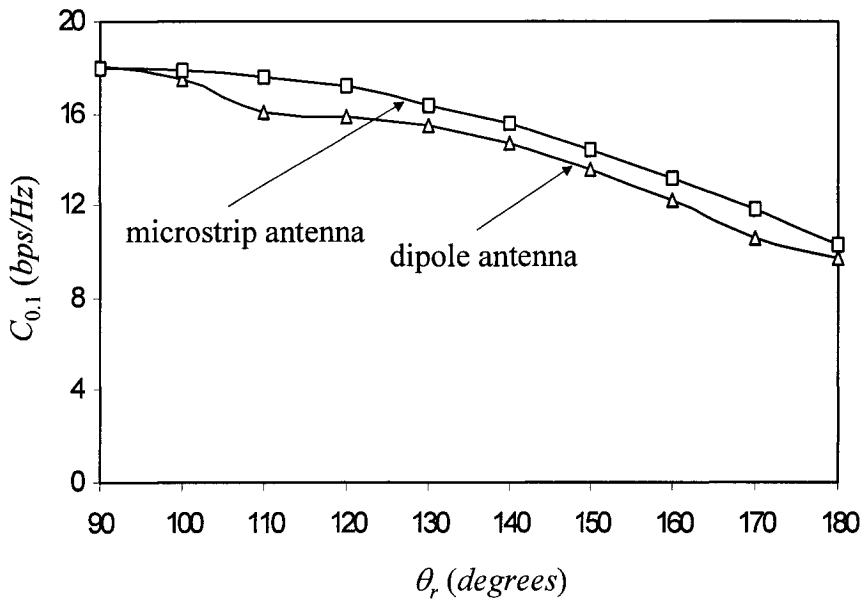

Fig. 5.9 The 10% outage capacity $C_{0.1}$ changes with θ_r for the vertical linear array.

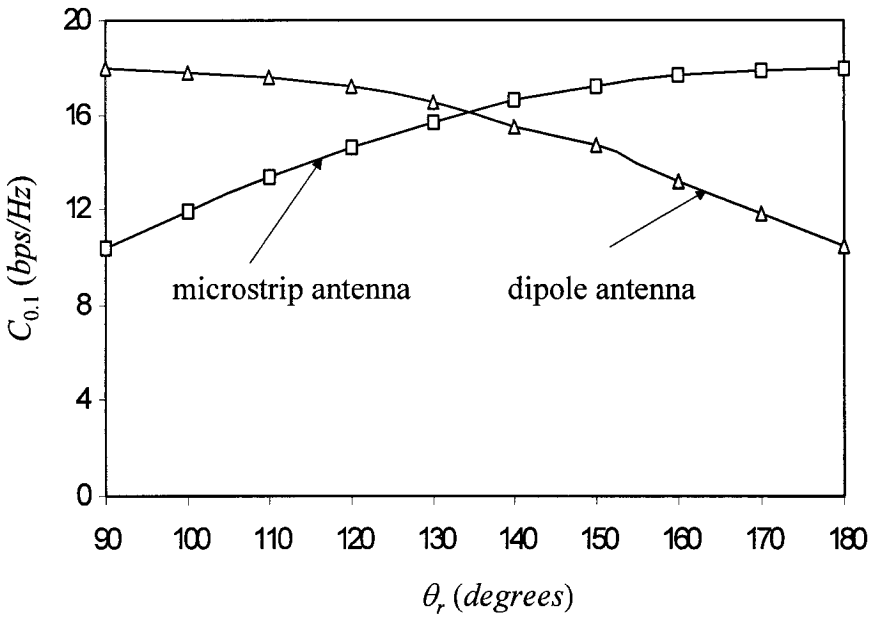

Fig. 5.10 The 10% outage capacity $C_{0.1}$ changes with θ_r for the horizontal linear array.

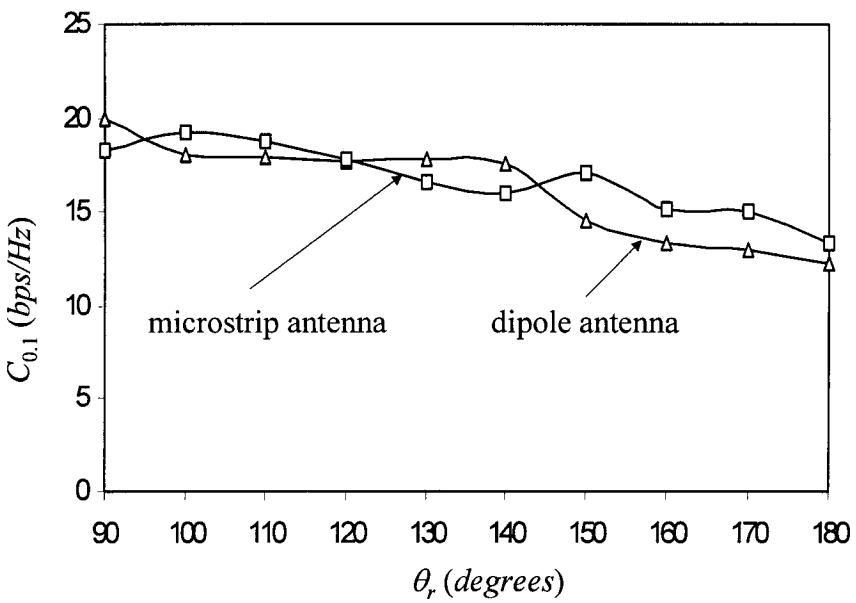

Fig. 5.11 The 10% outage capacity $C_{0.1}$ changes with θ_r for the hybrid linear array.

5.6 Summary

We have used the general path gain to derive a condition for zero-correlation, i.e., to achieve zero correlation, the receive antenna polarization matrix must be orthogonal with the incident source polarization matrix. This condition modified the condition of zero correlation in traditional communication systems.

Then, we derived a covariance matrix based on a statistical power spectrum with a Student's t-distribution of angle-of-arrival of incident waves in the limit where the antenna is not able to resolve the details of the distribution. The power spectrum is confirmed by indoor and outdoor measurements.

We have used the vertical linear array and horizontal linear array to investigate the effect of a half-wave dipole antenna and a half-wave patch microstrip antenna. It is found that the outage capacity is more sensitive to the spacing between two adjacent elements in a nonisotropic distribution of scatterers than in an isotropic distribution of scatterers. The microstrip elements have higher outage capacity than the dipole elements almost in every orientation of the antenna visible region in the vertical linear array, as they behave in the spherical model of uniform scatterers. However, the microstrip elements have a different variation of outage capacity versus orientation with the dipole elements in the horizontal linear array because of their patterns. These results with microstrip elements illustrate that the maximum directivity of antenna elements pointing to the incident waves is important. Nevertheless, the results with dipole elements don't show that it is important to have the maximum directivity of antenna elements pointed to the incident waves.

To investigate how to reduce the correlation in view of the condition for zero correlation, we study the hybrid linear array, in which two adjacent elements are crossly placed and form cross polarization. This linear array produces lower correlation and thus higher outage capacity than the vertical and horizontal linear arrays do.

Chapter 6 Summary

In this thesis, we first consider the history, motivation, and important research areas of multiple-input multiple-output communication systems. Then, we introduce the detailed derivation of the fundamental capacity formula of multiple-input multiple-output systems for a narrow band channel under the assumption that the transmitter does not know the channel state information, but the receiver does.

Based on the fundamental capacity formula, we show that the outage capacity of $n_T=N_1$ and $n_R=N_2$ is greater than the outage capacity of $n_T=N_2$ and $n_R=N_1$ when they are with the same *SNR* and $N_2> N_1$ for i.i.d. Rayleigh fading channels. Also, based on the formula, we use Monte-Carlo simulation to find the number of antennas for the point of diminishing return of outage capacity. In general, for a small number of transmit antennas, six receive antennas reach the point of diminishing return. However, for a small number of receive antennas, four transmit antennas reach the point of diminishing return.

Later in the thesis, we study the factor of correlation in the fundamental capacity formula. We extend the "one-ring" model to the spherical model so that we can consider the effects of the antenna parameters such as the antenna field pattern and orientation on the information-theoretic capacity. In this model, scatterers around the subscriber unit (receiver) are distributed over the sphere centered on the antenna array in the subscriber unit. Based on assumptions that the transmitting power is constant and the receiving power is the same for any type of receiving antennas if the incident waves are uniformly distributed over the sphere centered on the receiving antennas, we present the expressions of the channel transfer function and its covariance matrix, which is

appropriate for the study of different antenna types and different antenna orientations in the space in MIMO systems. In the simulations, the transmitting antenna elements are isotropic, and the receiving elements are half-wave dipole antennas and half-wave square patch microstrip antennas, respectively. The receiving isotropic antennas are taken for the purpose of comparison. In the transmitter, a linear array and a square array are chosen. In the receiver, a linear array and a rectangular array are set. We take 10 antennas and place four antenna elements in the transmitter and six in the receiver. The arrangement of unequal antenna numbers could be meaningful in a realistic communications system. In the uplink, more antennas in the base station (transmitter) having lower capacity are compensated by higher transmitting power of the base station. In the downlink, lower transmitting power of the mobile station (transmitter) having lower capacity is compensated by more antennas in the base station (receiver) having higher capacity.

When both the transmitter and receiver are linear and lie broadside to one another, the pdfs of the first eigenvalues with dipole and microstrip elements are almost the same, but the pdf of the second eigenvalue with microstrip elements has larger mean value and variance than that with the dipole elements, which gives the result that the outage capacities with the microstrip elements are higher than those with dipole elements for the same angle spread at different spread angles. The capacities with the microstrip elements are generally higher than those with the dipole elements for most of orientations. The maximum difference between them is about 1 bits/s/Hz or 10%. This means that the microstrip antennas provide lower correlation in the covariance matrix than the dipole antennas in the scatter-rich environment. It can be expected that antenna

directivity plays a more important role when its directivity is higher and the incident waves are not from uniformly distributed scatterers. Similar experimental observations can be found in [42]. Furthermore, the use of an antenna field pattern to achieve the parallel channels in the line of sight environment of MIMO systems can be found in [16].

In all inline cases, the capacities change very slightly with angular angle for any type of antenna because the correlations are high.

In the case that both the transmitting array and the receiving array are square and rectangular arrays, respectively, the variations of the capacities with angular angle are smoother than when the transmitting array is linear broadside.

Furthermore, we consider a realistic scattering environment instead of the uniform scatterers in the spherical model of Chapter 4 so that we can investigate the effect of antenna pattern in the correlation in a more realistic situation. We use the general path gain to derive a condition for zero-correlation, i.e., to achieve zero correlation, the receive antenna polarization matrix must be orthogonal with the incident source polarization matrix. This condition modified the condition of zero correlation in traditional communication systems.

Next, we derive a covariance matrix based on a statistical power spectrum with a Student's *t*-distribution of angle-of-arrival of incident waves in the limit where the antenna is not able to resolve the details of the distribution. The power spectrum is in good agreement with indoor and outdoor measurements.

We use the vertical linear array and horizontal linear array to investigate the effect of half-wave dipole antenna and half-wave patch microstrip antenna. It is found that the outage capacity is more sensitive to the spacing between two adjacent elements in a

nonisotropic distribution of scatterers than in an isotropic distribution of scatterers. The microstrip elements have higher outage capacity than the dipole elements almost in every orientation of the antenna visible region in the vertical linear array. However, the microstrip elements have a different variation of outage capacity versus orientation with the dipole elements in the horizontal linear array because of their pattern. These results with microstrip elements illustrate that the maximum directivity of antenna elements pointing to the incident waves is important. Nevertheless, the results with dipole elements don't show that it is important to have the maximum directivity of antenna elements pointed to the incident waves.

To investigate how to reduce the correlation in view of the condition for zero correlation, we study the hybrid linear array, in which two adjacent elements are crossly positioned and form cross polarization. This linear array produces lower correlation and thus higher outage capacity than the vertical and horizontal linear arrays.

As we have discussed above, we have made the following contribution to the MIMO :

1) The outage capacity of a wireless channel is capacity under the condition of a specified probability of outage. We have analytically verified the previously known result that the outage capacity of a MIMO system with N_1 transmit antennas and N_2 receive antennas is higher than that of a MIMO system with N_2 transmit antennas and N_1 receive antennas when they have the same signal-to-noise ratio and $N_1 < N_2$ in the independent and identically distributed Rayleigh fading channel;

2) We have numerically illustrated that six receive antennas reach the point of capacity diminishing returns for a small number of transmit antennas and four transmit antennas reach the point for a small number of receive antennas;

3) We have developed a spherical model to study the effect of antenna physics on the capacity of MIMO systems. We show that the microstrip patch antenna linear array has a higher capacity than the dipole linear array when they are in the broadside of the transmitter under the environment that scatterers are uniformly distribution over a sphere;

4) We have derived a condition of zero correlation for MIMO systems, i.e., the receive antenna polarization matrix must be orthogonal with the incident source polarization matrix, which extends the condition of zero correlation for the traditional communications systems, in which there is only one antenna in an end and multiple antennas in the another end;

5) We have derived a correlation model based on the Student's *t*-distribution of angle-of-arrival, which is accurate in the micro-cell environment. With this model, we have shown that the cross linear array has higher capacity than the vertical and horizontal linear arrays, indicating that this array is closer to the condition of zero correlation.

In brief, the effect of antenna pattern on the capacity strongly depends on the distribution of incident waves. In the vertical case, the microstrip antennas achieve higher capacity than the dipole antennas. In the scattering environment of Student's *t* distribution of angle-of-arrival, antennas have higher capacity than in the scattering environment with scatterers distributed uniformly around the receiver. Further study is required to show how to use the antenna array and antenna pattern to form a receive

antenna polarization matrix close to be orthogonal with the incident source polarization matrix in order to approach the condition of zero correlation.

In terms of present research, the future work is: 1) with the correlation models developed in this thesis, we continue to investigate effects of different antenna patterns on the capacity of MIMO systems and find out that what kind of pattern has higher capacity; 2) we continue to investigate more kinds of antenna arrays and find out that what kind of antenna array has higher capacity; 3) based on the theoretical work, we make an experiment. In the experiment, we first measure the distribution of the incident waves. And then, we measure the path gain with different type of antenna and find out the channel transfer matrix. At last, according to the capacity calculated from the measured data, we try to find the type of antenna having high capacity over different directions.

References

[1] W. C. Jakes, Ed., *Microwave mobile communications*, New York: Wiley, 1974.

[2] R. G. Vaughan and J. B. Andersen, "Antenna diversity in mobile communications," *IEEE Transaction on Vehicular Technology,* vol.36, pp.149-172, Nov.1987.

[3] A. Wittneben, "Base station modulation diversity for digital SIMULCAST," in *Proceeding of IEEE Vehicular technology Conference (VTC 41st),* pp.848-853, May 1991.

[4] A. Wittneben, "A new bandwidth efficient transmit antenna modulation diversity scheme for linear digital modulation," in *Proceeding of IEEE International Conference on Communications (ICC'93)*, pp.1630-1634, May 1993.

[5] N. Seshadri and J. H. Winters, "Two signaling schemes for improving the error performance of FDD transmission systems using transmitter antenna diversity," in *Proceeding of IEEE Vehicular Technology Conference (VTC 43rd),* pp.508-511, May 1993.

[6] J. H. Winters, "The diversity gain of transmit diversity in wireless systems with Rayleigh Fading," in *Proceeding of the1994 ICC/SUPERCOMM*, New Orleans, LA, vol. 2, pp.1121-1125, May 1994.

[7] S. M. Alamouti, " A simple transmit diversity technique for wireless communications," *IEEE Journal of Selected Areas in Communications,* vol.16, no.8, pp. 1451-1458, Oct. 1998.

[8] R. B. Ertel, P. Cardieri, K.W. Sowerby, T. S. Rappaport, and J. H. Reed, "Overview of spatial channel models for antenna array communication systems," *IEEE Personal Communications,* vol.5, pp. 10-22, Feb., 1998.

[9] J. Winters, "On the capacity of radio communication systems with diversity in a Rayleigh fading environment," *IEEE Journal of Selected Areas in Communications,* vol. 5, pp. 871-878, June,1987.

[10] G. J. Foschini and M. J. Gans, "On limits of wireless communications in a fading environment when using multiple antennas," *Wireless Personal Communications,* vol.6, pp.311-355,1998.

[11] G. J. Foschini, "Layered space-time architecture for wireless communication in a fading environment when using multi-element antennas," *AT&T Bell Labs Technical Journal,* pp.41-59, 1996.

[12] E. Telatar, " Capacity of multiantenna Gaussian channels," *AT&T Bell Laboratories, Technical Memo,* June, 1995.

[13] E. Telatar, "Capacity of multiantenna Gaussian channels," *European Transactions on Telecommunications,* ETT, vol.10, no.6, pp.585-595, 1999.

[14] G. Raleigh and J. M. Cioffi, "Spatial-temporal coding for wireless communications," *IEEE Transaction on Communications,* vol.46, pp.357-366, 1998.

[15] H. Bolcskei, D. Gesbert, and A. J. Paulraj, "On the capacity of OFDM based spatial multiplexing systems," *IEEE Transaction on Communications,* vol.50, pp.225-234, Feb. 2002.

[16] P. F. Driessen, G. J. Foschini, "On the capacity formula for multiple input-multiple output wireless channels: a geometric interpretation," *IEEE transaction on communications,* vol. 47, no. 2, pp. 173-176, Feb. 1999.

[17] Da-Shan Shiu, G. J. Foschini, M. J. Gans, and J.M. Kahn, "Fading correlation and its effect on the capacity of multielement antenna systems," *IEEE Transaction on Communications,* vol.48, no.3, pp.502-513, Mar. 2000.

[18] Ali Abdi, Mostafa Kaveh, "A space-time correlation model for multielement antenna systems in mobile fading channels," *IEEE Journal of Selected Areas in Communications,* vol.20, no.3, pp.550-560, 2002.

[19] Geoffrey J. Byers, and Fambirai Takawira, "Spatially and temporally correlated MIMO channels : modeling and capacity analysis," *IEEE Transaction on Vehicular Technology,* vol. 53, no.3, pp.634-643, 2004.

[20] M. Chiani, M.Z. Win, and A. Zanella, "On the capacity of spatially correlated MIMO Rayleigh-fading channels," *IEEE Transaction on Information Theory*, vol. 49, no.10, pp. 2363-2371, Oct. 2003.

[21] D. Chizhik, G. Foschini, and R. A. Valenzuela, "Capacities of multielement transmit and receive antennas: Correlation and keyholes," *Electronic Letters*, pp. 1099-1100, 2000.

[22] S. Loyka and A. Kouki, "New compound upper bound on MIMO channel capacity," *IEEE Communications Letters,* vol.6, no.3, pp. 96-98, Mar., 2002.

[23] X. Mestre, J. R. Fonollosa, Alba Pages-Zamora, "Capacity of MIMO channels : asymptotic evaluation under correlated fading," *IEEE Journal of Selected Areas in Communications,* vol. 21, no. 5, pp. 829-838, 2003.

[24] A. Goldsmith, S. A. Jafar, N. Jindal, and S. Vishwansth, "Capacity limits of MIMO channels," *IEEE Journal of Selected Areas in Communications,* vol. 21, no.5, pp. 684-702, 2003.

[25] D. Gesbert, H. Bolcskei, D. Gore, and A. Paulraj, "Outdoor MIMO wireless channels: models and performance prediction," *IEEE Transaction on Communications,* Vol. 50, No. 12, pp. 1926-1934, Dec., 2002.

[26] L. J. Greenstein, S. Ghassemzadeh, V. Erceg, and D. G. Michelson, "Theory, experiments, and statistical models," in *Proc. of the Second International Symposium on Wireless Personal Multimedia Communications (WPMC 99 Conf.),* Amsterdam, Sept., pp. 400-403, 1999.

[27] D. S. Baum, D. A. Gore, R. U. Nabar, S. Panchanathan, K. V. S. Hari, V. Erceg, and A. J. Paulraj, "Measurements and characterization of broadband MIMO fixed wireless channels at 2.5 GHz," in *Proceedings IEEE International Conference on Personal Wireless Communications (ICPWC 2000)*, Hyderabad, pp. 203-206, Dec., 2000.

[28] S. Pitchaiah, V. Erceg, D. Baum, R. Krishnamoorthy, and A. Paulraj, "Analysis and modeling of multiple-input multiple-output (MIMO) radio channel based on outdoor measurements conducted at 2.5 GHz for fixed BWA applications," in *Proc. International Conference on Communications*, Volume 1, pp.272 – 276, 28 April-2 May 2002.

[29] E. Green, "Radio link design for microcellular systems," *BELL SYSTEM TECHNICAL JOURNAL* , vol. 8, no.1, pp. 85-96, 1990.

[30] C.-N. Chuah, J. M. Kahn, and D. Tse, "Capacity of indoor multiantenna array systems in indoor wireless environment," in *Proc. IEEE GLOBECOM'98*, Sydney, Austrian, pp. 1894-1899, 1998.

[31] R. Stridh, B. Ottersten, and P. Karlsson, "MIMO channel capacity on a measured indoor radio channel at 5.8 GHz," in *Proc. Asilomar Conference on Signals, systems and computers*, pp.733-737, Oct., 2000.

[32] J. Fuhl, A. F. Molisch, and E. Bonek, "Unified channel model for mobile radio systems with smart antennas," in *Proc. Inst. Elect. Eng., Radar, Sonar Navigation*, vol. 145, pp.32-41, 1998.

[33] Chen-Nee Chuah, David N. C. Tse, Joseph M. Kahn, and Reinaldo A. Valenzuela, "Capacity scaling in MIMO wireless systems under correlated fading," *IEEE Transaction on Information Theory*, vol.48, no.3, pp. 637-650, Mar., 2002.

[34] S. J. Fortune, D. H. Gay, B. W. Kernighan, O. Landron, R. A. Valenzuela, and M. H. Wright, "WiSE design of indoor wireless systems: practical computation and optimization," *IEEE Computational Science and Engineering,* vol. 2, pp. 58-68, Mar., 1995.

[35] C. A. Zelley and C. C. Constantinou, "A three-dimensional parabolic equation applied to VHF/UHF propagation over irregular terrain," *IEEE Transactions on Antennas and Propagation,* vol. 47, pp. 1586-1596, Oct., 1999.

[36] Ronan Bradly and Peter James Cullen, "Incorporation of first-order polarization coupling in UHF propagation over gently undulating terrain using a perfect reflecting surface model," *IEEE Journal of Selected Areas in Communications,* vol. 20, no. 6, pp. 1144-1150, Aug., 2002.

[37] Andreas F. Molisch, Martin Steinbauer, Martin Toeltsch, Ernst Bonek, Reiner S. Thoma, "Capacity of MIMO systems based on measured wireless channels," *IEEE Journal of Selected Areas in Communications*, vol. 20, no. 3, pp. 561-569, Apr., 2002.

[38] Jean Philippe Kermoal, Laurant Schumacher, Klaus Ingemann Pedersen, Preben Elgaard, and Frank Frederiksen, "A stochastic MIMO radio channel model with experimental validation," *IEEE Journal of Selected Areas in Communications,* vol. 20, no. 6, pp. 1211-1226 , Aug., 2002.

[39] J. P. Kermoal, P. E. Mogensen, S. H. Jensen, J. B. Andersen, F. Frederiksen, T. B. Sorensen, and K. I. Pedersen, "Experimental investigation of multipath richness for multi-element transmit and receive antenna arrays," in *Proc. IEEE Vehicular Technology Conf.*, Tokyo, Japan, pp. 2004-2008, May 2000.

[40] P. Kyritsi, D. C. Cox, R. A. Valenzuela, and P. W. Wolniansky, "Correlation analysis based on MIMO channel measurements in an indoor environment, " *IEEE Journal of Selected Areas in Communications*, vol. 21, no. 5, pp. 713-720, Jun., 2003.

[41] P. Kyritsi, D. C. Cox, R. A. Valenzuela, and P. W. Wolniansky, "Effect of antenna polarization on the capacity of a multiple element system in an indoor environment," *IEEE Journal of Selected Areas in Communications,* vol. 20, no. 6, pp. 1227-1239, Aug., 2002.

[42] K. Sulonen, P. Suvikunnas, L. Vuokko, J. Kivinen, and P. Vainikainen, "Comparsion of MIMO antenna configuration in picocell and microcell environments," *IEEE Journal of Selected Areas in Communications,* vol. 21,no 5, pp. 703-712, Jun., 2003.

[43] M. Herdin, H. Ozcelik, H. Hofstetter and E. Bonek, "Variation of measured indoor MIMO capacity with receive direction and position at 5.2 GHz," *Electronics Letters*, vol. 38, no.21, pp. 1283-1285, oct., 2002.

[44] A. Wittneben, "A new bandwidth efficient transmit antenna modulation diversity scheme for linear digital modulation," in *Proceeding of IEEE International Conference on Communications (ICC'93)*, vol. 3, Geneva, Switzerland, pp. 1630-1634, 1993.

[45] N. Seshadri and J. H. Winters, "Two schemes for improving the performance of frequency-division duplex (FDD) transmission systems using transmitter antenna diversity," *International Journal of Wireless information networks*, vol. 1, pp. 49-60, Jan., 1994.

[46] V. Tarokh, N. Seshadri, and A. R. Calderbank, "Space-time codes for high data rate wireless communication: Performance criterion and code construction," *IEEE Transaction on Information Theory*, vol. 44, pp.744-765, Mar., 1998.

[47] M. P. Fitz and J. V. Krogmeier, "Further results on space-time codes for Rayleigh fading," in *Proc. Allerton conference on communicaion*, pp. 391-400, Sept., 1998.

[48] Q. Yang and R. S. Blum, "Optimum space-time convolutional codes for quasi-static slow fading channels," in *Proc. Wireless Communications and Networking Conf.*, pp. 1351-1355, Sept., 2000.

[49] S. Baro, G. Bauch, and A. Hansmann, "Improved codes for space-time trellis-coded modulation," *IEEE Communications Letters,* vol. 1, pp. 20-22, Jan., 2000.

[50] A. R. Hammons and H.E. Gamal, "On the theory of space-time codes for psk modulation," *IEEETranscction on Information Theory*, vol. 46, pp. 524-542, Mar., 2000.

[51] Z. Chen, J. Yuan, and B. Vucetic, "Improved space-time trellis coded modulation scheme on slow fading channels," in *Proc. IEEE International Conference on Communications*, Volume 4, pp.1110 – 1116, 11-14 June, 2001.

[52] Y. Liu, M. P. Fitz, and O. Y. Takeshita, "A rank criterion for QAM space-time codes," in Proc. *IEEE International Symposium on Information Theory*, pp. 3062-3079, Dec., 2000.

[53] S. Alamouti, "Space block coding: A simple transmitter diversity technique for wireless communications," *IEEE Journal of Selected Areas in Communications,* vol.16, pp. 1451-1458, Oct., 1998.

[54] V. Tarokh, H. Jafarkhani, and A. R. Calderbank, " Space-time block codes from orthogonal designs," *IEEE Transaction on Information Theory*, vol. 45, pp. 1456-1467, Jul., 1999.

[55] V. Tarokh, H. Jafarkhani, and A. R. Calderbank, "Space-time block codes for wireless communications: performance results," *IEEE Journal of Selected Areas in Communications,* vol. 17, pp. 451-460, Mar., 1999.

[56] G. Ganesan and P. Stoica, "Space-time diversity using orthogonal and amicable orthogonal designs," *Wireless Personal Communications,* vol. 18, pp. 165-178, Aug., 2001.

[57] H. Jafarkhani, "A quasi orthogonal space time block code," *IEEE Transaction on Communications,* vol. 49, pp. 1-4, Jan., 2001.

[58] D. Gesbert, L. Haumonte, H. Bolcskei, and A. Paulraj, "Technologies and performance for nonline-of-sight broadband wireless access networks," *IEEE Communication Magazine*, vol. 40, pp. 86-95, Apr., 2002.

[59] M. S. Pinsker, *Information and information stability of random processes*, Holden Bay, San Francisco, Chapter 10, 1964.

[60] G. J. Foschini and R. K. Mueller, "The capacity of linear channels with additive Gaussian noise," *BELL SYSTEM TECHNICAL JOURNAL*, pp. 81-94, 1970.

[61] M. S. Pinsker, *Information and information stability of random processes*, J. Wiley and Sons, New York, Chapter IV, 1968.

[62] S. Kullback, *Information theory and statistics*, Addison-Wesley, Massachusetts, 1974.

[63] D. B. Osteyee and I . J. Good, *Information weight of evidence, the singularity between probability measures and signal detection*, Springer-Verlag, New York, 1970.

[64] P. Lancaster and M. Tismenetsky, *The theory of Matrices*, Academic Press, P. 46, 1985.

[65] J. R. Pierce and E. C. Posner, *Introduction to communication science and systems*, Plenum Press, New York, Chapter 11, 1980.

[66] R. M. Fano, *Transmisssion of information*, John Wiley and Sons, New York, pp. 168-178, 1961.

[67] R. G. Gallager, *Information theory and reliable communication*, John Wiley and Sons, New York, Chapter IV, 1968.

[68] A.T. James, "Distributions of matrix variates and latent roots derived from normal samples," *The Annals of mathematical statistics,* vol.35, pp.475-501, pp.475-501,1964.

[69] J. B. Anderson, "Antenna arrays in mobile communications: gain, diversity and channel capacity," *IEEE Antenna and Propagation Magazine*, pp.12-16, Apr. 2000.

[70] D. Chizhik, F. Rashid-Farrokhi, J. Ling, and A. Lozano, "Effect of antenna separation on the capacity of BLAST in correlated channels," *IEEE communications Letters*, vol.4, pp.337-339, Nov. 2000.

[71] H.Boelcskei,A.J.Paulraj,K.V.S.Hari,R.U.Nabar, and W.W.Lu, "Fixed broadband wireless access: state of art,challenges, and future directions," *IEEE communication magazine*, pp.100-108, 2001.

[72] G.J.Foschini, D.Chizhik, M.J.Gans, C.Papadias, and R.A.Valenzuela, "Analysis and performance of some basic space-time architectures," *IEEE Journal of Selected Areas in Communications*, vol.21, no.3, pp.303-320, Apr. 2003.

[73] Franz E. Hohn, *Elementary matrix algebra*, second edition, the Macmillan company, Collier-Macmillan limited, London, 1970.

[74] R. A. Horn and C. R. Johnson, *Matrix analysis*, 1st ed Cambridge, Cambridge Univ. Press, U.K., 1990.

[75] G.J. Foschini and R. Valenzuela, "Initial estimation of communication efficiency of indoor wireless channel," *Wireless networks*, vol.3, pp.141-154, 1997.

[76] Claude Oestges, Vinko Erceg, and Arogyaswami J. Paulraj, "Propagation modeling of MIMO multipolarized fixed wireless channels," *IEEE Transaction on Vehicular Technology*, vol.53, no.3, pp.644-654, May 2004.

[77] T. Aulin, "A modified model for he fading signal at the mobile radio channel," *IEEE Transaction on Vehicular Technology*, vol.28, pp.182-202, Aug. 1979.

[78] J. D. Parsons and M. D. Turkmani, "Characterization of mobile radio signals: model description," *Proc. Inst. Elect. Eng.*, pt. I, vol. 138, pp.459-556, 1991.

[79] Ole Norklit and J. Bach Andersen, "Diffuse channel model and experimental results for array antennas in mobile environments," *IEEE transaction on Antennas and Propagation*, vol. 46, no.6, pp.834-840, June 1998.

[80] Yahya Z. Mohasseb and Michael P. Fitz, "A 3-D spatio-temporal simulation model for wireless channels," *IEEE Journal of Selected Areas in Communications,* vol. 20, no. 6, pp.1193-1203, August 2002.

[81] W.C.Y. Lee, " Effects on correlation between two mobile radio base station antennas," *IEEE Transaction on Communications*, vol.com-21, pp.1214-1224, Nov. 1973.

[82] R.E. Collin and F. Zucker, *Antenna theory*, part 1, New York: McGraw-Hill, 1969.

[83] Xiongwen Zhao, Jarmo Kivinen, Pertti Vainikainen, and Kari Skog, "Characterization of Doppler spectra for mobile communications at 5.3 Ghz," *IEEE Transaction on Vehicular Technology*, vol. 52, no. 1, pp.14-23, Jan. 2003.

[84] J.M. Wozencraft and I.M. Jacobs, *Principle of Communication Engineering*, New York: Wiley, 1965, pp.527-532.

[85] E.I. Telatar and D. Tse, "Capacity and mutual information of broad-band multipath fading channels," In *Proc. IEEE International Symposium on Information Theory*, p.188, 1998.

[86] K. Yu, M. Bengtsson, B. Ottersten, D. McNamara, P. Karlsson, and M. Beach, "Second order statistics of NLOS indoor MIMO channels based on 5.2 Ghz measurements," in *Proc. IEEE GLOBECOM'01*, San Antonio, Texas, USA, pp. 156-160, Nov. 2001.

[87] C.G. Khatri, " On certain distribution problems based on positive definite quadratic functions in normal vectors," *The Annals of mathematical statistics*, vol.37, pp.468-479, 1966.

[88] N.A.S. Crowther and D.J. de Waal, "On the distribution of a generalized positive semidefinite quadratic form of normal vectors," *South African Statistical Journal*, vol.7, pp.119-127, 1973.

[89] J. Gong, J.F. Hayes and M.R. Soleymani, "Comparison of capacities of the transmit antenna diversity with the receive antenna diversity in the MIMO scheme", In *Proc. IEEE CCECE 2003*, vol. 1, Montreal, pp.179-182, May 4-7, 2003.

[90] Warren L. Stutzman, Gary A. Thiele, *Antenna theory and design*, John Wiley and Sons, 2nd edition, New York, 1998.

[91] J. Salz and J. H. Winters, "Effect of fading correlation on adaptive arrays in digital wireless communications," in *Proc. IEEE Vehicular Technology Conference*, vol. 3, pp. 1758-1774, 1993.

[92] Q. H. Spencer, B. D. Jeffs, M. A. Jensen, and A. L. Swindlehurst, "Modeling the statistical time and angle of arrival characteristics of an indoor multipath channel," *IEEE Journal of Selected Areas in Communications*, vol. 18, pp.347-360, Mar. 2000.

[93] K. I. Pedersen, P. E. Mogensen, and B. Fleur, "A stochastic model of the temporal and azimuthal dispersion seen at the base station in outdoor propagation environments," *IEEE Transaction on Vehicular Technology*, vol. 49, pp.437-447, Mar. 2000.

[94] D. Astely and B. Ottersten, "The effect of local scattering on direction of arrival estimation with MUSIC," *IEEE Transaction on Signal Processing*, vol. 47, pp. 3220-3234, Dec. 1999.

[95] J. B. Andersen and K. I. Pedersen, "Angle-of-arrival statistics for low resolution antennas," *IEEE Transaction on Antennas and propagation*, vol. 50, pp. 391-395, Mar. 2002.

[96] S. Kozono, H. Tsuruhata, and M. Sakamoto, "Base station polarization diversity reception for mobile radio," *IEEE Transaction on Vehicular Technology*, vol. VT-33, no.4, pp. 301-306, 1984.

[97] W. C. Y. Lee and Y. S. Yeh, "Polarization diversity system for mobile radio," *IEEE Transaction on Communications*, vol. 20, no.5, pp. 912-923, 1972.

[98] J. B. Andersen, S. L. Lauritzen, and C. Thommesen, "Distribution of phase derivatives in mobile communications," *Proc. Inst. Elect. Eng.*, vol. 137, pp. 197-201, Aug. 1999.

[99] Q. H. Spencer, B. D. Jeffs, M. A. Jensen, and A. L. Swindlehurst, "A statistical model for angle of arrival in indoor multipath propagation," in *Proc. IEEE Vehicular Technology Conference*, pp. 1410-1414, May 1997.

[100] C. Oestges, Vinko Erceg, and A. J. Paulraj, "Propagation modeling of MIMO multipolarized fixed wireless channels," *IEEE Transaction on Vehicular Technology*, vol.53, no.3, pp. 644-654, 2004.

Appendix A

In this appendix, we will show that the determinant in Eq. 3.1 for (m, 2) has the same form as that of (2, m).

The determinant in Eq. 3.1 for (n, m) is

$$D_{mm,n} = \det[I_m + (\rho / n) HH^+] \,, \tag{A1}$$

where $D_{mm,n}$ denotes the determinant of a square matrix of order (m,m) with n transmit antennas, H is the channel transfer matrix of order (m,n) with each element being the normalized complex Gaussian RV, and the others have the same meaning as in Sec. 3.3. For convenience, we define $\overline{H} = (\rho / n)^{1/2} H$ and denote $A = \overline{H}\,\overline{H}^+$, which is a square matrix; thus, we have $D_{mm,n} = \det(I_m + A)$.

To facilitate the discussion, we introduce the following definition : a major determinant (the word "determinant" is often omitted) of a matrix of order (p, q) is any determinant of maximum order of the matrix[1] . Suppose now that B is of order (m, n) and that C is of order (n, m), where $m \leq n$. Then a major determinant of matrix B and a major determinant of the matrix C are said to be corresponding majors of B and C if and only if the columns of B used to form the major of B have the same indices as do the rows of C used to form the major of C.

[1] A detailed explanation of the matrix properties that are used in this paper can be found in Chapter 2 of Ref.73.

When the r rows and columns struck out of a square matrix A have the same indices, the remaining submatrix is located symmetrically with respective to main diagonal of A, and is called the *rth* principal minor of A.

First, let's check a pair of (2,3) and (3,2). After simple calculation, we can write determinants for the pair as

$$D_{22,3} = 1 + \sum_{i=1}^{2}\sum_{j=1}^{3} \left|\overline{H}_{ij}\right|^2 + \left\|\begin{matrix}\overline{H}_{11} & \overline{H}_{13} \\ \overline{H}_{21} & \overline{H}_{23}\end{matrix}\right\|^2 + \left\|\begin{matrix}\overline{H}_{12} & \overline{H}_{13} \\ \overline{H}_{22} & \overline{H}_{23}\end{matrix}\right\|^2 + \left\|\begin{matrix}\overline{H}_{11} & \overline{H}_{12} \\ \overline{H}_{21} & \overline{H}_{22}\end{matrix}\right\|^2$$

$$= 1 + \sum_{i=1}^{2}\sum_{j=1}^{3} \left|\overline{H}_{ij}\right|^2 + \sum_{i=1}^{\binom{3}{2}} \left|\overline{H}_{Mi,3}\right|^2, \qquad \text{(A2)}$$

for (3, 2) , where $\overline{H}_{Mi,3}$ is the i^{th} major of $\overline{H}$ of order (2, 3), $|a| = (a \cdot a^{+})^{1/2}$ represents the norm of a vector a, and $\left|\overline{H}_{Mi,3}\right|^2$ is the square of norm of the i^{th} major of H and represents the i^{th} product of the corresponding majors of $\overline{H}$ of order (2, 3) and $\overline{H}^{+}$ of order (3, 2). And

$$D_{33,2} = 1 + \sum_{i=1}^{3}\sum_{j=1}^{2} \left|\overline{H}_{ij}\right|^2 + \left\|\begin{matrix}\overline{H}_{11} & \overline{H}_{12} \\ \overline{H}_{21} & \overline{H}_{22}\end{matrix}\right\|^2 + \left\|\begin{matrix}\overline{H}_{21} & \overline{H}_{22} \\ \overline{H}_{31} & \overline{H}_{32}\end{matrix}\right\|^2 + \left\|\begin{matrix}\overline{H}_{11} & \overline{H}_{12} \\ \overline{H}_{31} & \overline{H}_{32}\end{matrix}\right\|^2$$

$$= 1 + \sum_{i=1}^{3}\sum_{j=1}^{2} \left|\overline{H}_{ij}\right|^2 + \sum_{i=1}^{\binom{3}{2}} \left|\overline{H}_{Mi,2}\right|^2, \qquad \text{(A3)}$$

for (2, 3), where $\overline{H}_{Mi,2}$ is the i^{th} major of $\overline{H}$ of order (3, 2) and $\left|\overline{H}_{Mi,2}\right|^2$ is the square of norm of i^{th} major of $\overline{H}$ of order (3, 2), representing the i^{th} product of the corresponding

majors of $\overline{H}$ of order (3, 2) and $\overline{H}^{+}$ of order (2, 3). The symbol $\binom{p}{q} = p!/q!(p-q)!$ denotes the number of combinations of q things from p. There are total $\binom{3}{2}$=3 ways to choose a major of order (2, 2) from H of either order (2, 3) or (3, 2).

It is explicitly seen from Eqs. A2 and A3 that $D_{22,3}$ and $D_{33,2}$ have the same forms as functions of each component of their corresponding $\overline{H}$.

If we check the pair of (2, 4) and (4, 2), their determinants are of the same form as Eqs. A2 and A3, respectively, except the orders in sum change correspondingly, i.e., $\sum_{j=1}^{3}$ replaced by $\sum_{j=1}^{4}$ in (A2), $\sum_{i=1}^{3}$ by $\sum_{i=1}^{4}$ in (A3), and $\sum_{i=1}^{\binom{3}{2}}$ by $\sum_{i=1}^{\binom{4}{2}}$ in the both cases.

For (n, 2) with n>4, the determinant $D_{22,n}$ can be calculated as a normal polynomial and is given by

$$D_{22,n} = \begin{vmatrix} 1+\sum_{j=1}^{n}\left|H_{1j}\right|^2 & \sum_{j=1}^{n} H_{1j}H_{2j}^{*} \\ \sum_{j=1}^{n} H_{2j}H_{1j}^{*} & 1+\sum_{j=1}^{n}\left|H_{2j}\right|^2 \end{vmatrix} = 1+\sum_{i=1}^{2}\sum_{j=1}^{n}\left|\overline{H}_{ij}\right|^2 + \sum_{i=1}^{\binom{n}{2}}\left|\overline{H}_{Mi,n}\right|^2, \qquad \text{(A4)}$$

where $\overline{H}_{Mi,n}$ is the i^{th} major of $\overline{H}$ of order (2, n) and $\left|\overline{H}_{Mi,n}\right|^2$ is the square of norm of i^{th} major of $\overline{H}$ of order (2, n), representing the i^{th} product of the corresponding majors of $\overline{H}$ of order (2, n) and $\overline{H}^{+}$ of order (n, 2). For (2, n), we assume that up to n $D_{nn,2}$ has the same form as (A3) with i ranging from 1 to n, i.e.,

$$D_{nn,2} = 1 + \sum_{i=1}^{n} \sum_{j=1}^{2} \left|\overline{H}_{ij}\right|^2 + \sum_{i=1}^{\binom{n}{2}} \left|\overline{H}_{Mi,2}\right|^2, \tag{A5}$$

where $\overline{H}_{Mi,2}$ is the i^{th} major of $\overline{H}$ of order (n, *2*) and $\left|\overline{H}_{Mi,2}\right|^2$ is the square of norm of i^{th} major of $\overline{H}$ of order (n, *2*), representing the i^{th} product of the corresponding majors of $\overline{H}$ of order (n, 2) and $\overline{H}^{+}$ of order (2, n). Now, we need to show that $D_{n+1n+1,2}$ for (2, n+*1*) has the same form as Eq. A3 with i ranging from 1 to n+1. In terms of Eq. A1, we have

$$D_{n+1n+1,2} = \begin{vmatrix} 1+\sum_{j=1}^{2}\left|H_{1j}\right|^2 & \sum_{j=1}^{2} H_{1j}H_{2j}^{*} & \cdots\cdots & \sum_{i=1}^{2} H_{1j}H_{n+1j}^{*} \\ \sum_{j=1}^{2} H_{2j}H_{1j}^{*} & 1+\sum_{i=1}^{2}\left|H_{2j}\right|^2 & \cdots\cdots & \sum_{j=1}^{2} H_{2j}H_{n+1j}^{*} \\ \cdot & & & \\ \cdot & & & \\ \sum_{j=1}^{2} H_{n+1j}H_{1j}^{*} & \sum_{i=1}^{n} H_{n+1j}H_{2j}^{*} & \cdots\cdots & 1+\sum_{i=1}^{n}\left|H_{n+1j}\right|^2 \end{vmatrix}$$

$$
=\begin{vmatrix}
1+\sum_{j=1}^{2}\left|H_{1j}\right|^2 & \sum_{j=1}^{2}H_{1j}H_{2j}^{*} & \cdots\cdots & \sum_{j=1}^{2}H_{1j}H_{n+1j}^{*} & 0 \\
\sum_{j=1}^{2}H_{2j}H_{1j}^{*} & 1+\sum_{j=1}^{2}\left|H_{2j}\right|^2 & \cdots\cdots & \sum_{j=1}^{2}H_{2j}H_{n+1j}^{*} & 0 \\
\cdot & & & & \\
\cdot & & & & \\
\sum_{j=1}^{2}H_{nj}H_{1j}^{*} & \sum_{j=1}^{2}H_{nj}H_{2j}^{*} & \cdots\cdots & 1+\sum_{j=1}^{2}\left|H_{nj}\right|^2 & 0 \\
\sum_{j=1}^{2}H_{n+1j}H_{1j}^{*} & \sum_{j=1}^{2}H_{n+1j}H_{2j}^{*} & \cdots\cdots & \sum_{j=1}^{2}H_{n+1j}H_{nj}^{*} & 1
\end{vmatrix}+
$$

$$
\begin{vmatrix}
1+\sum_{j=1}^{2}\left|H_{1j}\right|^2 & \sum_{j=1}^{2}H_{1j}H_{2j}^{*} & \cdots\cdots & \sum_{j=1}^{2}H_{1j}H_{nj}^{*} & \sum_{j=1}^{2}H_{1j}H_{n+1j}^{*} \\
\sum_{j=1}^{2}H_{2j}H_{1j}^{*} & 1+\sum_{j=1}^{2}\left|H_{2j}\right|^2 & \cdots\cdots & \sum_{j=1}^{2}H_{2j}H_{nj}^{*} & \sum_{j=1}^{2}H_{2j}H_{n+1j}^{*} \\
\cdot & & & & \\
\cdot & & & & \\
\sum_{j=1}^{2}H_{nj}H_{1j}^{*} & \sum_{j=1}^{2}H_{nj}H_{2j}^{*} & \cdots\cdots & 1+\sum_{j=1}^{2}\left|H_{nj}\right|^2 & \sum_{j=1}^{2}H_{nj}H_{n+1j}^{*} \\
\sum_{j=1}^{2}H_{n+1j}H_{1j}^{*} & \sum_{j=1}^{2}H_{n+1j}H_{2j}^{*} & \cdots\cdots & \sum_{j=1}^{2}H_{n+1j}H_{nj}^{*} & \sum_{j=1}^{2}\left|H_{n+1j}\right|^2
\end{vmatrix}. \qquad \text{(A6)}
$$

The first term in Eq. A6 is Eq. A5. For the second terms, repeating the process in Eq. A6 and so on for its following sub-determinants up to the determinants of order (*2, 2*), we have

$$
D_{n+1n+1,2}=D_{nn,2}+\det A+\sum_{1}^{\binom{n}{n-1}}\det A_{p,p}+\sum_{1}^{\binom{n}{n-2}}\det A_{pq,pq}+\cdots+\sum_{1}^{\binom{n}{1}}\det A_{pq\ldots k,pq\ldots k}+\sum_{j=1}^{2}\left|H_{n+1j}\right|^2
$$

,(A7)

where $A_{p,p}$ is the first principal minor of A obtained by striking out the pth row and column of A with p ranging from *1* to n, $A_{pq,pq}$ is the second principal minor of A obtained by striking out the pth and qth rows and columns of A with p and q ranging from *1* to n, $A_{pq...k,pq...k}$ is the $(n-1)$th principal minor of A obtained by striking out p^{th},q^{th},..., and k^{th} rows and columns of A with p, q,..., and k ranging from 1 to n. As $A = \overline{H}\,\overline{H}^{+}$, where $\overline{H}$ is a matrix of order $(n+1,2)$ and $\overline{H}^{+}$ of order $(2, n+1)$, det$A$=0 because the rows of $\overline{H}$ is larger than its columns as indicated by the theorem 2.11.3 of Ref. 72. $A_{p,p}$ can be written as $A_{p,p} = \overline{H}_p \overline{H}_p^{+}$, where $\overline{H}_p$ is obtained by deleting the pth row with p ranging from *1* to n. So det $A_{p,p}$=0 because $\overline{H}_p$ is a matrix of order $(n, 2)$ and $n>2$. So do the followings except the determinants in the last second term in (A7), $A_{pq...k,pq...k} = \overline{H}_{pq...k}\overline{H}_{pq...k}^{+}$ where $\overline{H}_{pq...k}$ is obtained by deleting $n-1$ rows with $p,q,...,k$ ranging from *1* to n, and is formed by

$$\begin{vmatrix} \sum_{j=1}^{2}\left|\overline{H}_{ij}\right|^2 & \sum_{j=1}^{2}\overline{H}_{ij}\overline{H}_{n+1j}^{*} \\ \sum_{j=1}^{2}\overline{H}_{ij}^{*}\overline{H}_{n+1j} & \sum_{j=1}^{2}\left|\overline{H}_{n+1j}\right|^2 \end{vmatrix} = \begin{vmatrix} \overline{H}_{i1} & \overline{H}_{i2} \\ \overline{H}_{n+11} & \overline{H}_{n+12} \end{vmatrix} \begin{vmatrix} \overline{H}_{i1}^{*} & \overline{H}_{n+11}^{*} \\ \overline{H}_{i2}^{*} & \overline{H}_{n+12}^{*} \end{vmatrix} = \begin{Vmatrix} \overline{H}_{i1} & \overline{H}_{i2} \\ \overline{H}_{n+11} & \overline{H}_{n+12} \end{Vmatrix}^2$$

, where $i=1,2,...,n$. A determinant of this kind is not zero due to the rows of $\overline{H}_{pq...k}$ equal to its columns, i.e., *2* by *2*. There are n determinants of this kind and they come from the products of the corresponding majors of $\overline{H}$ and $\overline{H}^{+}$ with the last row of $\overline{H}$ and last column of $\overline{H}^{+}$ being fixed. It is noted that n such square norms of the majors of H of

order ($n+1$, 2) with the last row being fixed plus $\binom{n}{2}$ square norms of the majors in $D_{nn,2}$ of Eq.A5 equals to $\binom{n+1}{2}$ combinational square norms of the majors of H of order ($n+1$, 2) according to the combinational method. Thus, we can rewrite Eq. A7 as

$$D_{n+1n+1,2} = 1 + \sum_{i=1}^{n+1} \sum_{j=1}^{2} \left|\overline{H}_{ij}\right|^2 + \sum_{i=1}^{\binom{n+1}{2}} \left|\overline{H}_{Mi,2}\right|^2, \tag{A8}$$

and we can say that Eq. A5 is true for any (n,2) based on (A8).

Comparing (A5) with (A4), we see that they have the same form.

Appendix B

The determinant in Eq. 3.1 for a system with m receive antennas and n transmit antennas, which refers to (n, m) here, is

$$D_{mm,n} = \det[I_m + (\rho / n) HH^+] \ , \tag{B1}$$

where $D_{mm,n}$ denotes the determinant of a square matrix of order (m, m) with n transmit antennas, H is the channel transfer matrix of order (m, n) with each element being the normalized complex Gaussian RV, and the others have the same meaning as they are mentioned in Sec.3.3. For convenience, we define $\overline{H} = (\rho / n)^{1/2} H$ and denote $A = \overline{H}\ \overline{H}^+$, which is a square matrix. So, $D_{mm,n} = \det(I_m + A)$. When the r rows and columns struck out of a square matrix A have the same indices, the remaining submatrix is located symmetrically with respective to main diagonal of A, and is called the r^{th} principal minor of A.

In terms of $\overline{H}$, $D_{mm,n}$ can be written as

$$D_{mm,n}=\begin{vmatrix} 1+\sum_{j=1}^{n}\left|\overline{H}_{1j}\right|^2 & \sum_{j=1}^{n}\overline{H}_{1j}\overline{H}_{2j}^{*} & \cdots\cdots & \sum_{j=1}^{n}\overline{H}_{1j}\overline{H}_{mj}^{*} \\ \sum_{j=1}^{n}\overline{H}_{2j}\overline{H}_{1j}^{*} & 1+\sum_{j=1}^{n}\left|\overline{H}_{2j}\right|^2 & \cdots\cdots & \sum_{j=1}^{n}\overline{H}_{2j}\overline{H}_{mj}^{*} \\ \cdot & & & \\ \cdot & & & \\ \sum_{j=1}^{n}\overline{H}_{mj}\overline{H}_{1j}^{*} & \sum_{j=1}^{n}\overline{H}_{mj}\overline{H}_{2j}^{*} & \cdots\cdots & 1+\sum_{j=1}^{n}\left|\overline{H}_{mj}\right|^2 \end{vmatrix}$$

$$=\begin{vmatrix} 1+\sum_{j=1}^{n}\left|\overline{H}_{1j}\right|^2 & \sum_{j=1}^{n}\overline{H}_{1j}\overline{H}_{2j}^{*} & \cdots\cdots & \sum_{j=1}^{n}\overline{H}_{1j}\overline{H}_{m-1j}^{*} & 0 \\ \sum_{j=1}^{n}\overline{H}_{2j}\overline{H}_{1j}^{*} & 1+\sum_{j=1}^{n}\left|\overline{H}_{2j}\right|^2 & \cdots\cdots & \sum_{j=1}^{n}\overline{H}_{2j}\overline{H}_{m-1j}^{*} & 0 \\ \cdot & & & & \\ \cdot & & & & \\ \sum_{j=1}^{n}\overline{H}_{m-1j}\overline{H}_{1j}^{*} & \sum_{j=1}^{n}\overline{H}_{m-1j}\overline{H}_{2j}^{*} & \cdots\cdots & 1+\sum_{j=1}^{n}\left|\overline{H}_{m-1j}\right|^2 & 0 \\ \sum_{j=1}^{n}\overline{H}_{mj}\overline{H}_{1j}^{*} & \sum_{j=1}^{n}\overline{H}_{mj}\overline{H}_{2j}^{*} & \cdots\cdots & \sum_{j=1}^{n}\overline{H}_{mj}\overline{H}_{m-1j}^{*} & 1 \end{vmatrix}+$$

$$\begin{vmatrix} 1+\sum_{j=1}^{n}\left|\overline{H}_{1j}\right|^2 & \sum_{j=1}^{n}\overline{H}_{1j}\overline{H}_{2j}^{*} & \cdots\cdots & \sum_{j=1}^{n}\overline{H}_{1j}\overline{H}_{m-1j}^{*} & \sum_{j=1}^{n}\overline{H}_{1j}\overline{H}_{mj}^{*} \\ \sum_{j=1}^{n}\overline{H}_{2j}\overline{H}_{1j}^{*} & 1+\sum_{j=1}^{n}\left|\overline{H}_{2j}\right|^2 & \cdots\cdots & \sum_{j=1}^{n}\overline{H}_{2j}\overline{H}_{m-1j}^{*} & \sum_{j=1}^{n}\overline{H}_{2j}\overline{H}_{mj}^{*} \\ \cdot & & & & \\ \cdot & & & & \\ \sum_{j=1}^{n}\overline{H}_{m-1j}\overline{H}_{1j}^{*} & \sum_{j=1}^{n}\overline{H}_{m-1j}\overline{H}_{2j}^{*} & \cdots\cdots & 1+\sum_{j=1}^{n}\left|\overline{H}_{m-1j}\right|^2 & \sum_{j=1}^{n}\overline{H}_{m-1j}\overline{H}_{mj}^{*} \\ \sum_{j=1}^{n}\overline{H}_{mj}\overline{H}_{1j}^{*} & \sum_{j=1}^{n}\overline{H}_{mj}\overline{H}_{2j}^{*} & \cdots\cdots & \sum_{j=1}^{n}\overline{H}_{mj}\overline{H}_{m-1j}^{*} & \sum_{j=1}^{n}\left|\overline{H}_{mj}\right|^2 \end{vmatrix},$$

(B2)

where * denotes the complex conjugate. The first term in (B2) equals to $D_{m-1m-1,n}$. Repeating above process for the second term and its followings until there is no "1" appearing in the entry of any determinant, we obtain

$$D_{mm,n} = D_{m-1m-1,n} + \det A + \sum_{1}^{\binom{m-1}{m-2}} \det A_{p,p} + \sum_{1}^{\binom{m-1}{m-3}} \det A_{pq,pq} + \cdots + \sum_{1}^{\binom{m-1}{1}} \det A_{pq\ldots k,pq\ldots k} + \sum_{j=1}^{n} \left|H_{mj}\right|^2 \quad , \text{(B3)}$$

where $A_{p,p}$ is the first principal minor of A obtained by striking out the pth row and column of A with p ranging from *1* to *m-1*, $A_{pq,pq}$ is the second principal minor of A obtained by striking out the pth and qth rows and columns of A with p and q ranging from *1* to *m-1*, $A_{pq\ldots k,pq\ldots k}$ is the $(m\text{-}2)^{th}$ principal minor of A obtained by striking out p^{th},q^{th},..., and k^{th} rows and columns of A with $p,q,\ldots$,and k ranging from *1* to *m-1*.

As it is defined, $A = \overline{H}\,\overline{H}^{+}$, where $\overline{H}$ is a matrix of order (m,n) and $\overline{H}^{+}$ of order (n,m). $A_{p,p}$ can be written as $A_{p,p} = \overline{H}_p \overline{H}_p^{+}$, where $\overline{H}_p$ is obtained by deleting the p^{th} row with p ranging from 1 to *m-1*. And $A_{pq\ldots k,pq\ldots k} = \overline{H}_{pq\ldots k}\overline{H}_{pq\ldots k}^{+}$ where $\overline{H}_{pq\ldots k}$ is obtained by deleting *m-2* rows with $p,q,\ldots,k$ ranging from *1* to *m-1*.

The determinant of A of the product of $\overline{H}$ and $\overline{H}^{+}$ can be either zero when $m>n$ or positive when $m<n$ in terms of theorems 2.11.1 and 2.11.3 of Ref. 72. So do the determinants of the products of $\overline{H}_p$ and $\overline{H}_p^{+}$ with $p=1, 2,\ldots m\text{-}1$, and the following. Thus, (B3) can be expressed as

$$D_{mm,n} = D_{m-1m-1,n} + P_m + \sum_{j=1}^{n} \left| H_{mj} \right|^2 , \tag{B4}$$

where P_m represents all other zero and positive terms except the first term and the last term in (B3). Similarly, we have

$$D_{m-1m-1,n} = D_{m-2m-2,n} + P_{m-1} + \sum_{j=1}^{n} \left| H_{m-1j} \right|^2 , \tag{B5}$$

where P_{m-1} represents all other zero and positive terms except the first and the last term in (B5). Repeating this step up to the minimum determinant of order *1*, which is $1 + \sum_{j=1}^{n} \left| H_{1j} \right|^2$, (B4) can be rewritten as

$$D_{mm,n} = 1 + \sum_{i=1}^{m} \sum_{j=1}^{n} \left| H_{ij} \right|^2 + P_T , \tag{B6}$$

where $P_T = P_m + P_{m-1} + \cdots + P_1$, which is positive.

List of publications

1. J. Gong, J. F. Hayes and M. R. Soleymani, "The effect of antenna physics on fading correlation and the capacity of multi-element antenna systems", submitted to IEEE trans. on Vehicular Technology, 2004.

2. J. Gong, J. F. Hayes, and M. R. Soleymani , "The effect of antenna physics on fading correlation and the capacity of multielement antenna systems," Proc. IEEE CCECE, Saskatoon, May 1-3, 2005.

3. J. Gong, J. F. Hayes, and M. R. Soleymani, "Comparison of capacities of the transmit antenna diversity with the receive antenna diversity in the MIMO scheme," Proc. IEEE CCECE 2003, Vol. 1, Montreal, May 4-7, 2003, pp.179-182.